12-13-2008

# Low-temperature halo-carbon homoepitaxial growth of 4H-SiC

Huang-De Hennessy Lin

# LOW-TEMPERATURE HALO-CARBON HOMOEPITAXIAL GROWTH OF 4H-SIC

By

Huang-De Lin

A Dissertation
Submitted to the Faculty of
Mississippi State University
in Partial Fulfillment of the Requirements
for the Degree of Doctor of Philosophy
in Electrical Engineering
in the Department of Electrical and Computer Engineering

Mississippi State, Mississippi

December 2008

LOW-TEMPERATURE HALO-CARBON HOMOEPITAXIAL GROWTH OF 4H-SIC

By

Huang-De Lin

Approved:

| | |
|---|---|
| Yaroslav Koshka<br>Associate Professor of Electrical and Computer Engineering<br>(Director of Dissertation) | Michael S. Mazzola<br>Professor of Electrical and Computer Engineering<br>(Committee Member) |
| Raymond S. Winton<br>Professor of Electrical and Computer Engineering<br>(Committee Member) | Seong-Gon Kim<br>Assistant Professor of Physics<br>(Committee Member) |
| James E. Fowler<br>Professor of Electrical and Computer Engineering<br>(Graduate Coordinator) | Sarah A. Rajala<br>Dean of the Bagley College of Engineering |

Name: Huang-De Lin

Date of Degree: December 12, 2008

Institution: Mississippi State University

Major Field: Electrical Engineering

Major Professor: Dr. Yaroslov Koshka

Title of Study: LOW-TEMPERATURE HALO-CARBON HOMOEPITAXIAL GROWTH OF 4H-SIC

Pages in Study: 131

Candidate for Degree of Doctor of Philosophy

New halo-carbon precursor, $CH_3Cl$, is used in this work to replace the traditional $C_3H_8$ gas as a carbon precursor for the homoepitaxial growth of 4H-SiC. The traditional $SiH_4$-$C_3H_8$-$H_2$ systems require high growth temperatures to enable the desirable step-flow growth for high-quality epilayers.

A well known problem of the regular-temperature growth is the homogeneous gas-phase nucleation caused by $SiH_4$ decomposition. However, the degree of Si cluster formation in the gas phase and its influence on our low-temperature epitaxial growth was unknown prior to this work.

Growth at temperatures below 1400$^o$C was demonstrated previously only for a limited range of substrate surface orientations and with poor quality. Mirror-like epilayer surface without foreign polytype inclusions and with rare surface defects was demonstrated at temperatures down to 1280-1300$^o$C for our halo-carbon growth.

Quantitatively different growth-rate dependences on the carbon-precursor flow rate suggested different precursor decomposition kinetics and different surface reactions in $CH_3Cl$ and $C_3H_8$ systems.

Photoluminescence measurement indicated the high quality of the epilayers grown at 1300$^{o}$C. A mirror-like surface morphology with rare surface defects was demonstrated for the growth on low off-axis substrates at 1380$^{o}$C.

The most critical growth-rate limiting mechanism during the low-temperature epitaxial growth is the formation of Si clusters, which depleted the Si supply to the growth surface, in the gas phase. Presence of chlorine in the $CH_3Cl$ precursor significantly reduces but does not completely eliminate this problem.

The addition of HCl during growths improved the growth rate and surface morphology drastically but also brought up some complex results, suggesting more complex mechanisms of HCl interaction with the gas-phase clusters.

These complicated results were explained partly by an additional mechanism of precursor depletion enhanced in presence of HCl.

Complex changes in the effective silicon-to-carbon ratio in the growth zone indicated that the supply of carbon species may also be enhanced at least at low HCl flow rates. This fact allowed us to suggest that the gas-phase clusters may contain a significant amount of carbon. The new model assuming coexistence of the silicon and carbon in the gas-phase clusters enabled the explanation of the complex experimental trends reported in this work.

ACKNOWLEDGEMENT

I would like to express my sincere gratitude to my major advisor, Dr. Yaroslov Koshka for not giving me up in the past 5 years. He is more than an advisor. Personally, he is like a friend. Academically, he taught me a lot. During the time I was down, he tried to pull me out of the mass. I also want to thank Dr. Mazzola, who alerted me about my work. That will definitely help me with my attitude toward my job. A special thank to Dr. Fowler, I would not be able to defense my dissertation on schedule without his help. Of course, all my friends and colleagues support me all the time and encourage me to face the problems no matter how hard they are. I would like to present my appreciation to our previous lab manager, Jeffery Wyatt. Without his help and instructions, my experiments won't be done so easily. The hardware experiences passed by him prepare me for the challenges in the future although he already left for another job. At last, I would like to dedicate all my love to my parents and my daughter. They complete me.

TABLE OF CONTENTS

Page

LIST OF TABLES

LIST OF FIGURES

FIGURE Page

CHAPTER 1

# INTRODUCTION

## 1.1 SiC Material

Silicon carbide (SiC) is currently under intensive investigations as a promising material for a variety of semiconductor devices in areas where silicon devices are not effective. Some of the unique properties of SiC that surpass that of silicon (Si) are: (1) large bandgap useful for high-temperature operation and better radiation hardness; (2) high electric breakdown field; (3) high saturation electron drift velocity for high-frequency operation; (4) significantly higher thermal conductivity that can manage heat more efficiently during the operation of high-power devices [1]. Table 1-1 shows some important electrical and physical properties of Si and commonly used SiC polytypes. More than 200 SiC polytypes exist [2-3]. These polytypes are differentiated by the different stacking sequence of the Si-C biatom layers. Most commonly used polytypes for

Table 1-1: Properties of typical SiC polytypes and Si

| Property \ Material | Si | 3C-SiC | 4H-SiC | 6H-SiC |
|---|---|---|---|---|
| Thermal conductivity (W/cm.k) | 1.5 | 4.9 | 4.9 | 4.9 |
| Bandgap(eV) | 1.12 | 2.4 | 3.2 | 3 |
| Transparency of intrinsic material | N | Y | Y | Y |
| Saturated electron velocity ($10^7$ m/s) | 1 | 2.7 | 2.7 | 2 |
| Electron mobility ($cm^2$/V-s) | 1450 | 1000 | 900 | 450 |
| Breakdown field (MV/cm) | 0.3 | 2 | 3 | 3 |

device applications are 3C-, 4H-, and 6H-SiC. Fig.1.1 shows the stacking sequences of 3C-, 4H-, and 6H-SiC polytypes. 3C-SiC is the only form that has the pure cubic zinc-

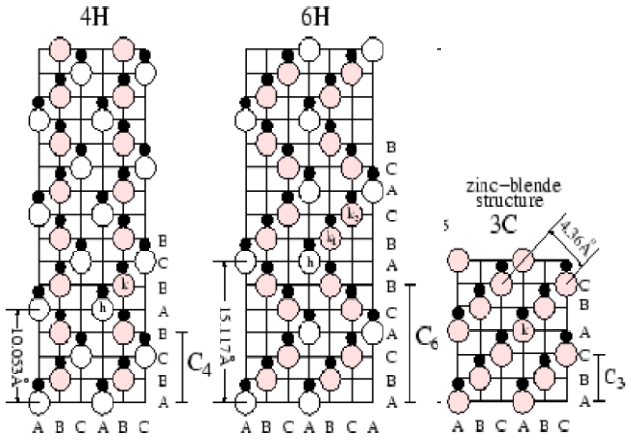


Fig.1.1: The stacking sequences of 4H-, 6H-, and 3C-SiC. The open circle denotes the Si atom, and the closed circle denotes the carbon atom, respectively.

blend structure. 3C-SiC is also referred to as β–SiC. 2H-SiC has a pure hexagonal symmetric structure. The other SiC polytypes have the mixtures of cubic or hexagonal bonding structures. In addition to 3C-SiC, all the other SiC polytypes are referred to as α–SiC. The most developed polytypes today are hexagonal 4H- and 6H-SiC. Those polytypes are commercially available today. 4H-SiC is the main object of this work.

### 1.2 Chemical Vapor Deposition (CVD) Epitaxial Growth of SiC

In order to realize the device applications of SiC materials, epitaxial SiC layers grown on the SiC bulk substrates are required. The crystalline quality of commercially

available 4H- and 6H-SiC wafers is often not sufficient for direct device fabrications, due to the presence of a variety of structural and crystallographic defects, such as sub-grain boundaries, dislocations, and micropipes, which will severely limit the SiC device performance [4-9]. More importantly, most of semiconductor device designs require values of conductivity in the near-surface layers (i.e., active device regions) different from that in the rest of the substrate. Epitaxial layers are commonly used to provide the desirable values of conductivity in the active device regions, while also reducing the concentration of crystallographic defects.

Chemical vapor deposition (CVD) is the most common technology for the epitaxial growth of SiC materials. Generally, CVD epitaxial growth of SiC is accomplished by supplying the carrier gas (which is usually $H_2$), and Si- and C-containing gases (i.e., growth precursors) into the growth chamber or the reactor. When passing through the hot zone of the reactor, the gaseous precursors undergo a chain of gas-phase reactions and provide growth species to the growth surface. By keeping the SiC substrates also at high temperature, the surface reactions for SiC growth are promoted on the substrate surface thus resulting in the epitaxial growth of SiC.

$SiH_4$-$C_3H_8$-$H_2$ gas system is the most conventional growth system used for the fabrication of 4H- and 6H-SiC epitaxial layers for high power and high frequency devices (i.e., silane and propane serve as the growth precursors supplying Si and C growth species, respectively). The conventionally used growth temperatures are in the range between 1500$^o$C and 1700$^o$C. Such high growth temperatures have been long considered to be absolutely required to ensure the favorable step-flow growth, which will be

discussed later in detail. If the growth temperature is below some critical value depending on the type of the reactor and the operating conditions, morphology degradation and crystalline quality deterioration occur, such as 3C-SiC inclusion, two-dimensional (2D) nucleation, step-bunching, etc.

However, the regular growth temperatures bring a number of disadvantages. The disadvantages include economics of the CVD process (e.g., susceptor degradation), higher rate of impurities released from the reactor hardware at high temperatures, etc. In addition, the traditional $SiH_4$-$C_3H_8$-$H_2$ system makes it very difficult to fabricate SiC microelectronic devices using the so called selective epitaxial growth (SEG) techniques [10]. The traditional masking materials for device fabrication cannot survive under such high temperatures, and novel high-temperature masks are required.

Off-axis cut substrates are used today to promote the step-flow mechanism. However, even with the off-axis wafers, the growth temperatures for device-ready epitaxial layers are still too high today. Simultaneously, use of off-axis substrates brings its own disadvantages. The existence of a large off angle reduces the available number of wafers that can be sliced from a single ingot. This problem will become worse at greater wafer diameters, i.e., a large portion of the SiC ingot will be wasted. In epitaxial growth, these off angles have a negative effect in that certain type of crystal defects in the substrate (e.g., basal plane dislocations that are known to be detrimental for performance of bipolar devices) propagate into the epitaxial layer [11]. Also, in the studies of substrates with mesa structures, large off angles caused the anisotropy in the epitaxial growth [12-13]. The mesa pattern deformed because of the different lateral growth rates

in different directions. In [13], the fastest growth direction was <11-20>, and the slowest growth direction was <1-100>. The original circular mesa pattern evolved into a hexagonal shape.

In this dissertation, an alternative halo-carbon precursor, $CH_3Cl$, was studied and compared to the traditional carbon precursor, $C_3H_8$. Different cracking mechanisms and different gas-phase chemical reactions of $CH_3Cl$, compared to $C_3H_8$, enabled the low-temperature epitaxial growths of electronic quality 4H-SiC epitaxial layers at temperatures down to and even below 1300$^o$C in this study.

In general, the growth-rate-limiting factors for the CVD epitaxial growth can be divided into two regimes, mass transfer and surface reaction modes. According to Grove's simplified CVD film-growth model [14], either one of the gas-phase processes (including the transport of the reactants across the boundary layer) or one of the surface processes (the surface film-forming chemical reaction) will limit the growth rate of the epitaxial layer. If the supply of the precursors is a constant, the growth rate is controlled by the small value of gas-phase mass-transfer coefficient ($h_g$) or chemical-surface-reaction-rate constant ($k_s$). If $h_g << k_s$, the growth is a mass-transfer-rate-limited case. This means that the concentrations of the reactants in the gas phase control the growth rate. If $k_s << h_g$, the growth is a surface-reaction-rate-limited case. In the surface-reaction-rate-limited case, chemical reactions on the surface of the growing epitaxial layer are often thermally activated. These surface reactions can be represented by an Arrhenius type equation:

$$k_s = k_0 e^{-E_A/kT} \tag{1.1}$$

where $k_s$ is the rate constant, $k_0$ is a temperature-independent frequency factor or pre-exponential factor, $k$ is the Boltzmanns constant (8.6e-5 eV/K), and $E_A$ is the activation energy of the reaction. According to a simplified consideration often used in CVD of silicon, the CVD growth is operating in the mass-transfer-rate-limited regime at high temperatures; for lower temperatures, the deposition rate of the CVD growth is usually surface-reaction-rate-limited. From equation (1.1), the surface reaction rate increases exponentially with the increasing temperature.

The objective of this study is to significantly reduce the growth temperature for 4H-SiC epitaxial growth by using $CH_3Cl$ as the carbon precursor. Intuitively, the surface mobility of the adatoms might be a major limiting factor to the growth. Therefore the initial approach of this study was based on the hypothesis that the surface mobility of the adatoms put the lowest limit on the growth temperature for the good quality homoepitaxial growth of 4H-SiC. The idea to use alternative precursors was initially aimed at increasing the surface mobility by enhancing the surface etching and providing different kinds of intermediate ad-species to the growth surface. However, as it is described in chapter 4, the experiments conducted in this study justified significant adjustments to the initial hypothesis and also indicated new opportunities towards improving the growth characteristics (i.e., growth rate and morphology) while further reducing the growth temperatures.

It will be shown that the homogeneous gas-phase nucleation (which is also often called condensation of Si vapor) profoundly limited the Si-related source supply and the growth rate of the epitaxial layers at low growth temperatures. The clustering of the Si-

atoms in the gas phase depletes the Si growth species and alters the Si/C ratios in the vicinity of the growing SiC layer surface. The low-temperature epitaxial growth by using $CH_3Cl$ has very different gas-phase and surface chemical reactions from that of the conventional CVD systems using $C_3H_8$ as the C-precursor. Formation of Cl-containing products of $CH_3Cl$ decomposition appears to bring significant advantages and enables the very possibility to conduct the homoepitaxial growth at such low temperatures with no morphology degradation and promising growth rates. However, use of the chlorinated carbon precursor chloromethane appears to only partially reduce the undesirable effect of the gas-phase nucleation, which limits significantly the growth rate at low temperatures.

In order to further reduce or eliminate the silicon clustering in the gas phase, HCl gas was added during the epitaxial growth. The objective of adding HCl during the epitaxial growth is to establish the feasibility of enhancing the reduction of Si clusters by providing additional Cl-containing vapor species; therefore the increase of the growth rate and the improvement of the epitaxial layer surface morphology were expected. The experimental results in chapter 4 confirmed the desirable effect of HCl addition. Both the growth rate and surface morphology were dramatically improved. The effect was proven to be due to suppressed homogeneous nucleation. However, some new undesirable mechanisms were identified.

### 1.3 Preview of This Dissertation

The main goal of this dissertation is application of the halo-carbon precursor, $CH_3Cl$, to achieve low-temperature CVD epitaxial growth for 4H-SiC. Chapter 2 covers the theoretical background of the electrical and physical properties of the most common

SiC polytypes, CVD epitaxial growth mechanisms, issues concerning the epitaxial growths of SiC, such as the step bunching problem, defects in the epitaxial layers, the effect of Si/C ratio on the surface morphology and on the dopant incorporation (i.e., so-called site-competition epitaxy), etc. The formation of Si clusters in the gas phase as a result of the pyrolysis of $SiH_4$ and prior research on the application of chlorinated gases to suppress this undesirable mechanism are also reviewed in Chapter 2

In Chapter 3, the characterization methods used for the grown epilayers are presented. The most common techniques include Nomarski differential interference microscopy (NDIM) for the epilayer morphology investigation, capacitance-voltage measurement for the doping profile in the epilayer, Fourier transform infrared spectroscopy for the thickness measurement of the epilayer, photoluminescence spectroscopy for the impurity energy level determination, and X-ray diffraction for crystal structure identification. The hardware for the CVD epitaxial growth is also demonstrated in chapter 3.

The experimental results and discussions are presented in Chapter 4. The comparison of the 4H-SiC epitaxial growths using $CH_3Cl$ versus the traditional $C_3H_8$ at normal growth temperatures (higher than 1450$^o$C) was conducted first. Subsequently, the growth conditions enabling epitaxial layers with mirror-like surface morphology were used as the starting point to explore the feasibility of reducing the epitaxial growth temperatures down to or even below 1300$^o$C. The dominant role of silicon clustering in the gas phase for the low-temperature halo-carbon epitaxial growth will be discussed in Chapter 4. The application of in-situ HCl flow with the $SiH_4$-$CH_3Cl$-$H_2$ system was

conducted to investigate the influence of HCl on silicon cluster dissociation, as well as to reveal some other growth limiting mechanisms. The capacitance-voltage (CV) measurements, photoluminescence measurements, and scanning electron microscopy (SEM) are employed to assess the quality of the epitaxial layers grown at low temperatures.

Conclusions and suggestions for the future work are presented in chapter 5. The promising aspects of replacing $C_3H_8$ with $CH_3Cl$ for the conventional $SiH_4$-$C_3H_8$-$H_2$ epitaxial growth systems are summarized. Future work for the successful development of the SiC low-temperature homoepitaxial growth method suitable for commercial applications is proposed.

# CHAPTER 2

# THEORETICAL BACKGROUND AND LITERATURE REVIEW

## 2.1 **Chemical Vapor Deposition (CVD)**

Chemical vapor deposition is a technique for depositing thin films of materials on wafers or substrates. Source gases are introduced into a reaction chamber, where the sample is positioned and the energy is supplied through heat, RF power, or other means that result in decomposition of the source gases and chemical reactions leading to the deposition of a solid film on a substrate. Various CVD processes are widely employed for the thin film growth including SiC epitaxial growth. The dominant use of CVD for the thin film growth can be attributed to 1) uniform thickness and doping concentration distribution over large area; 2) high-purity films can be achieved; 3) a great variety of chemical compositions can be deposited; 4) some films with acceptable film properties can only be achieved by CVD method; 5) good economy and process-control are possible for many CVD films. CVD systems usually contain the following subsystems: (1) gas sources, (2) gas feed lines, (3) mass-flow controllers (MFC), (4) a reaction chamber or reactor, 5) a heating element; 6) a temperature sensor; 7) a pumping system; and 8) a pressure controller ( items 7 and 8 are for low-pressure CVD systems (LPCVD)) [15]. Generally, different types of CVD reactors can be defined in terms of the chamber pressure, the gas flow direction, or heating source and heating mechanism. With respect

to the operating pressure, the configuration for the reactor can be atmospheric-pressure CVD (APCVD) or low-pressure CVD (reduced pressure) (LPCVD). If only the wafer (or the substrate) and the susceptor are heated during the operation, this is the cold-wall CVD reactor. If the temperature of the reactor walls is the same as the wafer, it is a hot-wall CVD reactor. For LPCVD type of reactors, if part of the energy is supplied by the plasma as well as by thermal energy, they are known as plasma-enhanced-CVD (PECVD). Different types of CVD reactors are designed for different applications based on the economic and purpose-oriented reasons. The next section will explore advantages and drawbacks of different types of CVD reactors. After understanding the basic aspects of different types of CVD reactors, the discussion of a simplified CVD epitaxial growth model will help us understand better the limitations and mechanisms of CVD epitaxial growths.

## 2.2 Advantages and Disadvantages of Different Types of CVD Reactors

### 2.2.1 APCVD

Operating at atmospheric pressure keeps the reactor design simple and allows for high film-deposition-rates. However, APCVD suffers from undesirable gas-phase reactions, especially in the case of silane-related reactant gases, and poor step-coverage. Generally APCVD processes are conducted in the mass-transport-limited regime; therefore the design of the reactor geometry and the control of gas-flow patterns are extremely important to provide a homogeneous delivery of the reactant-flux to all parts of

every wafer or substrate in the reactor. Poor uniformity and particulate contamination render APCVD systems little use in VLSI and ULSI fabrication today.

### 2.2.2 LPCVD

Operating at medium vacuum, LPCVD systems result in better uniformity and step coverage, as well as lower particulate contamination, than APCVD systems for some film types [16-17]. At reduced pressure, the diffusivity of the reactant gas molecules is sufficiently increased so that typically the surface reaction rate rather than mass-transport becomes the limiting factor. The surface reaction rate is very sensitive to temperature (Eq.1.1). Therefore the control of a homogeneous temperature distribution for the LPCVD systems is very important. However the surface reaction rate is also directly proportional to the surface concentration. If a local depletion of reactants from a gas by their deposition on the wafers or substrates near to the gas inlet happens, the non-uniform gas-phase concentrations can result in deposition non-homogeneity. The growth rate of the deposited film could decrease from the upstream (inlet side) sample to downstream (outlet side) sample. The main disadvantage of LPCVD processes is their relatively low deposition rates for monocrystalline thin film depositions. The undesired gas-phase nucleation tends to occur when attempting to increase the deposition rates by increasing the partial pressures of the reactants (i.e., increasing the inlet reactant-gas-flow rate).

The LPCVD reactors are widely used in semiconductor industry because of their superior economy, throughput, uniformity, and ability to accommodate large diameter wafers. Operating in the surface-reaction-rate-limited regime for LPCVD reactors allows

the wafer arrangement more flexible since the homogeneous delivery of reactant gases to every part of the wafer or substrate in the reactor is not as large an issue.

### 2.2.3 PECVD

Plasma enhanced chemical vapor deposition (PECVD) initiates and sustains chemical reactions by using an rf-induced glow discharge to transfer energy to the reactant gases, as well as the thermal energy. PECVD has two advantages compared to the conventional CVD methods: low process temperature and flexible film properties. The former satisfies the low thermal budget requirement for most production, and the latter makes it possible to tailor film properties for specific device characteristics such as the formation of $SiO_2$ and silicon nitride over aluminum [18]. Desirable properties for VLSI and USLI applications can be achieved by PECVD, such as good adhesion, low pinhole density, good step coverage, adequate electrical properties, and compatibility with fine-line pattern transfer processes. However the highly reactive radicals formed in the plasma discharge also present some problems. By-products and incidental species (especially hydrogen, nitrogen, and oxygen), are incorporated into the resultant films. The excessive incorporation of these contaminants may lead to various problems [19-20], including: 1) outgassing and contaminant bubbling, 2) cracking or peeling during later thermal cycling, 3) shifts in the threshold voltage of MOSFETs, and 4) increased susceptibility to degradation from hot carrier effects in MOSFETs. The control and optimization of a PECVD process is dependent in a very complex way on several deposition parameters besides those of an LPCVD process. Furthermore, PECVD is typically surface-reaction-rate-limited, which is similar to the case of an LPCVD process.

An adequate substrate temperature control is needed to ensure a uniform film thickness. Therefore PECVD is more often used to grow amorphous or polycrystalline films and rarely used for high-quality epitaxial growths of semiconductors. Table 2-1 briefly summarizes the characteristics and applications of the aforementioned CVD processes.

Table 2-1 Characteristics and Applications of CVD Reactors

| Process | Characteristics & Advantages | Disadvantages | Applications |
|---|---|---|---|
| APCVD | Mass-transport-limited regiem, Simple reactor, Fast deposition, Low temperature, | Poor step coverage, Particulate contamination, | Low temperature oxides (doped and undoped), Epi films. |
| LPCVD | Surface-reaction-rate-limited, Excellent purity and uniformity, Conformal step coverage, Large wafer capacity, | Low deposition rate, Requires vacuum systems, Source depletion, High temperature, | High temperature oxides (doped and undoped), Silicon nitride, Poly-Si, Epi films. |
| PECVD | Surface-reaction-rate-limited, Low temperature, Fast deposition, Good step coverage, better ability to tailer the properties of the deposited films. | Impurity incorporation (e.g., $H_2$, $O_2$, and $N_2$), More complicated control of the process parameters, Particulate contamination. | Low temperature insulators over metals, Passivation (nitrides). |

## 2.3 An Overview of SiC Material Growth

### 2.3.1 The Bulk Growth for SiC Materials

For the past several decades, the single crystalline SiC bulk growth has been implemented by physical vapor transport (PVT) or SiC seed sublimation growth method. The SiC bulk growth method was first proposed by Lely in 1955 [21]. The crucible was heated to approximately 2500$^{o}$C in an atmosphere of Ar at atmospheric pressure. The SiC crystal quality grown by Lely method can be very high, however the yield of Lely process is low, the size of the SiC crystal is irregular, the shape is normally hexagonal, and the polytype control of the grown SiC is not available. The Lely method was improved later by Tairov and Tsvetkov in 1978 [22]. The method proposed by [22] is

also known as a seeded sublimation method, in which the growth rate is mainly governed by the temperature, the quality of the seed, the pressure and the temperature gradient inside the crucible. An easier control of the grown crystal polytype and the size of the crystal and a higher yield can be achieved by the latter method or the modified Lely method. A schematic drawing of the modified Lely crucible configuration is shown in Fig.2.1. The sublimation method has become the most mature process to date for the SiC bulk growth.

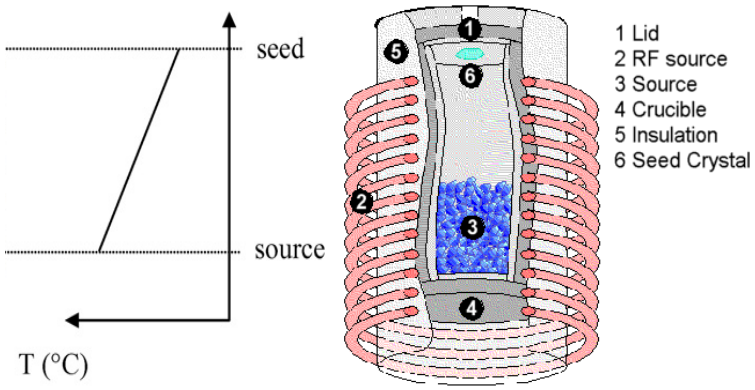


Fig.2.1 Schematic drawing of a modified Lely crucible.

The SiC powders are placed in the graphite crucible. Typically the growth temperatures could be 2500$^{o}$C for the SiC source and 2200$^{o}$C for the seed. The SiC powder sublimes at higher temperatures, transports to the seed, and crystallize the Si- and C-containing gas species at a slightly cooler single crystal seed. The ambient atmosphere is filled with Ar inside the crucible. Large dimension boules, up to 100mm both in diameter and in length, have been produced [23].

The possibility of eliminating different kinds of structural defects on small-size wafers with dislocation density near 100 $cm^{-2}$ has been reported [24]. Also the micropipe-free single crystalline ingot has been demonstrated [25]. The main advantages of the classical PVT technique are the availability of well developed standard industrial processes and lower costs for both growth machine setup and running. However, maintaining the thermal and chemical conditions for the controlled growth of a long single crystal at a high rate and without defects is a challenge. It has been very difficult to obtain high-purity boules and to accurately control the doping level by PVT technique. Although the PVT technique dominates SiC wafer production, other processes have been investigated. The other techniques include high temperature chemical vapor deposition (HTCVD) [26-27], modified-PVT (M-PVT) [28-29], and continuous feed-PVT (CF-PVT) [30-32]. To date these emerging processes are not mature; however, their potentials of improving some intrinsic limitations of PVT technique should make them more and more attractive in the future.

### 2.3.2 The CVD Epitaxial Growth for SiC Materials

Although the potentials of SiC materials have been recognized for a long time, the availability of large and high-quality monocrystalline SiC substrates is the main obstacle for realizing the full-potential device applications of SiC materials. SiC crystals grown by the modified Lely method are still not suitable for device fabrications directly, due to micropipes, dislocations, low angle grain boundaries, edge, basal plane, and screw dislocations [1,4]. These as-grown defects deteriorate the performance of SiC devices [4-6,33]. High-quality epitaxial layers grown on the commercially available SiC wafers are

required for device applications. No less importantly, most of semiconductor device designs require presence of active device region with conductivity different from that of the substrate or even multiple layers having different conductivities. Chemical vapor deposition (CVD) is the most common method for the epitaxial growth of SiC materials. The CVD epitaxial growth has advantages in the precise control and uniformity of epitaxial layer thickness and impurity doping. The reactant gases are carried by $H_2$, He, or Ar. The reactant gases and the carrying gas are fed into the reactor at a certain pressure maintained by the pressure controller and the pumping system. The substrates are heated up to the desired growth temperatures. The reactant gases diffuse to the surface of the substrate, where the chemical reactions produce Si- or C-atoms participating in the epitaxial growth and by-products. The unused gases and the by-products of the chemical reactions are pumped out of the reactor.

The understanding of thin film growths is constructed on the thermodynamic behavior of the reactants and the reaction kinetics. In gaseous CVD systems, the film

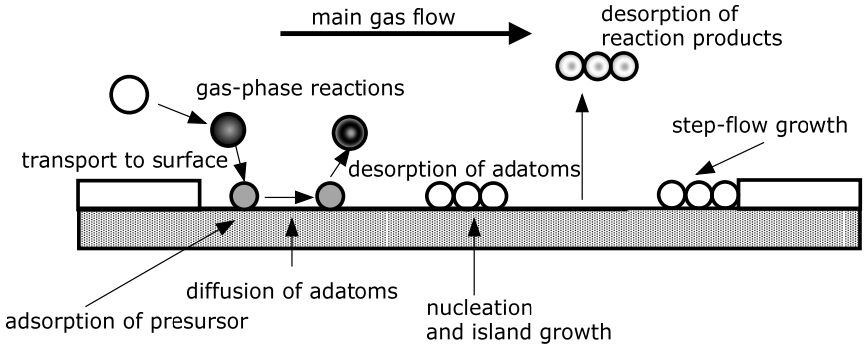


Fig.2.2: the microscopic view of the CVD process happened on a substrate

growth process consists of the main gas flow, gas phase reactions, transportation of the precursors to the surface, surface diffusion, nucleation and (undesirable) island growth and (desirable) step-flow growth, desorption of precursors, and desorption of volatile surface reaction products. Fig.2.2 shows the epitaxial growth process on the atomic level.

The gas-phase reaction products (black balls in Fig.2-2) transport to the surface. Decomposition occurs on the substrate surface. Basically the substrate is heated to a determined growth temperature, usually between 1300$^{o}$C and 1850$^{o}$C. The chemical reaction and the pyrolysis happen during this stage. The adsorbed precursor diffuse to any available atomic site and forms bonds with the surface atoms before the desorption of the precursor occurs. In some conditions, this growth scenario could lead to a 2-D nucleation or a 3-D island growth, which is undesirable. The basic aspects of a CVD process consist of the following steps:

1. The reactant gases are introduced into the reaction chamber. The products of gas-phase chemical reactions or decompositions diffuse to the wafer surface through the boundary layer, which exists between the main gas flow and the surface of the wafer.
2. The reactants are adsorbed on the substrate surface and called adatoms.
3. These adatoms migrate to proper growth sites, where chemical reactions take place and form the solid film and gaseous by-products.
4. The gaseous by-products desorb from the surface and diffuse into the main gas flow and are removed from the reactor chamber toward the exhaust.

If the diffusing precursor could reach the step of the surface and start growing from the step, this is the so-called step-flow growth, which is the desired growth mode. If not, an undesired 2D-nucleation or an island growth could be initialized. The reaction by-products will be pumped out of the reactor along with the remnant main gas flow. The following sections will briefly describe the mechanisms of the CVD epitaxy.

### 2.3.3 Thermodynamics of CVD

In thermodynamics, the Gibb's free energy or free energy is a thermodynamic potential, which is (or can be) available to do useful work, from an isothermal and isobaric thermodynamic system. The Gibb's free energy is a state function, which is defined only in terms of state functions, enthalpy and entropy, and the state variable temperature. The definition of free energy is

$$G = H - TS \text{ or } \Delta G = \Delta H - T\Delta S \tag{2.1}$$

where $G$ is the Gibb's free energy, $H$ is the enthalpy, $S$ is the entropy, and $T$ is the absolute temperature.

From the second expression of Eq.(2.1), $\Delta G = \Delta H - T\Delta S$,

1) if $\Delta G < 0$, the chemical process favors the forward reaction (spontaneous reaction), no external energy is needed for the chemical reaction;

2) if $\Delta G = 0$, neither the forward nor the reverse reaction prevails (in equilibrium);

3) if $\Delta G > 0$, external energy is needed for the forward reaction.

For a chemical reaction, if the conditions of a system, which was initially at equilibrium, are changed, the equilibrium will shift in such a way as to restore the original conditions, which is called Le Chatelier's principle. The quantitative description for the forward or

the reverse reaction, and reactions in equilibrium can be expressed by the Law of Mass Action [34]. The Law of Mass Action has two aspects: 1) the composition of a reaction mixture at equilibrium, 2) the rate equations for elementary reactions. A chemical reaction can be expressed as:

$$aA + bB + \ldots\ldots \leftrightarrow xX + yY + \ldots\ldots \quad (2.2)$$

where A, B, … are reactants, X, Y, … are products, and a, b, …, x, y, … are the coefficients balancing the chemical equation on both sides. The reaction rate is proportional to the product of the concentrations of the participating molecules; therefore the forward and the reverse reaction rates are proportional to

$$[\text{forward reaction rate}] \propto k_1[A]^a[B]^b\ldots \text{, and}$$

$$[\text{reverse reaction rate}] \propto k_{-1}[X]^x[Y]^y\ldots .$$

$$\text{In equilibrium, } k_1[A]^a[B]^b = k_{-1}[X]^x[Y]^y.$$

where $k_1$ and $k_{-1}$ are the forward and reverse reaction rate constants, respectively. We can use the partial pressures of the participating molecules since the reaction rate is proportional to the number of collisions; the number of collisions is proportional to the density of the reactant; the density is proportional to the pressure of the reactant or the product. We can rewrite the reaction rates as :

$$[\text{forward reaction rate}] \propto k_1P_1^aP_2^b\ldots \text{, and}$$

$$[\text{reverse reaction rate}] \propto k_{-1}P_3^xP_4^y\ldots .$$

In equilibrium, $k_1P_1^aP_2^b \ldots = k_{-1}P_3^xP_4^y \ldots$; where $P_1^a, P_2^b, P_3^x, P_4^y, \ldots$ are the partial pressures of each reactants or products. The constant of equilibrium can be defined as:

$$K(T)=\frac{k_{-1}}{k_1}=P_1^a P_2^b P_3^{-x} P_4^{-y}... \quad (2.3)$$

The equilibrium constant depends on the temperature. Therefore, the change of the partial pressure in one reactant (product) will affect the partial pressures of the others.

By the thermodynamics analysis of different gaseous precursor systems depending on the thin films deposited, the most possible gas-phase chemical reactions corresponding to the growth temperatures could be used to simulate the growth conditions. This simulation will help set up the closest growth conditions for the growth, such as the carrier gas flow rate and the precursors' gas flow rates. There may be a variety of different reactions, but different reactions would have different reaction coefficients and would play different role depending on the thermodynamics factors discussed in this section.

### 2.3.4 Gas Mass Transport in CVD

The design of the CVD epitaxial growth system has two main requirements: 1) deliver gaseous products of gas-phase reactions uniformly to the substrate and 2) optimize the flow of the gas for the maximum deposition rate. In general, two gas flow regimes exist during the gas transportation process - Molecular flow and Viscous flow.

1. Molecular flow: This is about the diffusion in gas. From the kinetic theory of gases, the diffusion coefficient D is approximately proportional to $T^{\frac{3}{2}}/P$, which indicates that a reduced pressure or a higher temperature increases D or deposition rate. Molecular flow is usually implemented in Molecular Beam Epitaxy (MBE)

growth systems. It is not used during regular CVD epitaxial growth of SiC.

2. Viscous flow: When fluid flows in a direction parallel to a boundary, the flow velocity distribution, shown in Fig.2.3, is a parabolic function of distance along the carrier gas flow direction. Low flow rates produce the laminar flow (provided the reactor geometry is optimized), which is desired. High flow rates produce the turbulent flow, which should be prevented. The desired laminar flow is shown in Fig.2.4, where δ represents the thickness of the boundary layer, within which the flow velocity varies with the distance between the location within the boundary layer and the substrate surface. The flow velocity is zero near the plate, and the layer on the plate is called a stagnant layer. The gas phase precursors diffuse to the surface of the plate (or a substrate) through the stagnant layer. Deriving a mathematical relationship to predict CVD growth rates based on the steps described in section 2.3.2 is difficult. A less complex growth-rate model called Grove's simplified CVD film-growth model has been created. This simplified model explains many phenomena observed in CVD processes and predicts many film growth rates quite accurately. The Grove's model is based on the processes that occur (1) in the gas phase (gas-phase processes) and (2) on the substrate and predicts many film growth rates quite accurately. The Grove's model is based on the processes that occur (1) in the gas phase (gas-phase processes) and (2) on the substrate surface or chamber-wall surfaces (surface processes). The Grove's model assumes that only one of the gas-phase growth steps or one of the surface processes is the rate-limiting step for the growth rate of the CVD growth [18].

Fig.2.5 depicts the essentials of Grove's model. The flux $F_1$ represents the number of atoms or molecules diffusing from the bulk of the gas to the surface of the growing film through the boundary layer. The flux $F_2$ corresponds to the consumption of the reactant gas arriving at the surface to form the solid film. The flux $F_1$ is approximately proportional to the concentration difference between the reactant in the bulk of the gas $C_g$ and that at the surface of the substrate, $C_s$. The flux $F_2$ is assumed to be linearly proportional to the surface concentration of the reactant.

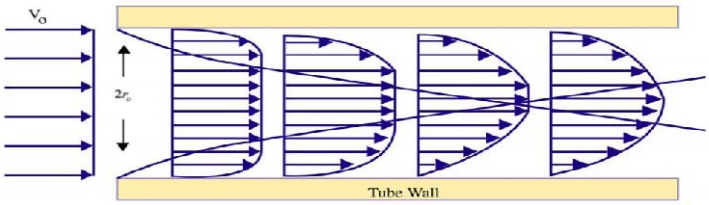


Fig.2.3: Gas flow velocity distribution inside a tube wall.

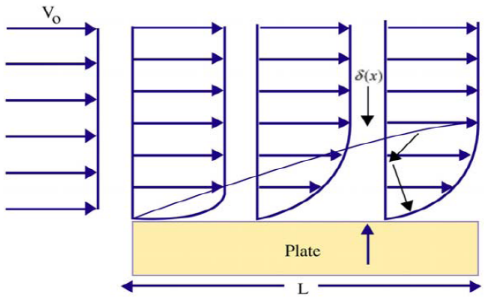


Fig.2.4: Laminar flow across a plate.

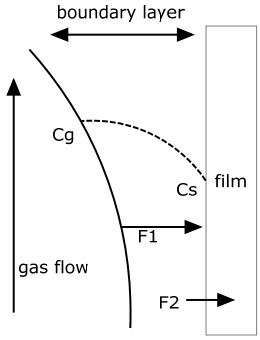


Fig.2.5: Grove's model depicting the transport and reaction fluxes $F_1$ and $F_2$.

The relationships for $F_1$ and $F_2$ are:

$$F_1 = h_g(C_g - C_s) \tag{2.4}$$

$$F_2 = k_s C_s \tag{2.5}$$

where $h_g$ is the gas-phase mass-transfer coefficient and $k_s$ is the chemical-surface-reaction-rate constant. Under steady state conditions, which mean no build-up or depletion of the material, the two fluxes must be equal: $F_1=F_2=F$. The surface concentration of reactants, $C_s$, can be expressed as

$$C_s = \frac{C_g}{1 + k_s / h_g} \tag{2.6}$$

There are two limiting cases of Eq.(2.6):

1) $h_g \gg k_s$, the value of $C_s$ approaches $C_g$. This is the surface-reaction-rate limited case. The surface-reaction-rate (film-forming processes) is slower than the mass transfer of the reactant gases. This slower process limits the growth rate of the epitaxial film.

2) $h_g \ll k_s$, the value of $C_s$ approaches zero. This is the mass-transfer-rate limited case. The surface-reaction-rate is faster than the mass transfer of the reactant gases; therefore the reactant concentration on the surface, $C_s$, is almost depleted. The growth rate of the film is limited by the mass transfer of the reactant gases.

For the estimation of the growth rate, let's assume N is the number of atoms incorporated into a volume of the film. The steady state flux, F, is in the unit of (number of atoms/area*sec). The growth rate, G, of the film can be expressed by:

$$G = \frac{F}{N} \text{ (thickness/sec)} \tag{2.7}$$

Substituting Eq. (2.5) and (2.6) into Eq.(2.7), we obtain:

$$G = \frac{k_s h_g}{k_s + h_g} \frac{C_g}{N} \tag{2.8}$$

In most of the CVD processes, the reactant gas is diluted in an inert carrier gas. The concentration of the reactant gas can be defined as $C_g = C_T Y$, where $Y$ is the mole fraction of the reaction species and $C_T$ is the total number of molecules per unit volume in the gas. Substituting $C_g = C_T Y$ into Eq.(2.8), we obtain the general expression for the film deposition or growth rate for Grove's CVD model:

$$G = \frac{k_S h_G}{k_S + h_G} * \frac{C_T}{N} Y \tag{2.9}$$

where $C_T$ is the total concentration of molecules in the gas phase, $k_S$ is the surface reaction rate (cm/sec), $h_G$ is the mass transfer coefficient (cm/sec), $N$ is the number of atoms incorporated per unit volume in the film, and $Y$ is the mole fraction of the incorporating species.

If $k_S \ll h_G$, we have a surface reaction controlled case, in which the growth rate is very sensitive to the temperature due to $k_S$. If $h_G \ll k_S$, we have a gas phase transfer or a mass transfer controlled case, in which the growth rate is not temperature sensitive. Eq.(2.9) indicates that the growth rate should be proportional to the reactant gas concentration, which is directly proportional to the flow rate. The chemical reactions at the substrate surface are often thermally activated. If this is the case, the surface-reaction-rate constant, $k_s$, can be represented by an Arrhenius type equation, which can be written as

$$k_s = k_0 e^{-E_A/kT} \tag{2.10}$$

where $k_o$ is a temperature-independent frequency factor, and $E_A$ is the activation energy of the reaction. Eq.(2.10) indicates that if the CVD growth is operating in the surface-reaction-rate-limited regime, the growth rate is very sensitive to variations in the temperature. When the growth temperature is sufficiently low, the arrival rate of the reactants exceeds the rate at which they are consumed by the surface chemical reactions, and the deposition rate becomes surface-reaction-rate-limited.

Take one of the growths in this study for example, the growth conditions are: $H_2$ = 1 slm, $SiH_4$ = 30 sccm, $CH_3Cl$ = 4 sccm, T = 1300$^o$C, and P = 150 torr. The density of SiC is 3.21 g/cm$^3$; therefore $N$ in Eq.(2,9) is 4.83x10$^{22}$ atoms/cm$^3$. The growth rate from the experiment in this particular run is about 1.6 μm/hr, which is used as $k_s$. Each SiC molecule needs one silicon atom and one carbon atom, and $CH_3Cl$ supply is less than $SiH_4$; therefore $CH_3Cl$ will limit the growth rate. The estimation is under the assumption

that $SiH_4$ and $CH_3Cl$ will completely decompose and all the Si and C atoms incorporate in the film growth. The product of $C_T$ and $Y$ will be 1.075e20 x 0.004 atoms/cm$^3$. The estimated growth rate by using this simplified model is

$$G = \frac{1.075 \times 10^{20} \times 0.004 \times 1.6}{4.83 \times 10^{22}} \cong 8.9 \ (\mu m/hr)$$

The estimated growth rate is obviously higher than the actual growth rate. The possible chemical reactions in the gas phase and the Si clustering are ignored during the calculation. Besides, in this particular case, the growth-rate-limiting factor is the Si gas-phase condensation, instead of the surface reaction. A large portion of Si species in the gas phase were not able to participate the film growth. More complicated model and mechanism will be needed for the numerical simulation. (But in general, this kind of analysis here is good).

### 2.3.5 Arrhenius Behavior of Thermally Induced Chemical Reactions

In many cases, the reaction-rate dependence of a chemical reaction can be well predicted by a relationship known as the Arrhenius equation, which can be written as:

$$R(T) = R_0 e^{(E_a/kT)} \tag{2.11}$$

where *R(T)* is the rate constant at temperature *T* (in units of Kelvin, or K), $R_0$ is the frequency factor or the pre-exponential factor, *k* is the Boltzmanns constant (8.6e-5 eV/K), and $E_a$ is the activation energy (in units of eV). If a reaction rate depends on temperature, it is necessary to check if it also obeys the Arrhenius relationship. If the reaction rate does follow the Arrhenius relationship, we could extract the values of $R_0$ and

$E_a$ from the reaction-rate data. We can rewrite Eq.(2.11) in a logarithmic form to facilitate the computation of $R_0$ and $E_a$. Eq.(2.11) can be expressed as

$$\ln R(T) - \ln R_0 = \frac{E_a}{k} \times \frac{1}{T} \tag{2.12}$$

The activation energy $E_a$ can be extracted from the slope, $E_a/k$, of this dependence. If the experimental data does not follow this trend, a more complex reaction is involved than that described by the Arrhenius equation.

By using the content mentioned above, many SiC epitaxial growth models were proposed depending on the process gas, the growth temperature and pressure, the geometry of the reactor, and the carrier gas, etc [35-40]. For the traditional $SiH_4$-$C_3H_8$-$H_2$ system at regular growth temperatures, more than 81 gas-phase chemical reactions (including $SiH_4$ and $C_3H_8$ with $H_2$) could be included in the models. Table 2-2 [40] only lists some of the reactions for $SiH_4$ and $C_3H_8$ for example. Si- and C-containing species obtained from the thermal decomposition of the gases diffuse to the surface of the substrate, where the surface reactions occur. Table 2-3 lists few of the surface reactions. The rate constants in the tables are written in the Arrhenius form, $k = AT^n e^{-E_a/RT}$ where the unit of $A$ depends on the reaction, containing moles, cubic centimeters, seconds, and kelvins. In Table 2-3, S and B in the parenthesis denote the surface and bulk species, respectively. The molecules in the topmost surface layer are referred to as surface species, which become bulk species later. The reactions with very small reaction rates ($k$) are discarded in those models.

| Table 2-2 Gas-phase reaction | *A* | *n* | $E_a$*(cal/mole)* |
|---|---|---|---|
| $SiH_4 \leftrightarrow SiH_2+H_2$ | $6.671*10^{29}$ | -4.795 | 63450 |
| $SiH_4 \leftrightarrow SiH_3+H$ | $3.690*10^{15}$ | 0 | 93000 |
| $SiH_2 \leftrightarrow Si+H_2$ | $1.06*10^{14}$ | -0.88 | 45000 |
| $C_3H_8 \leftrightarrow CH_3+C_2H_5$ | $1.698*10^{16}$ | 0 | 84840 |
| $CH_3+C_3H_8 \leftrightarrow CH_4+iC_3H_7$ | $1.097*10^{15}$ | 0 | 25140 |
| $CH+C_2H_2 \leftrightarrow C_3H_2+H$ | $1.0*10^{14}$ | 0 | 0 |

| Table 2-3 Surface reaction | *A* | *n* | $E_a$*(cal/mole)* |
|---|---|---|---|
| $H+Si(S) \rightarrow HSi(S)+Si(B)$ | $2.18*10^{12}$ | 0.5 | 0 |
| $H+C(S) \rightarrow HC(S)+C(B)$ | $2.18*10^{12}$ | 0.5 | 0 |
| $2HSi(S)+2Si(B) \rightarrow 2Si(S)+H_2$ | $7.230*10^{24}$ | 0 | 61000 |
| $2HC(S)+2C(B) \rightarrow 2C(S)+H_2$ | $7.230*10^{24}$ | 0 | 61000 |
| $Si_2H_2+2C(S) \rightarrow 2C(B)+2SiH(S)$ | $4.07*10^{20}$ | 0.5 | 0 |
| $H_2CCCH+3Si(S) \rightarrow$ | $4.58*10^{29}$ | 0.5 | 0 |

## 2.4 CVD Epitaxial Growths for SiC Materials

### 2.4.1 The Conventional CVD System for SiC Epitaxial Growths

$SiH_4$-$C_3H_8$-$H_2$ gas system is the most common CVD epitaxial growth system used for the fabrication of 4H- and 6H-SiC epitaxial layers needed for high-power and high-frequency devices (i.e., silane and propane serve as the growth precursors supplying Si and C growth species, respectively) [41-42]. This traditional system requires high growth temperatures (in excess of 1500$^o$C) for achieving device-quality homoepitaxial layers of SiC, by ensuring the favorable step-flow growth. The growth temperatures usually are in the range between 1500$^o$C and 1700$^o$C [43-45]. If the growth temperature is below a critical value, morphology degradation and crystalline quality deterioration occur, such as

3C-SiC inclusion, 2-D nucleation, and step-bunching, etc [46,48]. Besides the growth temperature, the pressure, the input Si/C ratio (effective Si/C ratio), off-axis angle of the substrate, the defect density and wafer polishing damages of the substrates, the surface polarity of the SiC substrate (Si-face or C-face), and other epitaxial growth process conditions all contribute to the surface morphology and the crystalline quality of the grown epitaxial layer [43,45,49-51]. The following paragraphs will describe these variables further.

### 2.4.2 Off-Axis Angle Substrates and Step-flow Growth

The most influential breakthrough of SiC epitaxial growth is probably the application of vicinal or off-axis substrates [52-56]. The off-axis substrates provide shorter terrace widths on the steps, where the adatoms (Si- or C-atoms) can more easily migrate to the proper growth sites before desorption of the ad-species or the undesired 2-D nucleation take place. Figs. 2.6(a)(b) show the lateral views of an on-axis and an off-axis substrates, respectively. The off-axis cut substrate provides more and shorter steps. The adatoms have enough time to migrate to the edge of the step and implement the step-flow growth. The diffusion lengths of the ad-species on the SiC substrate decreased with the reduction of the growth temperature [48]. If the diffusion length is longer than the terrace width, the adatoms can reach the proper growth sites (the terrace step edge shown in Fig.2.2) and duplicate the identical crystal structure of the substrate. The application of off-axis surface orientation enables the step-flow epitaxial growth at much lower temperatures since the shorter migration path compensates for the lower diffusion length

Fig.2.6(a): a regular on-axis cut substrate

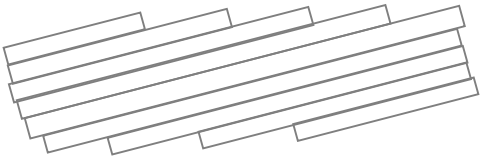

Fig.2.6(b): an off-axis cut substrate

of the adatom at such temperatures. If the adatoms are not able to reach the proper growth sites before they desorb from the steps or incorporate into the substrate, the reduction of growth rate or 2-D island nucleation will take place, respectively.

### 2.4.3 The Influences of Si/C Ratio

During the CVD process, the chemical reactions also take place in the gas phase. Some of the gas-phase reactions classified as the homogeneous-nucleation reactions are undesirable. The gas phase nucleation forms clusters in the gas phase. These clusters can rain down on the growing film and cause defects in the film. In addition, the homogeneous reactions deplete the reactants and thus cause the reduction of deposition rate and increase the non-homogeneity of the growth rate over the substrate along the gas flow direction. The desirable growth mechanism is the heterogeneous reaction, in which the chemical reactions take place at the surface of the growing film. In SiC growth, the homogeneous-nucleation of silicon in the gas-phase will alter the actual (or effective) Si/C ratio near the growing film due to the depletion of the Si related precursors.

The Si/C ratio is a very important process parameter for CVD epitaxial growth techniques. The Si/C ratio is used to control the dopant incorporation [57-60] and to

influence the surface morphology of the grown epitaxial layers [58-59]. The doping control technique based on adjusting the Si/C ratio within the growth reactor to effectively control the amount of dopant incorporated into substitutional SiC crystal lattice sites is called site-competition epitaxy [60]. The site-competition epitaxy technique enables much wider range of doping and more precise doping control than what was previously possible. The principle of the site-competition is based on the competition between nitrogen and carbon for the C sites and between aluminum and silicon for the Si sites of the growing SiC epilayer [60]. By increasing the C-source concentration, the n-type dopant (nitrogen) concentration in a growing SiC epilayer will decrease because C atoms outcompete N atoms for the C sites. Analogously, increasing the Si-source concentration will decrease the p-type dopant (aluminum) concentration in a growing SiC epilayer because Si atoms outcompete Al atoms for the Si sites. Site-competition has been investigated as a mean of control of nitrogen (N), phosphorus (P), aluminum (Al) and boron (B) dopants incorporation during the CVD epitaxial growth of SiC on Si- and C-face epilayers [57,61-62]. Use of site-competition technique has resulted in improved device performance which includes the first multi-kilovolt rectifiers [63], ohmic contacts [64], and high-temperature JFETs [65].

Finally, the value of the effective Si/C ratio is often critical for achieving good crystal quality of the epitaxial layer and avoiding surface morphology degradation. Since proper control of the effective Si/C ratio involves more than providing certain flows of the silicon and carbon precursors (i.e., input Si/C ratio), this issue deserves special attention in developing new epitaxial growth processes. It will be demonstrated in this

work that understanding the factors influencing the effective Si/C ratio was critical in developing the novel low-temperature halo-carbon epitaxial growth process.

### 2.4.4 Step Bunching In Step-Controlled Epitaxy

The step bunching problem in step-controlled epitaxy for different SiC polytypes is an on-going issue for the researchers. Step bunching is the formation of multiple Si-C bilayers at steps. Each bunched step may contain different numbers (more than one) of Si-C bilayers [66]. The step bunching phenomenon is more pronounced on the Si-face than on the C-face SiC substrates for both 6H- and 4H-SiC. The macrosteps normally have a terrace width of 220 – 280 nm and a step height of 3 – 6 nm for 6H-SiC and a terrace width of 110 – 160 nm and a step height of 10 – 15 nm for 4H-SiC, respectively [67]. This wavy structure often appears on grown surfaces with off-orientation from a low-index plane [68-69]. Several models for the step bunching mechanism have been proposed [68,70-74]. Tsunenobu Kimoto *et al.* revealed that the dominating numbers of Si-C bilayer height are three or six for 6H-SiC and two or four for 4H-SiC [67]. They introduced a model, which suggested that surface energies are different for each Si-C bilayer plane, owing to the peculiar stacking sequence [75], based on the report of Chien *et al* [76]. The lower the surface energy is, the higher probability the adatoms incorporate on the plane. This model leads to an explanation of the formation of three or six Si-C bilayer height at the steps for 6H-SiC and of two or four bilayer height for 4H-SiC. The surface energy on the Si-face is higher than that on the C-face for both 6H- and 4H-SiC [46], and single Si-C bilayer-height steps are dominant on C-faces for both 6H- and 4H-SiC polytypes. This may be one reason why epilayers grown on C-face exhibit a flatter

surface and much less or even no step bunching. The influence of the growth temperature on step bunching remains unclear today. It will be demonstrated in this work that use of lower growth temperatures has a potential of alleviating this problem.

### 2.4.5 The Effects of the Substrate's Quality on the Epitaxial Growth

The morphology of the grown epitaxial layers is sensitive to substrate defects and polishing damage, especially on the Si-face of 4H-SiC substrate [7]. Triangular pits, on which most often 3C-SiC nucleation occurs, and macrosteps are formed at the substrate defect sites [77]. Fig.2.7 and 2.8, which are the micrographs of our halo-carbon epitaxial growth at 1300$^{o}$C, show the triangular pits grown on the 4H-SiC substrates. The triangular pits were grown along the scratches (Fig.2.7) or possibly originated from the defect sites on the substrate (Fig.2.8). Such defects can be suppressed by improving the

Fig.2.7: Triangular pits were grown on the 4H-SiC substrate along the polish scratches.

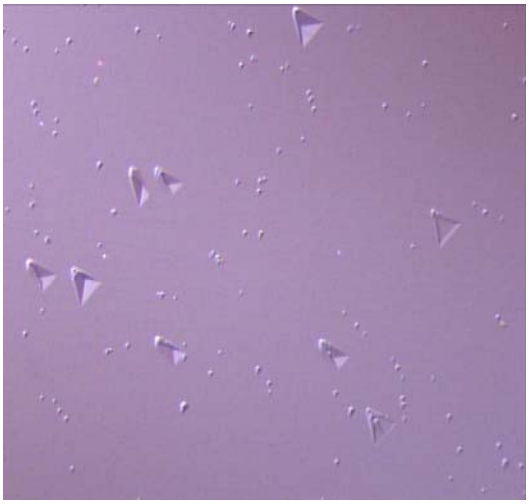

Fig.2.8: Triangular pits originated probably from the defect sites on the as grown 4H-SiC substrate.

surface perfection and CVD processes [10]. The commercially available 4H- and 6H-SiC wafers with chemical mechanical polishing (CMP) surface process demonstrated better substrate surfaces for subsequent epitaxial growth as determined by the surface morphology and roughness of the grown epitaxial layers [78].

The lattice defects in the substrate, like dislocations or micropipes, will induce the morphological degradation of the subsequently grown epitaxial layer. Screw dislocations originated in commercial 4H- and 6H-SiC wafers can propagate parallel to the crystallographic c-axis through the entire homoepilayers grown by CVD. Screw dislocations with large Burgers vectors are referred to as micropipes. The micropipes are tubular voids that will extend along the crystal c-axis (the <0001> growth direction) through the entire epitaxial layer [79]. Micropipe is a major device killer among all types of crystal defects in SiC wafers, while screw dislocation, edge dislocation, low-angle grain boundary, and stacking fault may also influence device characteristics [80-81]. The performance of High-field SiC devices suffers from the existence of the micropipes [82-84]. For SiC diodes, the reverse breakdown voltage is significantly reduced by the presence of micropipes [85-86]. With the improvement of the sublimation SiC bulk growth technique, 4-inch (100mm) micropipe-free n-type 4H-SiC is available now. This can significantly improve device yields and expand the range of products using SiC substrates.

### 2.4.6 Gas-Phase Nucleation of Si In CVD Epitaxial Growths

As mentioned in section 2.4.3, the homogeneous gas-phase nucleation of Si may alter the actual (effective) Si/C ratio at the vicinity of the growing film surface and

depletes the Si source. The thermal decomposition of $SiH_4$ can result in aerosol particle formation under certain conditions [87-88]. The formation of Si clusters in the gas phase negatively impacts the SiC CVD epitaxial growth, in terms of the growth rate, the impurity doping control, and the surface morphology of the epitaxial layer. By now, the thermal decomposition of $SiH_4$ has been investigated through a wide range of temperature from 600K to 2000K [89-102]. Silane pyrolysis is a complex process including numerous homogeneous and heterogeneous steps. The heterogeneous stages prevail at pressures less than 1 kPa, and the solid depositions form on the reactor walls and on the substrates [103-105]. At higher pressures (> 1 kPa), it is believed that the primary monosilane decomposition occurs as a homogeneous reaction [87,106-107]. The growth conditions of our epitaxial layers fall in this range; therefore, the gas-phase decomposition reactions dominate during the 4H-SiC epitaxial growths. The main process of the decomposition of monosilane pyrolysis in the early stage includes the following reactions [108-109]:

$$SiH_4 \rightleftharpoons SiH_2 + H_2$$

$$SiH_2 + SiH_4 \rightleftharpoons Si_2H_6$$

$$SiH_2 + Si_2H_6 \rightleftharpoons Si_3H_8$$

$$SiH_2 + Si_3H_6 \rightleftharpoons Si_4H_{10} \qquad (2.13)$$

In the above reactions, silylene ($SiH_2$) initiates the consecutive reactions to form disilane ($Si_2H_6$), trisilane ($Si_3H_8$), and tetrasilane ($Si_4H_{10}$), etc. It was generally believed that the formation of $SiH_2$, which forms the higher silanes, initializes the subsequent polymerization and gas phase nucleation from the higher silanes [100,108-109]. Recently,

numerical process simulation models indicated that the most influential gas-phase products due to the decomposition of $SiH_4$ during SiC epitaxial growth are Si and $SiH_2$ [110-112], and mainly Si droplets in SiC CVD [113].

There is a certain critical concentration of $SiH_4$, above which the aerosol formation occurs under certain conditions. The investigations of aerosol formation indicated that the critical concentration of silane is inversely proportional to temperature [87,109,114-119]. Use of different carrier gasses also strongly influences the critical concentration of silane. Homogeneous nucleation in inert gases began at relatively lower temperatures. The aerosol formation was observed only at much higher temperatures in the experiments with mixtures of silane and hydrogen. It was suggested that the excessive hydrogen favors reverse reactions with silylene, such as $SiH_2 + H_2 \rightarrow SiH_4$, and reduces the concentration of aerosol particle precursors.

The mechanism of aerosol formation is still not conclusive. The formation of particles could be from Si and $Si_2$ [93-94,119], $(SiH_m)_n$ particles [120], silicon hydride clusters [121], or $Si_nH_{2n+2}$, $Si_nH_{2n}$, $Si_2H_2$, and $Si_n$ clusters [106]. It is believed that the initial stage of aerosol formation is the formation of $Si_mH_n$ clusters [109].

A. Ellison et al suggested the formation of Si-$Si_xC_{1-x}$ in the Si clusters [122]. A study of 4H-SiC epitaxial growth by CVD conducted by Yuuki Ishida et al showed that clusters in the gas phase may consist of not only Si droplets but also SiC particles [123].

Recently, chlorinated precursors or (and) HCl additive are being reconsidered in applications of SiC epitaxial CVD growth. Especially by adding HCl during CVD epitaxial growth at regular growth temperatures, the homogeneous nucleation of $SiH_4$ can

be effectively reduced and the epilayer growth rate and the epilayer quality can be improved. However, not much is known about the effects of adding HCl during low-temperature SiC epitaxial growth. The next section will discuss in more details the role of HCl during the epitaxial growth of SiC.

### 2.4.7 The Reduction of Homogeneous Nucleation for SiC CVD Epitaxial Growths

One of the main problems for $SiH_4$-based high-temperature CVD (HTCVD) SiC epitaxial growth systems is the silicon clusters in the gas phase [122]. The formation of solid/liquid particulates in the gas phase causes the depletion of the gas phase precursors available for deposition [123,124-125]. Recently, epitaxial growths at regular temperatures also revealed the Si clustering problem in the gas phase [124-125,110-112]. The gas-phase nucleation of silicon at regular growth temperatures could deplete the Si precursors supplied to the growth surface, reduce the growth rate, and alter the effective Si/C ratio near the growth surface. To conquer these problems, halide CVD has been under intensive investigations around the world. Either halide Si-precursors or halide C-precursors were suggested to replace the traditional $SiH_4$ or $C_3H_8$ precursors. The other alternative is to add HCl during the epitaxial growth.

The use of chlorinated precursors or simply the HCl addition was developed approximately simultaneously with this work on the halo-carbon precursor as applied to lower-temperature growth. The purpose was to reduce the degree of the silicon droplets formation in the gas phase and to improve the growth rate and quality of the epilayers [113,119,126-138]. A more traditional approach without using chlorinated precursors to overcome the gas-phase nucleation is to lower the total pressure in the reactor and/or to

increase the carrier gas flow; therefore, the faster gas flow can transport the aggregates out of the susceptor, but the growth rate can be reduced [137,139-140]. The chloride-based epitaxy is based on the idea that the chemical binding between Si and Cl atoms is stronger than that between Si atoms in clusters. The presence of species that more strongly bind to silicon can dissolve the silicon clusters. Table 2-4 lists the average bond enthalpies at 25$^{o}$C for the halogen-containing molecules, which are appropriate candidates for this purpose [113,141]. Bromine and iodine atoms are too large and have relatively weak bonds to Si, and fluorine has too strong bond of a bond to Si. Such a strong bond is hard to break (needs more energy or higher temperatures). The etching effect may dominate over the epitaxial growth under regular growth conditions. Therefore, the best choice appears to be chlorine.

Table 2-4: The comparison of average bond enthalpies between silicon and halogen

| species | Si-Si | Si-F | Si-Cl | Si-Br | Si-I |
|---|---|---|---|---|---|
| bond enthalpy (kJ/mole) | 226 | 597 | 400 | 330 | 234 |

Chlorinated precursors that were used in the CVD reactor include HCl [136-137,142-143], $SiH_xCl_y$ [144-146], $CH_xCl_y$ [124], or $SiC_xH_yCl_z$ [113]. The growth rate exceeding 110 μm/h has been reported [142]. The homologs, which mean any compound in the series of $SiH_4$, $SiH_3Cl$, $SiH_2Cl_2$, $SiHCl_3$, and $SiCl_4$, containing the most hydrogen often produce more silicon particulate due to homogeneous nucleation [119].

The Cl/Si ratio for chloride-based SiC epitaxial growth is an important process parameter. The input Cl/Si ratio must be optimized for the given growth temperatures for a balance between growth and etching.

The addition of HCl during epitaxial growth can substantially promote the growth rate and also decrease the defects present in the epitaxial layers [133]. From the report of L. Calcagno et al., the large band between 2100 and 2700 meV, which is related to the formation of stacking faults in the epitaxial layers, of the room-temperature photoluminescence spectra decreased to zero with the Cl/Si ratio greater than 0.5 [133]. The leakage current of the diodes manufactured on these epitaxial layers grown with HCl reduced one to two orders of magnitude.

For the on-axis 6H-SiC epitaxial growth, the extra advantage of HCl is to prevent the formation of 3C-SiC polytype by preferentially etching 3C-SiC islands that form on the surface [131].

Another advantage of using HCl is that the most abundant species of halide chemical vapor deposition during the growth is $SiCl_2$, which has a higher sticking coefficient and surface mobility to improve the growth rate and quality of the grown epitaxial layer [113,126,134].

The main goal of this dissertation was to replace the traditional C-containing precursor, $C_3H_8$, with the halo-carbon precursor chloromethane ($CH_3Cl$). By using $CH_3Cl$, the different thermal decomposition mechanisms of this precursor and its influence on gas phase and surface reactions enabled the 4H-SiC epitaxial growth at temperatures around 1300$^{o}$C, which are significantly lower than the traditional growth temperatures

that are above 1500-1600$^0$C [124-125]. New knowledge about the properties of gas-phase clusters and their influence on epitaxial growth at low temperatures was obtained. Understanding of the HCl effect on the homogeneous nucleation was significantly enhanced by investigating the HCl addition during low-temperature epitaxial growth.

# CHAPTER 3

# EQUIPMENTS AND EXPERIMENTAL METHODS

## 3.1 **The CVD Reactor System**

The CVD system for our epitaxial growth consists of five major subsystems: the gas supply and control system, the pumping system, the pressure control, the CVD chamber, and the heating system. The carrier gas and the process gases are listed in Table 3-1. $H_2$ was used as a carrier gas and purified by Palladium (Pd) membranes. The Palladium membrane is typically a metallic tube comprising a palladium and silver alloy material processing the unique property of allowing only monatomic hydrogen to pass through its crystal lattice when it is heated above 300$^{o}$C. The hydrogen gas molecule, coming into contact with the Pd membrane surface, dissociates into monatomic hydrogen and passes through the membrane. On the other surface of Pd membrane, the monatomic hydrogen is recombined into hydrogen molecular hydrogen – the ultrapure hydrogen used in semiconductor process. The silane ($SiH_4$) gas cylinders in our lab contain 3% (diluted in $H_2$) or pure $SiH_4$. Both of them were used alternatively as the Si-containing source gas for the 4H-SiC epitaxial growth. Propane ($C_3H_8$) was used as the traditional C-containing source for the epitaxial growth. Chloromethane ($CH_3Cl$) was the alternative chlorinated carbon precursor for this study. Hydrogen chloride (HCl) was also used to study effect of additional chlorine in the growth chamber on the Si-cluster etching in the gas phase. The gas flow rates were controlled by mass flow controllers (MFCs). The pumping system

Table 3-1: Gas Supply System

| | |
|---|---|
| Hydrogen ($H_2$) | purified by $H_2$ purifier |
| Silane ($SiH_4$) | 3% diluted in $H_2$ and 100% |
| Propane ($C_3H_8$) | 3% diluted in $H_2$ |
| Nitrogen ($N_2$) | Used for $N_2$ doping |
| Trimethylaluminium (TMA) | Used for Al doping |
| Chloromethane ($CH_3Cl$) | 100% |
| Hydrogen Chloride (HCl) | 100% |

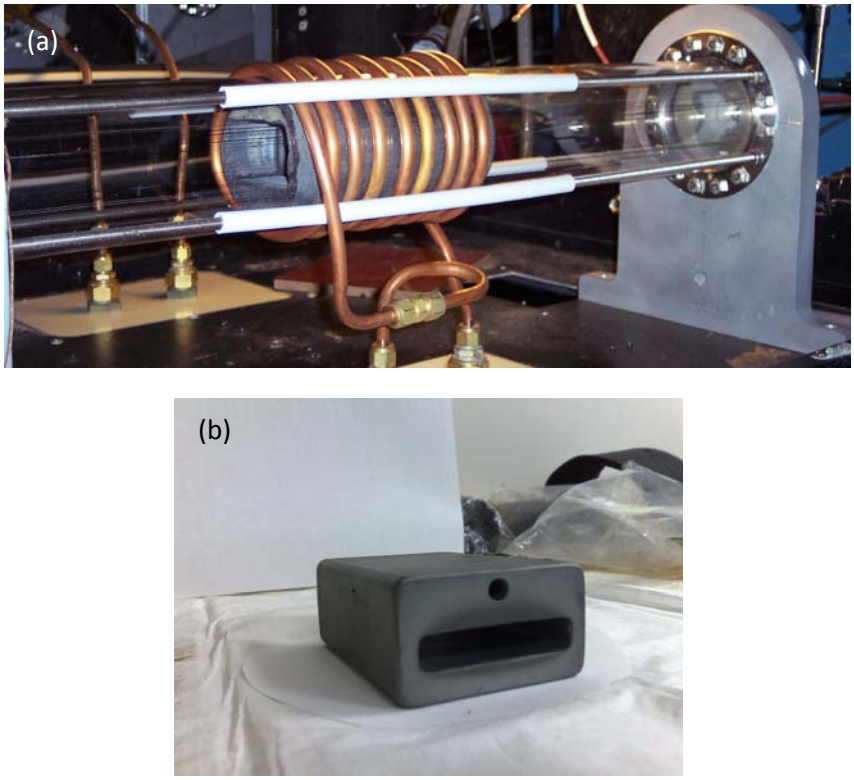


Fig.3.1: The hot-wall CVD reactor for the 4H-SiC epitaxial growth (a). The graphite insulation foam was positioned in the middle of the quartz tube wrapped with the inductance coil, which was used to heat the susceptor. The SiC coated graphite susceptor (b).

consisted of a dry pump and a booster pump. Along with the pressure controller, the pumping system maintained a certain pressure for each epitaxial growth runs. The CVD reactor consists of a 720mm long quartz tube with the diameter of 100 mm. An RF coil is wrapped around the center of the tube to heat a graphite susceptor, which served as a heating element to provide the targeted growth temperature. The susceptor was SiC-coated to prevent out diffusion of impurities from the susceptor at elevated temperatures. Fig.3.1 shows the CVD reactor (a), and the susceptor (b).

The SiC substrates were cleaned by acetone and isopropanol using a supersonic bath tub before they were loaded into the CVD reactor. The typical size of the substrates was 8x10 $mm^2$. Occasionally, growth on full 2-inch diameter substrate was also conducted.

## 3.2 **Nomarski Differential Interference Contrast Microscope (NDIC)**

Nomarski differential interference contrast microscope (NDIC) is a very common technique to examine the surface morphology of SiC epitaxial layers. In NDIC, a polarized light is used to improve the contrast of the surface image. The incident light is polarized and separated into two beams with $90^o$ phase difference with each other, the sampling and reference rays. The two rays are focused by a condenser and pass through two adjacent points in the sample, around 0.2 μm apart. The sample is illuminated by two coherent light sources with $90^o$ phase difference. These two coherent light sources are not aligned and are lying slightly offset with respect to each other. The rays travel through two different and adjacent areas of the sample. They will experience two different optical path lengths where the areas differ in refractive index or thickness. This causes a phase

change in one ray relative to the other. When they recombine, interference between them gives an amplitude contrast image. Usually, the system allows for appropriate phase adjustment for optimum contrast. The edge of a raised portion can appear bright against a dark background or dark against a light background. NDIC is more sensitive to gradual topographical sample changes and is able to detect step heights as small as 3 nm, making this technique suitable for planar and etch pit studies.

## 3.3 **Capacitance-Voltage Measurement**

The Capacitance-Voltage (C-V) measurement is used to evaluate the impurity doping concentration in the epitaxial layer. The C-V technique relies on the fact that the width of the reverse-biased space-charge region (scr) of a metal-semiconductor junction depends on the applied voltage [147]. The C-V technique uses the width of the scr region for the extraction of the characterization depth. The change of the capacitance with the applied bias is used to determine the doping concentration at the particular depth.

For the doping profiling of our grown epitaxial layers, a mercury probe was used to make a Schottky contact to the epilayer surface. A small AC voltage (30 mV) was superimposed on the applied dc bias. The capacitance for a Schottky diode can be represented by Eq.(3.1) assuming that the impurity doping concentration does not vary over the increased depletion width induced by the AC voltage.

$$C = qAN_A(W)\frac{dW}{dV} \tag{3.1}$$

where $q$ is the electrical charge, $A$ is the area of the mercury contact, and $N_A$ is the doping density. The capacitance of a reversed-biased junction, when considered as a parallel plate capacitor, is

$$C = \frac{K_s \varepsilon_0 A}{W} \tag{3.2}$$

where $K_s$ is the semiconductor dielectric constant, $\varepsilon_0$ is the permittivity of free space ($8.854 \times 10^{-14}$ F/cm), $W$ is the depletion width, and $A$ is the contact area of the mercury probe. Differentiating Eq.(3.2) with respect to voltage and substituting $dW/dV$ into Eq.(3.1) gives

$$N_A(W) = \frac{2}{qK_s \varepsilon_0 A^2 d(1/C^2)/dV} \tag{3.3}$$

Then the doping density, $N_A(W)$ can be obtained from the slope $d(1/C^2)/dV$ of a $1/C^2$-$V$ curve, and the depth at which the doping density is evaluated is

$$W = \frac{K_s \varepsilon_0 A}{C} \tag{3.4}$$

## 3.4 **Fourier Transform Infrared Spectroscopy**

Fourier-transform infrared (FTIR) reflectance spectroscopy methods have been applied for the characterizations of semiconductor materials because this technique allows nondestructive measurement of the thickness of a grown thin film on a substrate. The light source at the wavelength of 632.8 nm was employed in the set-up used in this work. The implementation of FTIR measurement is based on the Michelson interferometer, which consists of a fixed and a movable mirror. A schematic representation of a Michelson interferometer is shown in Fig.3-2. The detector collects

reflectance date from the epilayer for all wavelengths used in the IR source. Normally the SiC substrate and the epilayer have substantially different doping levels. The indices of refraction will be different. The distances of the optical paths that the light travels are different for the light reflected from the air/epilayer interface and that reflected from the epilayer/substrate interface. The optical path difference will cause the phase difference between the light reflected from the movable mirror and the one from the epilayer. When the two path lengths of the split beam are equal (solid lines in Fig.3.2), the beam is nearly coherent, and the maximum signal is detected. When the movable mirror is at a distance equal to the optical path length of the IR beam in the epitaxial layer, a second coherence is detected and termed side-bursts. The distance between the center and the first side-bursts is twice the product of the epi thickness and index of the refraction of the epi film. The advantage of FTIR measurement is that this technique is extremely fast (one

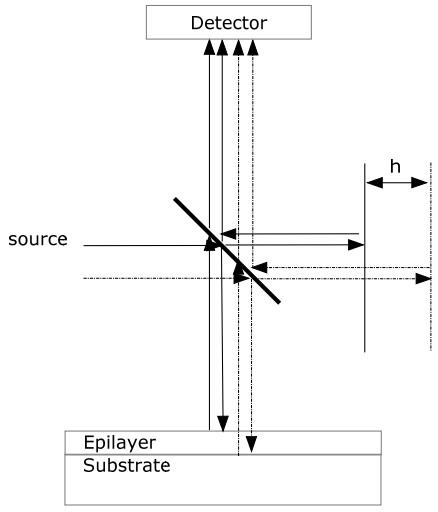


Fig.3.2: A schematic representation of a Michelson interferometer for the epilayer thickness measurement.

measurement/sec). Except the measurement of the epi thickness, FTIR technique also allows nondestructive measurement of parameters, not discussed here, such as multiple-film thickness, free-carriers concentration, index of refraction, dopant concentration in dielectrics, and alloy composition.

## 3.5 **Photoluminescence (PL) Measurement**

Photoluminescence is the optical emission caused by photon excitation (usually a laser). PL measurement allows non-destructive characterization of semiconductors. Usually, PL measurement is used to identify the type of impurities (i.e., bandgap levels). PL can provide information on many types of impurities, but only those impurities that produce radiative recombination can be detected. In our lab, an Ar+ laser was used as an excitation source. The PL spectra were detected using an SPEX 500M grating spectrometer coupled with a Hamamatsu R928 multi-alkali photo-multiplier tube (PMT). The testing samples were mounted on the cold finger of a liquid He closed-cycle cryostat, which can operate in the temperature range between 15 K and 350K.

## 3.6 **X-ray Diffraction (XRD)**

X-ray diffraction is a non-destructive technique for determining crystal structures. The X-ray source can be generated by x-ray tubes or synchrotron radiation. The incident X-ray will interact with the crystal lattice. The reflected X-ray from different lattice sites will interfere and form a diffraction pattern of the arrangement and the spacing between the lattice planes due to the periodicity of the lattice. Different crystal structures (i.e., different spacing distance between two adjacent crystal planes) create unique patterns.

The interpretation of the XRD data is based on the Bragg's Law. In the application to characterizing thin films, the reflection geometry is used for the measurement as the substrates are generally too thick for transmission geometry. Rocking curve measurement is one of the analyses using X-ray diffraction technique. A nearly perfect crystalline structure will give a narrow Gaussian curve. Any crystalline defect induced during the epitaxial growth or other sample processes will broaden the Rocking curve. Therefore, a Rocking curve measurement can be used as an indication of the film quality.

In this study, the powder-XRD technique, which is most widely used for the identification of unknown crystalline materials, was used to identify the composites of the polycrystalline islands grown in some specific growth conditions. By changing the incident angle ($\theta$) between the X-ray and the surface of the sample and recording the intensities of the diffracted beams within the angle of $2\theta$ between the incident and diffracted beams, a resulting $2\theta$ versus intensity plot is obtained. The unknown crystalline material(s) can be identified by comparing the obtained peaks and intensities to the standard reference data.

# CHAPTER 4

# 4H-SiC EPITAXIAL GROWTH BY CVD USING $CH_3Cl$ AS THE CARBON PRECURSOR

## 4.1 4H-SiC Epitaxial Growths at Regular Temperatures

As was discussed in Chapter 2, the fabrication of 4H and 6H-SiC layers for high power and high frequency devices is traditionally conducted by chemical vapor deposition epitaxial growth technique using the $SiH_4$-$C_3H_8$-$H_2$ reaction-gas system [45,148]. The growth rates in the range of several-to-tens of microns per hour are normally utilized at moderately high growth temperatures below 1700$^o$C. Higher growth rates are possible at higher temperatures [149]. However, the economics of SiC manufacturing suffers from using too high growth temperatures. Unfortunately, the surface dynamics of the epitaxial process makes it more difficult to sustain the step-flow growth conditions at low temperatures [46].

The initial work of this study used our CVD epitaxial growth system (Fig.4.1) to explore the expected advantages of the halogenated carbon precursor chloromethane ($CH_3Cl$) and to establish the process parameters that favor the step-flow growth and suppress 2D nucleation. The experiments were conducted with $CH_3Cl$ replacing the traditional propane as the carbon source during the CVD epitaxial growth. As was described in Chapter 2 chloromethane was previously utilized in the diamond growth [150] as well as in growth of heteroepitaxial 3C-SiC [130]. To the best of our knowledge,

the present study is one of the first attempts to utilize chloromethane for homoepitaxial growth of 4H- or 6H-SiC materials. The objectives of the initial part of this study were to explore anticipated differences between the $CH_3Cl$-based growth and the traditional $SiH_4$-$C_3H_8$-$H_2$ system including (1) kinetics of the precursor cracking, (2) domination of different reaction products at the growth surface, and (3) formation of Cl-containing products and their influence on gas-phase and surface reactions.

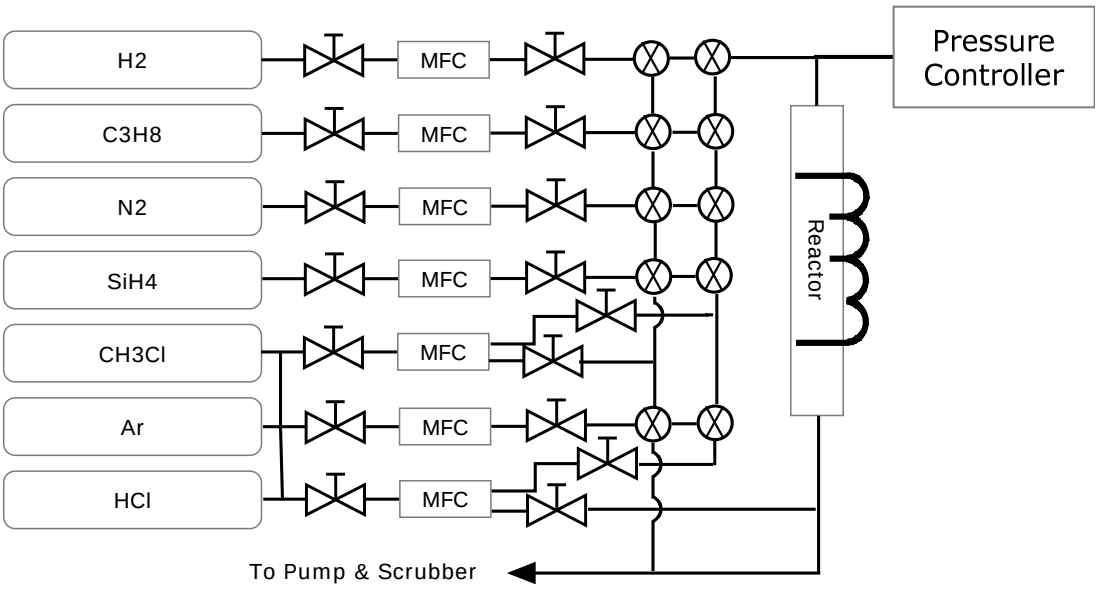


Fig.4.1: A schematics of our CVD epitaxial growth system (the TMA system is not shown in the schematic).

### 4.1.1 Experimental Approach

The optimal process parameters for the $CH_3Cl$ system were first determined at a conventional homoepitaxial growth temperature of 1600$^oC$ and pressure of 400 torr in a hot-wall CVD reactor. $H_2$ was used as the carrier gas. The process gases were $SiH_4$ (3% in $H_2$) and $CH_3Cl$ serving as the silicon source and carbon source, respectively. Growth runs using the traditional $SiH_4$-$C_3H_8$-$H_2$ gas system were conducted at similar conditions for comparison. The typical growth time was 30 minutes. Longer runs (up to 2 hours) were occasionally implemented to provide thicker epilayers for more comprehensive characterization purpose. The surface morphology of the grown epilayers was examined by Nomarski differential interference contrast microscope (NDIC). The quality of the epilayer was characterized by photoluminescence (PL) spectroscopy. The capacitance-voltage (C-V) measurement was employed to determine the doping concentration. While not always optimal for achieving the best growth rate homogeneity across the wafer surface, lower than typical carrier gas flow conditions were found to be favorable for investigating the difference between the two gas systems with respect to the chemistry of the gas phase reactions, influence of silicon droplet formation and dissociation, surface reaction mechanisms, etc. Therefore, the $H_2$ flow rates were a few times lower than what is typically used for the standard $C_3H_8$ growth.

### 4.1.2 The Surface Morphology at Regular Growth Temperatures

The surface morphology was compared in two selected growth runs with the new $CH_3Cl$ precursor (Fig. 4.2a) and the traditional $C_3H_8$ precursor (Fig.4.2b). When using $CH_3Cl$, it was possible to increase the growth rate up to about 7 μm/hr without any

detectable surface morphology degradation by increasing the $SiH_4$ flow (Fig.4.2(a)). For these particular growth conditions, the growth rate increased in the downstream direction and was higher for the downstream sample (location 2). To achieve these results, the carrier gas flow was reduced more than 25% compared to that for the optimized growth with the traditional $SiH_4$-$C_3H_8$-$H_2$ system. For the same growth conditions, the outcomes for $C_3H_8$- and $CH_3Cl$-based systems are different, and this indicates that the gas-phase kinetics is different. Therefore, the optimized growth conditions for the $CH_3Cl$-based system are different. The trend of the growth rate change in the direction parallel to the gas flow (growth rate increases from upstream to downstream) is shown in Fig.4.3. The initial results at regular growth temperatures showed that (1) the gas-phase kinetics is different for the $CH_3Cl$-based system and (2) a significant increase of $R_g$ can be achieved with the $SiH_4$-$CH_3Cl$-$H_2$ system.

The morphology of the growth with the traditional $SiH_4$-$C_3H_8$-$H_2$ system when using the same carrier gas flow but different Si/C ratio optimized for this precursor system produced a very different result, which is shown in Fig.4.2(b). The morphology degradation took place at much lower growth rates than that in $CH_3Cl$ growths. A less than perfect morphology was obtained at significantly lower growth rate than when the chloromethane was used at the same carrier gas flow, silane flow, and temperature. However, if the traditional $SiH_4$-$C_3H_8$-$H_2$ process is used in our reactor under optimized growth conditions, the growth rate for the good-morphology epilayers would normally be larger than what is shown in Fig.4.2b. When the silane flow rate was further increased

compared to the conditions used in Fig.4.2(a) during the $CH_3Cl$ growth, the achievable growth rate increased to about 10 µm/hr without morphology degradation.

While this portion of the experimental results is insufficient to make any conclusion about the growth mechanisms or relative advantages/disadvantages of the two precursor systems, obvious differences in the precursor decomposition kinetics and their influence on the epilayer morphology were demonstrated.

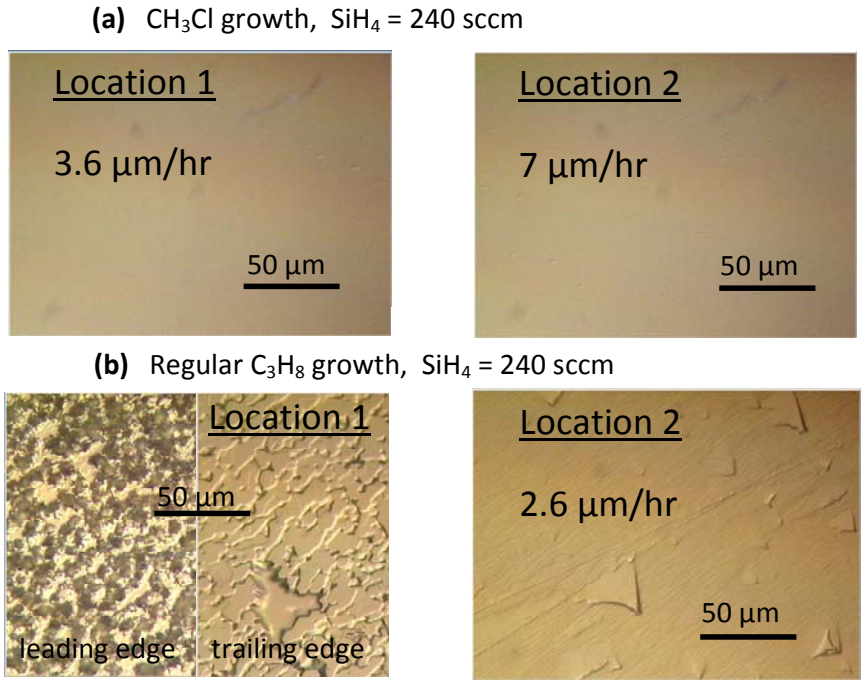


Fig.4.2: The surface morphology of epilayers grown with $SiH_4$+$CH_3Cl$ (a) compared to $SiH_4$+$C_3H_8$ growth at the same conditions (b). In each experiment, location 1 was located closer to the upstream edge of the susceptor, and location 2 was closer to the downstream edge.

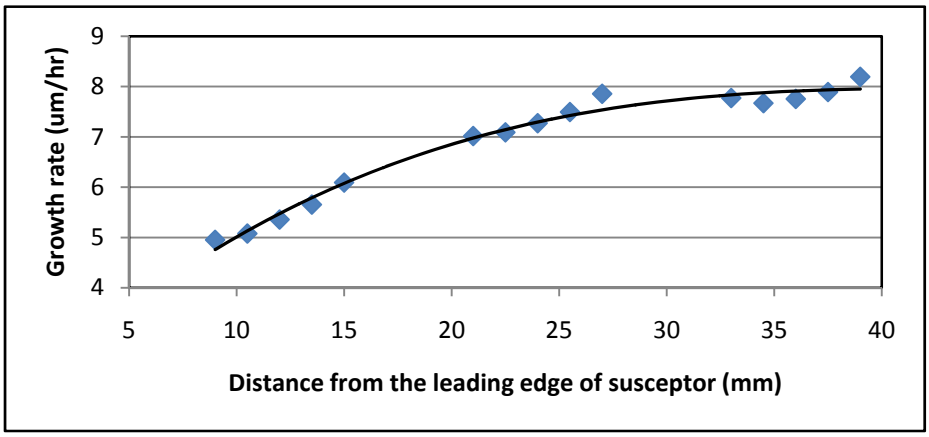


Fig.4.3: The $R_g$ increased from upstream to downstream at higher $H_2$ flow rates for the $CH_3Cl$ growth.

### 4.1.3 The Epilayer Quality

In general, it is expected that the presence of the Cl-containing products of the chloromethane decomposition may cause a favorable difference in the mechanisms for the epitaxial growth. Fig.4.4 shows the photoluminescence spectra of a 10 μm-thick epilayer grown with the $CH_3Cl$ carbon precursor. The main spectroscopic features typical for the normal-quality epitaxial layers include the $Q_0$ line due to nitrogen donor bound exciton and the Al-BE line due to aluminum acceptor bound exciton. The shape of the spectra and the absolute intensity of the PL signal are at least as good as that of the epilayers grown with the traditional $SiH_4$-$C_3H_8$-$H_2$ system at similar conditions and susceptor purity. The presence of the sharp lines due to hydrogen complex with silicon vacancy (i.e., lines $H_1$ and $H_1^{c\text{-}s}$) [151] is a normal signature of the boron-rich growth related to the degraded purity of the susceptor in our experiments.

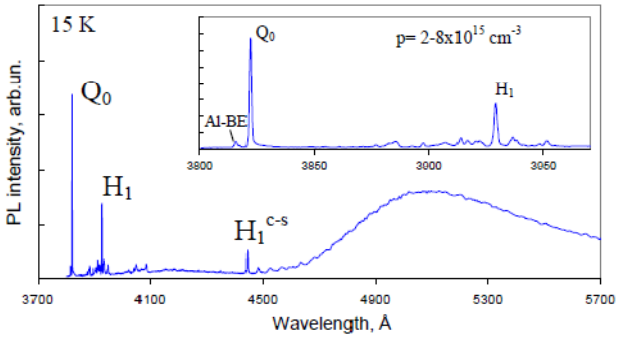


Fig.4.4: Photoluminescence spectra of a 10 µm epilayer grown with $SiH_4$-$CH_3Cl$ system. The background of Al and B acceptors is similar to the traditional $SiH_4$-$C_3H_8$ growth using the same susceptor (old). Presence of H-lines is typical for B-doped epilayers.

### 4.1.4 Growth Rate Dependence

For the given input C/Si ratio, the growth rate of $CH_3Cl$ epitaxy initially increased with increasing the $SiH_4$ flow rate until it saturated at a certain value proportional to the growth temperature. The conditions of the saturated growth rate correspond to the extremely heavy droplet cloud inside the susceptor and at the downstream portion of the reactor in particular.

When the temperature was increased from 1600°C to 1700°C, the maximum achievable growth rate almost doubled from below 10 µm/hr to more than 20 µm/hr with mirror-like surface morphology. The apparent rate of droplet formation was observed to decrease for the same growth conditions with increasing temperature. This allowed us to suggest that for a given mode of the epitaxial process, the droplet formation and

dissociation limited the growth rate of SiC, even in presence of Cl species supplied by the $CH_3Cl$ precursor.

At the low-$H_2$ flow used in this study, the growth rate dependence on $CH_3Cl$ flow exhibited a non-linear trend. The dependence of the growth rate on the $CH_3Cl$ flow for low-$H_2$ flow conditions at 1700°C is shown in Fig.4.5. At low $CH_3Cl$ flow rates, increasing the $CH_3Cl$ flow resulted in an increase of the growth rate. The growth rate maximum shifted from the downstream toward the center and upstream of the susceptor with the increase of $CH_3Cl$ flow at higher rates. At higher $CH_3Cl$ flows, further increase of the $CH_3Cl$ flow led to a reduction of the growth rate (especially at the downstream portion of the susceptor (Fig.4.5)). Simultaneously, severe morphology degradation appeared at the leading edge. A qualitatively similar but quantitatively different non-linear trend was also observed for $C_3H_8$ growths.

When the $CH_3Cl$ flow was further increased, the region of morphology

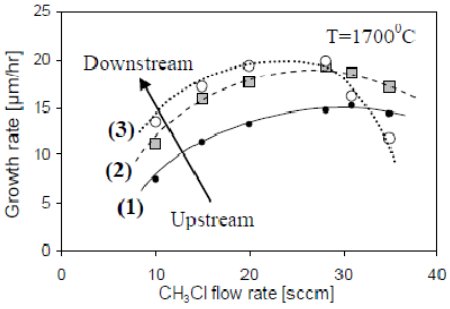


Fig.4.5: Dependence of the growth rate on the $CH_3Cl$ flow for low-$H_2$ flow conditions: (1) the upstream sample, (2) the middle of the susceptor, and (3) the downstream sample.

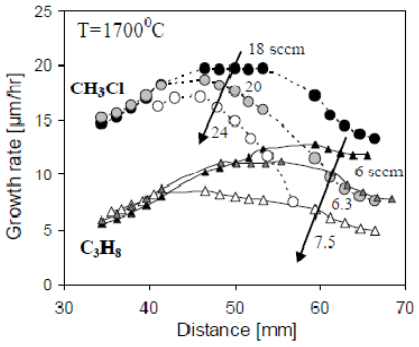


Fig.4.6: Growth rate distribution along the growth direction for $CH_3Cl$ and $C_3H_8$ growth conducted at the same $SiH_4$ and $H_2$ flow conditions. The distance is from the leading edge of the susceptor.

degradation expanded from the upstream toward the center of the susceptor, while the growth rate was continuing to decrease (especially at the downstream regions).

A strong dependence of the growth rate distribution along the growth direction on C/Si ratio (at low $H_2$ flow rates) is shown in Fig.4.6. The three growth rate distributions shown in Fig.4-6 correspond to the high-$CH_3Cl$ flow region of Fig.4.5, when the growth rate was decreasing with an increase of $CH_3Cl$ flow. A qualitatively similar trend was also observed for the $C_3H_8$ growth conducted at the same growth conditions (Fig.4.6). However, the quantitative differences were very significant. The maximum growth rate that we were able to achieve for any propane flow at the same temperature and $H_2$ flow was by a factor of two lower than that of $CH_3Cl$ growth (Fig.4.6). While the growth rate and its distribution along the growth direction also strongly depend on the C/Si ratio, the maximum growth rate at the center of the susceptor was achieved with a lower ratio of the carbon to silicon source in comparison to $CH_3Cl$ growth. Further increase of the C/Si

ratio of $C_3H_8$ growth did not cause increase of the growth rate, while resulting in morphology deterioration. At any C/Si ratio, the maximum achievable growth rate for the same temperature, carrier gas and silane flows was almost two times higher when $CH_3Cl$ precursor was used.

The pattern of the growth rate distribution along the gas flow direction and its complex dependence on the flow of carbon precursor gas were attributed to the enhanced rate of homogeneous nucleation at the leading edge of the susceptor. This resulted in (1) polycrystalline growth upstream and (2) depletion of the precursors downstream in the susceptor. The observation of a somewhat similar but quantitatively very different pattern of this trend for $C_3H_8$ growth (Fig.4.6) is an indication of the different kinetics of $CH_3Cl$ and $C_3H_8$ precursor decomposition as well as possibly different influences of the two carbon precursors on Si droplet formation and dissociation.

### 4.1.5 Changes of the Effective Si/C Ratio in the Growth Zone.

An expected trend of the doping dependence on the input C/Si ratio was observed in accordance with the site-competition mechanism [57-60]. As shown in Fig.4.7, a shift to higher values of the net donor concentration took place with decreasing the carbon source gas flow. However, a somewhat unusual outcome of the selected growth conditions is a pronounced variation of the doping along the growth direction, with the conductivity changing from low p-type (for the leading sample) to n-type (for the trailing sample). The net free carrier concentrations along the growth direction for two different $CH_3Cl$ flows are shown in Fig.4.7. The mechanism of this change is attributed to (1) a change in the effective C/Si ratio as a result of gas phase reactions and droplet

formation/dissociation as well as (2) a variation of the growth rate along the growth direction, which is different in $CH_3Cl$ and $C_3H_8$ processes. These different processes will be discussed in the following paragraphs.

Different gas-phase and surface reactions between $CH_3Cl$ and $C_3H_8$ systems resulted in very different surface morphology shown in Fig.4.2. The lower Si/C ratio in the $C_3H_8$ growth caused the polycrystalline growth on the sample located at the upstream portion of the growth zone (location 1). When the gas flow approached the middle of the growth zone, the higher temperatures dissociated the Si-clusters in the gas phase more efficiently and increased the Si/C ratio, which improved the surface morphology downstream (location 2). When we increased $C_3H_8$ flow rates, the Si species were consumed at more upstream regions and caused the decrease of the growth rate downstream (Fig.4.6). The growth was in the Si-supply-limited mode.

For $CH_3Cl$ precursor growth, the chlorinated species of the gas-phase reactions initiated the dissociation of the gas-phase Si clusters upstream before entering the growth zone. Therefore the surface morphology at the upstream portion of the growth zone improved (compared to the $C_3H_8$ growths). Also the growth rate was higher than that of $C_3H_8$ growths. When $CH_3Cl$ flow rate was increased, more Si-species was consumed upstream, and this caused the rapid decrease of the growth rate downstream. At this normal growth temperatures, large amount of Si and C species were consumed upstream and deposited on the susceptor/or carrier wafer (instead of SiC samples). From Fig.4.7, the increase of the donor concentration along the gas flow direction indicates the increase

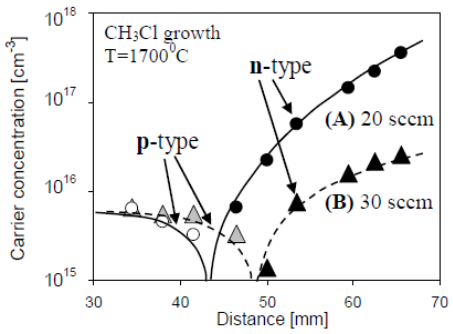


Fig.4.7: Distribution of the net free carrier concentration along the growth direction for $CH_3Cl$ growth: (A) for $CH_3Cl$ flow of 20 sccm, and (B) for $CH_3Cl$ flow of 30 sccm. From upstream to downstream, doping changes from p-type to n-type.

of Si/C ratio from upstream to downstream. The carbon species were depleted faster than silicon species upstream, probably because the Si supply (and consequently is depletion) was limited by the silicon gas-phase condensation.

No further investigation of the mechanisms responsible for the differences between the two precursor systems at the moderate-to-high growth temperatures was conducted. However, the hypothesis outlined above was used as guidance for more detailed investigation of the reaction kinetics for the more important low-temperature-growth experiments described in the subsequent sections.

### 4.1.6 Surface Morphology During the Growth on Substrates Having Different Off-axis Surface Orientations.

Experiments were conducted to explore the possibility of using the $CH_3Cl$ precursor for improving the morphology of the epitaxial growth on substrates having lower off-axis angles with the surface orientation. As was discussed in Chapter 2, 8-

degree off-axis cut substrates are traditionally used in order to implement the step-flow growth at lower temperatures. It is desirable to grow epitaxial films at lower-angle-cut substrates. However, use of lower angles requires higher $T_g$ for the step-flow growth.

At temperatures above 1600°C, the major form of the surface morphology degradation for the growth on 2° off-axis cut substrates was a pronounced step-bunching. The micrographs of the epilayers grown on different off-axis substrates with $CH_3Cl$ and $C_3H_8$ carbon precursors are shown in Fig.4.8. No significant differences in the growth morphology between the $CH_3Cl$ and $C_3H_8$ systems could be observed on the 8° off-axis cut substrates. Epitaxial layers grown on 2° off-axis substrates exhibited a similar degree of step-bunching regardless of what carbon precursor was used.

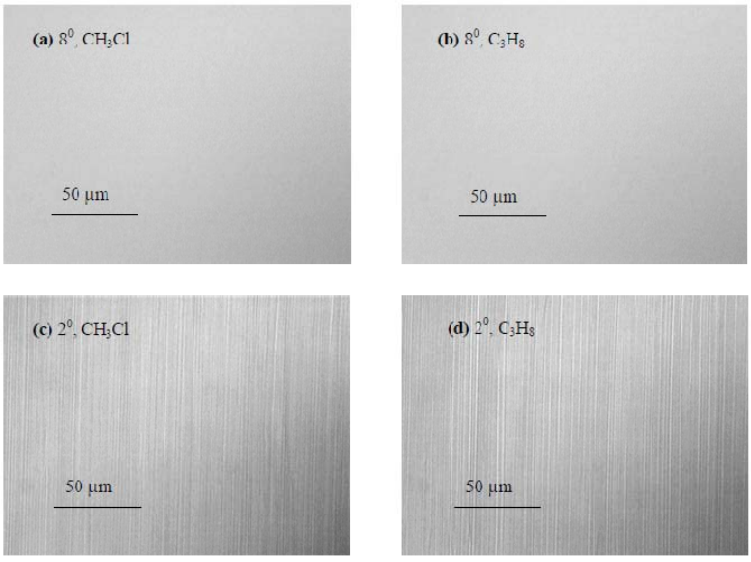


Fig.4.8: Interference contrast optical micrograph of epilayers grown on standard 8° off-axis 4H-SiC substrates (a),(b) and on 2° off-axis 4H-SiC substrates (c),(d). The $CH_3Cl$ was used for (a) and (c), and $C_3H_8$ was used for (b) and (d).

### 4.1.7 Summary

Investigation of the new $CH_3Cl$-based precursor system at traditional high growth temperatures indicated that the epitaxial growth with chloromethane appears to have significantly different gas-phase precursor decomposition kinetics and different surface reaction mechanisms. The preliminary data indicated that the maximum achievable growth rate resulting in good surface morphology is noticeably higher for the $CH_3Cl$-based growth. The maximum growth rate (for the particular growth reactor) that we were able to achieve was by a factor of two higher for the $CH_3Cl$ precursor than for the $C_3H_8$ precursor at the same temperature and flow conditions. The trend of the growth rate dependence on $CH_3Cl$ flow was different from that on $C_3H_8$ flow, and that serves as an indication of different kinetics of $CH_3Cl$ and $C_3H_8$ precursor decomposition, as well as difference in Si droplet formation and dissociation.

The initial attempt of the epitaxial growth on the low off-axis cut ($2^o$) substrates showed a severe step-bunching problem for both of the carbon precursors at regular growth temperatures.

## 4.2 Homoepitaxial Growth at Low Temperatures

From the results obtained at regular growth temperatures, the new carbon precursor, chloromethane, showed different properties promising for achieving high-quality 4H-SiC epitaxial growth at much lower temperatures than the temperatures presently used in the state-of-the-arts SiC homoepitaxial growth techniques. As was discussed in Chapter 2, investigation of the possibility to reduce the growth temperature of SiC homoepitaxy has a long history [152-153]. However, in the previous studies,

epilayers of promising quality were obtained only on 6H-SiC substrates with particular surface orientations. Recently, chlorine-containing growth precursors gained significant attention in SiC epitaxy [113,123-126,133-137]. The results of our regular-temperature growth showed the possibility of a higher growth rate with chloromethane precursor without increasing the growth temperature. The investigation of the $CH_3Cl$ growth mechanisms at low growth temperatures was conducted to answer the following questions: (1) if the use of halo-carbon growth precursor chloromethane can enable the device-quality growth at reduced temperatures, (2) the role of the Si cluster nucleation in the gas phase (which was shown to be important in the growths at regular temperatures), (3) how the condensation of the silicon vapor affects the Si/C ratio above the growth surface , and (4) the dependence of the morphology of the grown epilayers on the Si/C ratio when the growth temperature ($T_g$) is reduced.

As was discussed in Chapter 2, high $T_g$ values are used to ensure favorable surface reaction mechanisms in SiC epitaxy. Suppression of 2D nucleation at the growth surface in favor of the step-flow growth requires a high surface diffusion length ($L_D$) of the ad-species [48,55]. This can be achieved by a combination of low pressure, low precursor supersaturation, large substrate vicinal angles (i.e., small inter-step distances), and higher growth temperatures. An estimation for the onset of 2D nucleation as a function of vicinal angle and temperature was conducted by Kimoto and Matsunami [55]. Recently, Nakamura et al. re-evaluated the conditions of the onset of 2D nucleation [154]. It was suggested that the value of $L_D$ in modern SiC substrates is higher than that evaluated for the substrates used in Ref.[55], that is due to the improved surface preparation techniques

used by the modern SiC wafer industry. The improved substrate surface provides the minimum $L_D$ values required for the step-flow growth at significantly lower temperatures than previously believed. If temperature limitations on surface mechanisms are indeed relieved, the possibility to achieve the desirable step-flow growth at lower temperatures would be determined by our ability to ensure favorable Si/C ratio above the growing surface. For all the other conditions being the same, Si/C ratio can be different at lower $T_g$ values compared to conventional $T_g$ values because of different kinetics of gas-phase reactions, homogeneous nucleation, and silicon aerosol formation in the carrier gas, etc. Intuitively, halogen-containing precursors (such as $CH_3Cl$ used in this work) could alter gas-phase reaction kinetics and reduce Si aerosol formation, as well as enhance surface diffusion and promote the step-flow growth mechanism by producing different intermediate species (like $SiCl_2$).

The purpose of this study is to explore the possibility of growing high-quality SiC epilayers while operating at significantly lower temperatures with the virtues of halide precursors exhibited at regular growth temperatures. More favorable gas-phase kinetics of the new precursor system are explored to improve control of the Si/C ratio over the growing surface. Suppression of 2D nucleation by virtue of different surface reactivates and migration rates, and possible etching by Cl-containing intermediates and reaction products, was explored. The step-flow epitaxy at temperatures below 1300$^{o}$C was achieved by utilizing these combined gas-phase and surface kinetic advantages. Mechanisms limiting further increase in $R_g$ at low $T_g$ values were also investigated.

### 4.2.1 Experimental Approach

The process conditions suitable for achieving high-quality growth at significantly lower growth temperatures that was previously considered not possible were established by gradually reducing the temperature from 1600$^{o}$C down to 1290$^{o}$C in a series of runs. The growth on a 2" full wafer was conducted to examine the growth rate homogeneity at the established low-temperature growth conditions. The growth experiments for the low-temperature epitaxial growth were conducted at the pressure range between 150-400 torr. $H_2$ was used as the carrier gas. $SiH_4$ (3% in $H_2$) and $CH_3Cl$ were used as the silicon and carbon source, respectively.

### 4.2.2 Morphology Dependence on Si/C Ratio

$T_g$ was successfully lowered below 1300$^{o}$C, while adjusting other process conditions. Good epilayer morphology was obtained with the optimized Si/C ratios (Fig.4.9(b)). $R_g$ values in excess of 2 μm/hr were achieved at this temperature.

However, it was established that the process window for achieving featureless epilayer morphology without island nucleation and defect generation narrowed with decreasing growth temperature. The surface morphology for different values of the Si/C ratios at 1300$^{o}$C is shown in Fig.4.9. High $SiH_4$ flows were found to be relatively safe for the low-temperature growth. However, depending on the carrier-gas flow, an excessive Si/C ratio could result in oriented triangular defects (Fig.4.9(a)). A scanning electron micrograph of the triangular defects from Fig.4.9(a) is shown in Fig.4.10(a). Sometimes the triangular defects were accompanied by other types of defects including semi-circular regions of disturbances (Fig.4.9(a) and Fig.4.10(b)).

In all experiments, dense clouds of silicon particulates were observed inside the susceptor. It is suggested that high concentration of silicon clusters in the gas phase could create disturbances, resulting in surface defects (Fig.4.9(a) and Fig.4.10). These defects are probably caused by silicon clusters initially formed and subsequently evaporated/etched at the growth surface. Alternatively, a detrimental influence of substrate defects cannot be excluded.

Use of low Si/C ratios caused island nucleation, resulting in grainy surfaces and polycrystalline films (Fig.4.9(c)). It is not merely the high concentration of carbon-containing species but rather excess of C over Si that is responsible for the degradation shown in Fig.4.9(c).

Intermediate Si/C ratios resulted in a mirror-like morphology, with very few defects related to substrate imperfections and/or particulates produced by the hot-wall susceptor (Fig.4-9(b)). The epilayer shown in Fig.4-9(b) was grown at 2 μm/hr.

An interesting trend of morphology degradation was observed at lower Si/C ratios.

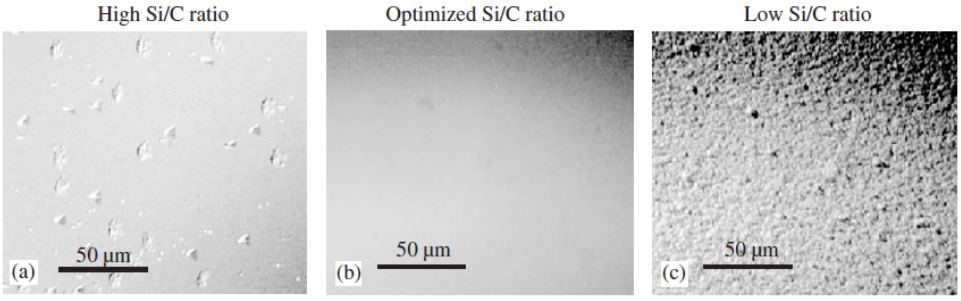


Fig.4.9: Interference contrast optical micrographs of 4H-SiC epitaxial layers grown at 1300°C, 150 Torr, and the same $H_2$ flow rate, but with different input Si/C ratios. (a) High Si/C ratio generated surface defects, and (c) low Si/C ratios resulted in island nucleation and polycrystalline growth.

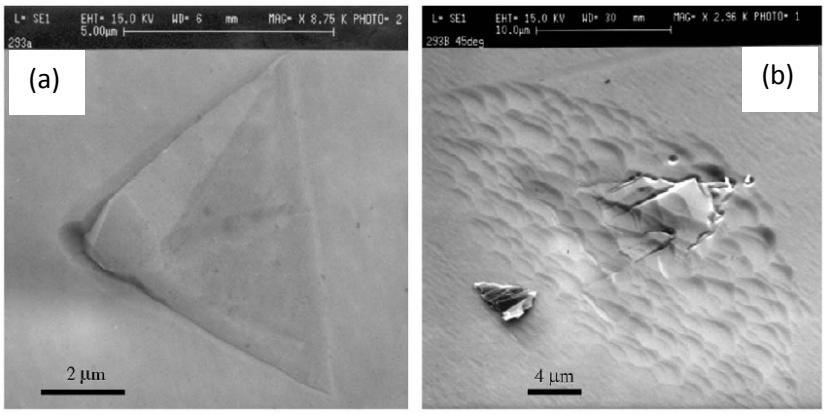


Fig.4.10: SEM images of the two types of defects from Fig.4-9(a): (a) oriented triangles and (b) semicircular areas of disturbances.

Micrographs of epilayers grown at different locations along the gas flow direction are shown in Fig.4.11. For the chosen growth conditions, the concentration of nucleated islands increased from very few upstream (Fig.4.11(a)) to increasingly higher concentration towards the center (Fig.4.11(b)). The grainy structure further downstream (Fig.4.11(c)) is a result of high concentration of nucleated islands merged together to form a nearly-polycrystalline film. Measurement of the temperature distribution inside the susceptor using Si melting test indicated that the non-homogeneity of the temperature was rather small (Fig.4.18). Therefore, the temperature variation was not sufficient to cause the differences in epilayer morphology shown in Fig.4.11. Another parameter that can significantly affect the surface morphology of the epilayers is the effective Si/C ratio above the growth surface. Also by the visual observation of the silicon clusters in the gas phase during the epitaxial growth, the Si/C ratio from upstream to downstream may be varied significantly. The variation could be due to different kinetics of gas-phase

reactions involving Si and C gaseous species in combination with silicon depletion by the clustering process as well as release of Si due to cluster evaporation/etching. Preliminary measurements of the doping variation along the gas-flow direction confirmed the possibility of Si/C ratio variation from upstream to downstream. Consequently, lower Si/C ratios downstream are thought to be responsible for poor morphology of the epilayer in Fig.4.11(c) in comparison to the upstream regions (Fig.4.11(a)(b)).

In summary, the growth at low temperatures showed strong sensitivity to the effective Si/C ratio above the growth surface. At $1300^0$C, the effective Si/C ratio strongly depends on the growth conditions. Evidences of the change of the Si/C ratio from upstream to downstream were identified at some growth conditions, which in turn influenced the epilayer morphology. This could be caused either by depletion of Si-related species downstream by Si aerosol formation or higher concentration of C-related species downstream as a result of the particular kinetics of the gas-phase reactions. The depletion of Si-related species downstream appears to be more likely as follows from the discussion of growth rate dependence on the precursor flows in the next section.

### 4.2.3 $R_g$ Dependence on the Precursor Flow and the Temperature

As expected, the growth rate ($R_g$) was found to increase with increasing the $CH_3Cl$ flow (Fig.4.12). However, $R_g$ did not saturated at higher C/Si ratios by transition to Si-supply limited growth mode (which is generally observed at regular $T_g$ values [55]). Instead the morphology degradation initiated. Morphology degradation at higher C/Si ratios limited the possibility to further increase $CH_3Cl$ flow and to reach $R_g$ saturation.

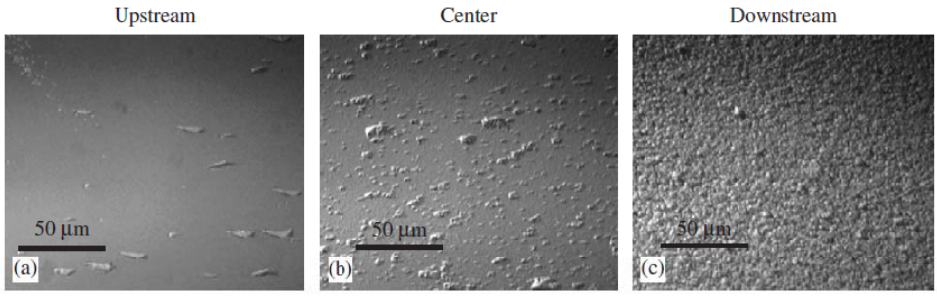


Fig.4.11: Interference contrast optical micrographs of 4H-SiC epitaxial layers grown at 1300°C and lower than optimal Si/C ratio ($CH_3Cl$ flow at 4 sccm and $SiH_4$ flow at 30 sccm). The three films shown were grown at different locations of the susceptor along the gas flow direction: (a) 40 mm from the upstream edge of the susceptor, (b) in the middle of the susceptor, and (c) 60mm from the upstream edge of the 100-mm-long susceptor. The real Si/C ratio above the growth surface decreases along the gas flow direction, and that makes morphology degradation increase from upstream to downstream.

$R_g$ dependence on $SiH_4$ flow showed more complex behavior (Fig.4.13). At lower $SiH_4$ flow rates, $R_g$ initially increased with increasing $SiH_4$ flow. However $R_g$ saturated at high $SiH_4$ flows for all $CH_3Cl$ flows investigated in this study. An important feature of this trend is that the $SiH_4$ flow corresponding to the onset of saturation was independent of $CH_3Cl$ flow. The experimental data were fitted with an exponential dependence (shown in Fig.4.13 as solid lines), described by

$$R_g(<SiH_4>) \; \alpha \; 1\text{- exp}\left(-\frac{<SiH_4>}{\tau_{SiH_4}}\right) \qquad (4.1)$$

where $R_g$ is the growth rate, $<SiH_4>$ is the silane flow rate, and $\tau_{SiH4}$ is the exponential rate coefficient for the $SiH_4$ flow dependence. The value of $\tau_{SiH4}$ extracted from the experimental data presented in Fig.4.13 was found to be independent of the $CH_3Cl$ flow.

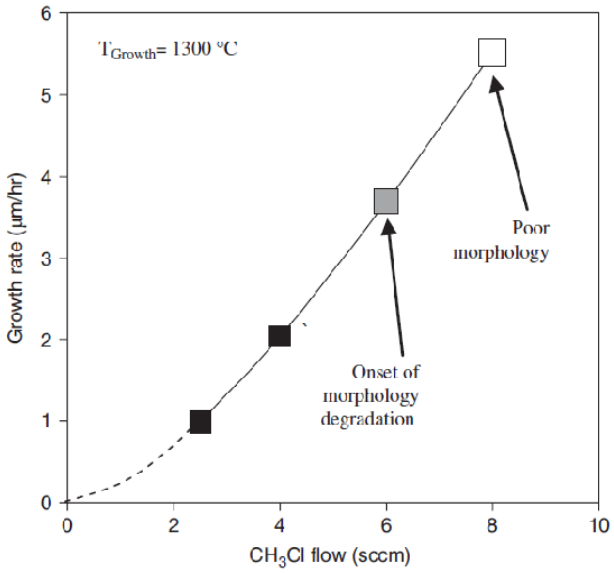


Fig.4.12: Growth rate dependence on $CH_3Cl$ flow for the fixed value of $SiH_4$ flow of 30 sccm. The grey square corresponds to the onset of morphology degradation. The highest $CH_3Cl$ flow in this figure corresponds to the nearly-polycrystalline growth shown in Fig.4.11(c).

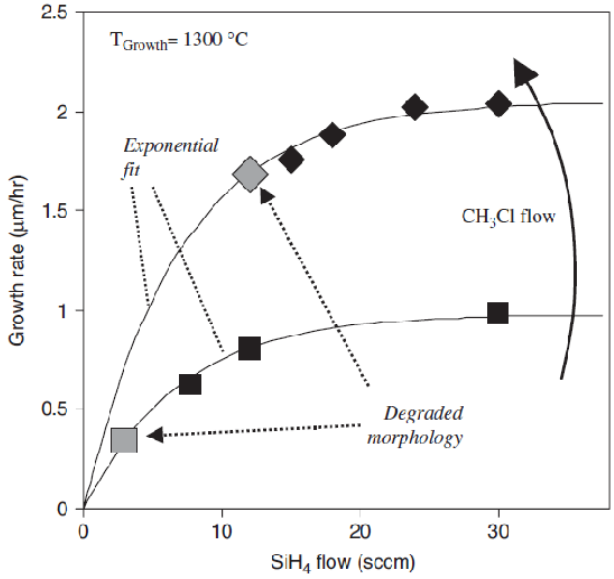


Fig.4.13: $R_g$ dependence on $SiH_4$ flow for two different $CH_3Cl$ flows at 2 and 6 sccm. The solid lines represent the exponential fit. Rate constants of the exponential fit are independent of $CH_3Cl$ flow.

This confirmed that the $SiH_4$ flow rate corresponding to the transition from the increasing $R_g$ with $SiH_4$ flow to its saturation is independent of the Si/C ratio.

It could be speculated that the saturation in Fig.4.13 is due to the conventional mechanism of transition from Si supply-limited to C supply-limited mode. However, in this case the onset of saturation would be at increasingly higher $SiH_4$ flows for higher higher $CH_3Cl$ flows (which quantitatively means that the value of $\tau_{SiH4}$ would be increasingly higher for higher $CH_3Cl$ flow rates). The independence of $\tau_{SiH4}$ on $CH_3Cl$ flow suggested that the observed saturation is a result of silicon vapor condensation, which is also observed as a pronounced droplet cloud inside the susceptor and at the downstream portion of the reactor.

Whilst independent of $CH_3Cl$ flow rate for the fixed set of the growth conditions, the exponential rate coefficient $\tau_{SiH4}$ depends on the carrier-gas flow and $T_g$. Higher $H_2$ flow rates require lower $SiH_4$ flows (i.e., lower Si vapor concentration in the growth zone) before the saturation occurs. Simultaneously, the saturated value of $R_g$ was lower for higher $H_2$ flow rates. This trend can be related to the kinetics of the gas-phase reactions. It is suggested that when the gas flow velocity inside the susceptor is increased (e.g., in the range of 1-1.5 m/s typical for our experiments), silicon precursors have less time to approach equilibrium between Si cluster formation and their etching/evaporation compared to lower carrier-gas velocity, with the balance shifted towards higher concentrations of Si clusters and consequently lower concentration of Si-carrying ad-species contributing to the film growth.

In order to gain more insight in the mechanism of the Si condensation and its influence on the growth rate, the temperature dependence of the growth was investigated. For a constant carrier-gas flow, the temperature dependence of $R_g$ over the wide range of $T_g$ in our reactor was complex. It was influenced by non-linear effects such as precursor depletion. For relatively low gas flow velocities in the range of 1-2 m/sec inside the susceptor, precursor depletion due to high deposition at the upstream portion of the susceptor drastically reduced the value of $R_g$. The depletion effect is more pronounced at higher temperatures (above 1500$^o$C) resulting in $R_g$ decreasing with increasing $T_g$. Because of the precursor depletion, $R_g$ is also very non-homogeneous along the gas flow direction at low gas-flow velocities.

However, the expected Arrhenius dependence of $R_g$ on $T_g$ was observed below 1500$^o$C (Fig.4.14(a)). The dependencies of $R_g$ on $SiH_4$ similar to those shown in Fig.4.13 were obtained and the values of the exponential rate coefficient $\tau_{SiH4}$ were extracted for each temperature. The temperature dependence of the exponential rate coefficient $\tau_{SiH4}$ is shown in Fig.4.14(b). When the growth was conducted at higher temperatures, $R_g$ dependence on $SiH_4$ flow entered saturation at higher $SiH_4$ flows than that at lower temperatures. Quantitatively, this is equivalent to larger values of $\tau_{SiH4}$ at higher temperatures. It was established that the values of $\tau_{SiH4}$ follow the Arrhenius temperature relationship. A striking result is that the activation energy of $\tau_{SiH4}$–temperature dependence (Fig.4.14(b)) and that for $R_g$ (Fig.4.14(a)) is the same within experimental error (and also independent of the $CH_3Cl$ flow rate). Thus the mechanism responsible for $R_g$ saturation with increasing $SiH_4$ flow (which is, as we established above, purely Si

supply-limited) is also the main factor determining the temperature dependence of $R_g$. This indicates that changes in the values of $R_g$ with temperature are also predominantly dictated by changes in Si supply, and are less dependent on C supply. This mechanism is further discussed below.

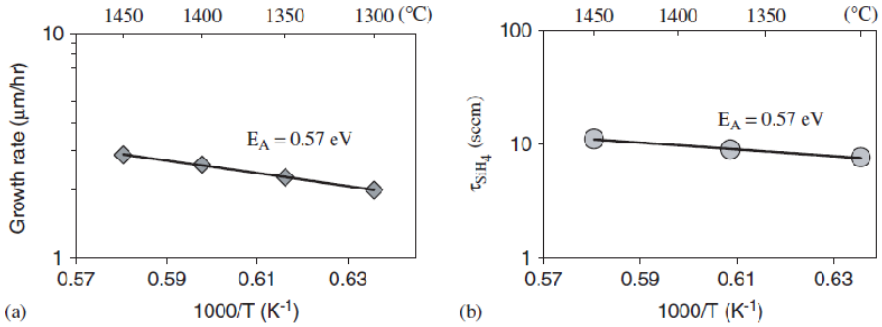


Fig.4.14: Arrhenius plot for (a) $R_g$ and (b) the exponential rate coefficient $\tau_{SiH4}$ of Eq.(4.1) for $R_g$ dependence on $SiH_4$ flow (Fig.4-13) in the temperature range of 1300-1450°C. Values of activation energy $E_A$ for both Arrhenius plots are the same within experimental error.

### 4.2.4 Discussion of the Growth-Rate-Limiting Mechanisms

The distinctive features of low-temperature epitaxial growth experiments reported here are the relatively low flow rates of the carrier gas and high flow rates of silicon and carbon precursors. The results of the study indicated that the silicon vapor condensation process became a critical mechanism influencing $R_g$ and epilayer morphology at these conditions.

One of the expected possibilities was that $R_g$ saturation at high $SiH_4$ flows happened due to the well-known transition from the Si supply limited to C supply limited mode. However, in this case, the saturation would happen at higher $SiH_4$ flows when for higher $CH_3Cl$ flow rates (which quantitatively means that the value of $\tau_{SiH4}$ would be increasingly higher for higher $CH_3Cl$ flow rates). Analysis of $R_g$ dependence on silane flow (Fig.4-13) indicated that $R_g$ saturation at high $SiH_4$ flows is solely determined by silicon condensation, independent of the carbon supply. Whilst $R_g$ strongly depends on $CH_3Cl$ flow rate, the exponential rate coefficient $\tau_{SiH4}$ does not depend on $CH_3Cl$ supply. Thus $R_g$ saturation at high $SiH_4$ flow cannot be explained by a transition to carbon-diffusion-limited mode. In fact, due to high precursor flows, $R_g$ is likely to be surface-reaction-rate-limited (at least for the silicon supply). Let us consider a generalized relationship for the surface reaction rate leading to formation of epitaxial SiC:

$$R_{surf} \ \alpha \ \sum_{n,m} [\mathrm{Si}_n]^{\alpha} \times \ [\mathrm{C}_m]^{\beta} \tag{4.2}$$

where $[Si_n]$ and $[C_m]$ represent concentrations of all possible silicon- and carbon-carrying species that participate in the surface reactions to produce epitaxial SiC.

Eq.(4.2) would result in $R_g$ that is independent of flow rate of one of the precursors (i.e., saturation of $R_g$ in Fig.4.13), only if the concentration of the corresponding ad-species arriving at the surface does not change (i.e., does not increase with increasing precursor flow). In the present case, for silane flow rates exceeding a certain value, $[Si_n]$ should remain constant, independent of the $SiH_4$ flow rate, to provide the experimentally observed $R_g$ dependence.

The silicon condensation is suggested to be responsible for this trend. As discussed in Chapter 2, according to classical nucleation theory [155], high silicon vapor concentrations (a product of silane decomposition) result in silicon aerosol formation. The Si clusters formed in the gas phase have low diffusivity, making them effectively unavailable for epitaxial growth surface reactions [122]. The mechanism of this process is complex, with the rate of cluster formation depending on temperature, temperature gradient, pressure, etc. Despite this complexity, the rate of conversion of silicon vapor into Si clusters is proportional to the excess silicon vapor. Increasing the $SiH_4$ flow rate results in a surplus of Si vapor that is converted into Si clusters. If the reactor geometry and $SiH_4$ flow rate provide sufficient time for the silicon vapor condensation process to approach thermodynamic equilibrium, most of the excess silicon vapor, beyond a critical concentration, will be converted to clusters. Thus the number of silicon species available for surface reactions (i.e., the value of $[Si_n]$ in Eq.(4.2)) becomes independent of the $SiH_4$ flow rate when the $SiH_4$ flow rate is too high.

If the $T_g$ increases, there are two independent effects of the temperature increase on $R_g$ can be expected:

(1) Cluster formation will be suppressed (and cluster evaporation/etching will be enhanced) at higher temperatures. For the same $SiH_4$ flow, this increases the concentration of Si-carrying species available for surface reactions (not involved in clusters), which contributes to $R_g$ increase, which was observed experimentally as described in 4.1.3.

(2) $R_g$ also depends on carbon supply (Fig.4.13 and Eq.(4.2)). If gas-phase reactions involving carbon have sufficiently strong temperature dependence, $R_g$ would further increase with temperature.

The overall $T_g$ dependence of $R_g$ (i.e., the activation energy for $R_g$) should reflect both of these contributions if they were present.

In contrast to the $R_g$ dependence on $T_g$, the activation energy of the temperature dependence of the $\tau_{SiH4}$ coefficient, according to this model, would exclusively reflect the temperature-dependent rate of aerosol formation and evaporation/etching. The coincidence of the values of the two activation energies determined from Figs.4.14(a) and 4.14(b) indicates that the overall temperature dependence of $R_g$ is also predominantly determined by cluster formation/evaporation process, and is nearly independent of carbon-related process in our experimental temperature range.

This model can also help interpret the observed morphology variations along the gas flow direction (Fig.4.11). As mentioned previously, in the absence of essential temperature non-homogeneity, reduction in Si/C ratio is likely responsible for the morphology degradation of the downstream sample (Fig.4.11(c)). Since $R_g$ does not significantly change from upstream to downstream, the Si/C ratio variation is likely caused by variation in silicon-related species concentration available for surface reactions (i.e., the value of $[Si_n]$ in Eq.(4.2)), while the concentration of the carbon species (i.e., the value of $[C_m]$ in Eq.(4.2)) remains relatively unchanged along the gas flow direction. The reduction in $[Si_n]$ can be caused by the kinetics of silicon particulate condensation

consuming increasingly more silicon from the gas phase when the gas flow approaches the trailing edge of the substrate.

### 4.2.5 Low-Temperature Growth on Low Off-Axis Cut Substrates

In this portion of our work, the $CH_3Cl$-based epitaxial growth process, developed for $8^o$ vicinal substrates, was applied to lower vicinal angle substrates. The main outcomes for epilayer morphology are summarized in Table 4-1. As was described in Chapter 4.1.6, growth on $2^o$ off-axis cut substrates at conventional high temperatures produced similar results between $C_3H_8$- and $CH_3Cl$-based epitaxial processes. In contrast to the mirror-like growth morphology on $8^o$ vicinal surfaces (Fig.4.15(a)), growth on $2^o$ vicinal substrates at $1600^oC$ produced severe step-bunching for both $C_3H_8$ and $CH_3Cl$ precursors (Fig.4.15(b)).

When $T_g$ of the $2^o$ growth was reduced to $1300^oC$, severe 2D nucleation resulted. Obviously, $L_D$ at such low temperatures was not sufficient to provide nucleation-free step-flow growth for the higher average terrace width on the $2^o$ vicinal substrates, while it was sufficient for the terrace width on $8^o$ substrates.

Table 4-1: Surface morphology of $8^o$ and $2^o$ off-axis epilayers at different growth

| Temperature ($^oC$) | 1600 | 1380 | 1300 |
|---|---|---|---|
| $8^o$ off-axis | No step-bunching, mirror-like surface | No step-bunching, mirror-like surface | No step-bunching, mirror-like |
| $2^o$ off-axis | Step-bunching, no defect | No step-bunching, rare surface defects | No step-bunching, heavy |

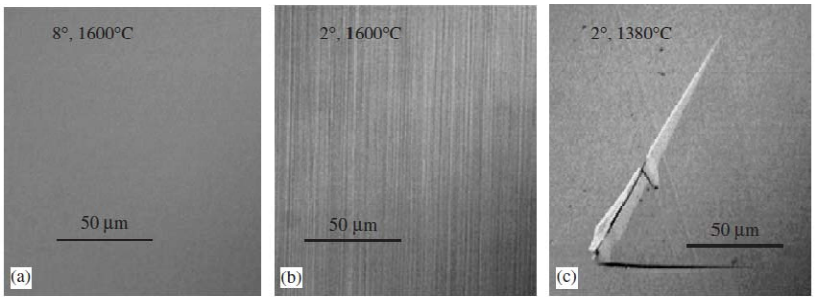


Fig.4.15: Interference contrast optical micrograph of epilayers grown on (a) standard $8^o$ off-axis 4H-SiC substrates, (b),(c) $2^o$ off-axis 4H-SiC substrates at optimized gas flow conditions. $CH_3Cl$ was used in all three cases. $T_g$ was $1600^oC$ in (a) and (b), and $1380^oC$ in (c). While high-temperature growth on $2^o$ substrates results in the well know step-bunching (b), reduction in $T_g$ significantly alleviates this problem (c).

An encouraging result was obtained by using $CH_3Cl$-based growth at temperatures higher than $1300^oC$ but still lower than conventional $T_g$ values. The morphology of the $2^o$ vicinal film at $1380^oC$ is shown in Fig.4-15(c). A location on the epilayer showing a triangular defect was deliberately selected for this figure. While these defects could be observed across the sample, the major fraction of the film area was defect free. It is apparent that use of halo-carbon precursor enabled suppressing the nucleation of defects and 3C-SiC polytype inclusion on the low off-axis substrates at reduced temperatures. More important, the step-bunching problem was eliminated by performing the growth at a temperature lower than the conventional temperatures of traditional propane/silane 4H-SiC homoepitaxy.

Consequently, the low growth temperatures enabled by the use of the halo-carbon precursor may offer an additional advantage of reducing or completely eliminating the step-bunching problem in low off-axis epilayers.

### 4.2.6 Characterization of the Quality of the Epilayers Grown at Low Temperatures

High crystalline quality was confirmed by low-temperature PL spectroscopy in Fig.4.16 and 4.17. Both growth runs (at 1300°C and at 1700°C) were conducted at the flow conditions optimized for the corresponding $T_g$ values. The two spectra in Fig.4.17 were measured at identical conditions. The absolute intensity of the excitonic lines was found to be very close in the 1300 and 1700°C samples. For the epilayers with similar concentrations of donors and acceptors, this indicated that there is virtually no degradation in crystal quality as $T_g$ was lowered by 400°C. The spectrum of the epilayer grown at 1300°C showed strong nitrogen and aluminum bound-exciton lines (e.g., $Q_0$ and Al lines) as well as nitrogen-aluminum and nitrogen-boron donor-acceptor pairs (DAP). Relatively high concentrations of dopants (above $10^{16}$ $cm^{-3}$ for nitrogen and above $10^{15}$ $cm^{-3}$ for aluminum) were confirmed by SIMS. However, the absolute intensity of the PL signal and the sharpness of the excitonic lines were found to be at least as good as that of epitaxial layers grown at 1700°C (Fig.4.17).

### 4.2.7 2-Inch Full Wafer Epitaxial Growth

The epitaxial growth on a 2" wafer was conducted to explore the possibility of a commercial scale growth. All the growth experiments were conducted in a small hot-wall CVD reactor that is not exactly suitable for a 2"-wafer growth. The distance between the sidewalls of the susceptor is only 7 mm larger than the diameter of the 2" wafer substrate. The geometrical restriction of our reactor makes the usual "sweet-spot" of the growth noticeably smaller than two inches; therefore, the reactor is more suitable for the process development on smaller substrates.

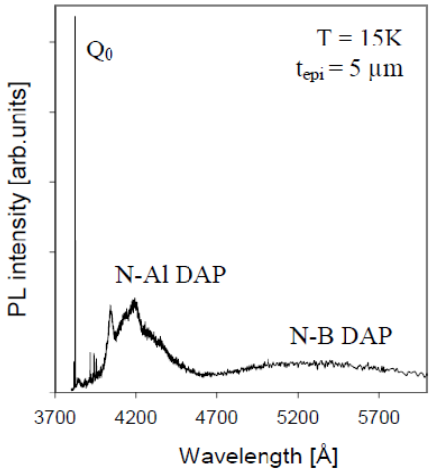


Fig.4.16: Low-temperature PL spectrum of a 5µm-thick epitaxial layer grown at 1300°C using $CH_3Cl$ precursor.

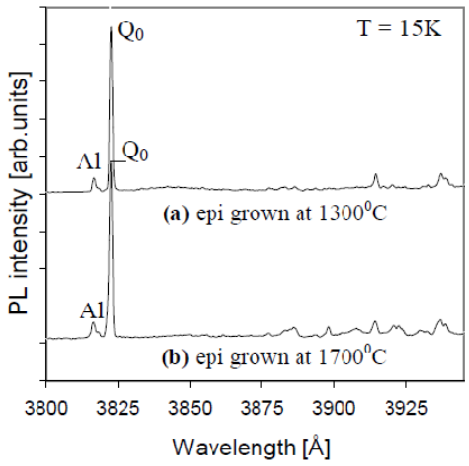


Fig.4.17: Near-bandgap part of the PL spectra of an epitaxial layer grown (a) at 1300°C and (b) at 1700°C. $CH_3Cl$ was the C-source precursor.

However, prior to scaling the lower-temperature process toward the larger CVD reactor, the growth on a 2" substrate at 1300°C was attempted in this small reactor. The surface morphology was found to be mirror-like everywhere except for the regions about 2 mm wide at the left and right edges of the substrate close to the susceptor walls. In addition, the homogeneity of the growth rate was much better than what was expected (Fig.4.18). The growth rate homogeneity along the gas flow direction was better than 7% although a significant reduction of the growth rate was found near the regions with the degraded morphology close to the susceptor walls (which is natural for the small size of the susceptor used). A non-optimized temperature distribution along the gas flow direction (right picture in Fig.4.18) is responsible for the major part of the growth rate

inhomogeneity. The temperature distribution was obtained by the temperature calibration using melting of silicon pieces placed inside the susceptor. The melting point of silicon is 1414$^{o}$C. We recorded the temperatures at which the silicon substrate started melting from the reading of a pyrometer. The differences between the reading of the pyrometer and the actual melting temperature of silicon were used to evaluate the temperature distribution inside the susceptor.

### 4.2.8 Summary

The experimental results reported in this section showed that use of chloromethane as a carbon precursor was beneficial for achieving device-quality homoepitaxial growth of 4H-SiC on regular commercial substrates at temperatures below 1300$^{o}$C.

A complex growth mechanism was investigated. A model was proposed to explain the quantitative trends. Condensation of the silicon vapor at high silane flows, which causes the growth rate saturation, appears to be one of the major obstacles toward obtaining higher growth rates in excess of 2 μm/hr, while retaining a good quality. Proper control of the Si/C ratio through control of silicon condensation could enable significantly higher $R_g$ values without morphology degradation.

$CH_3Cl$ precursor-based growths at a temperature of 1380$^{o}$C allowed avoiding 2D nucleation on 2$^{o}$ vicinal substrates, with complete elimination of step-bunching, which is an omnipresent challenge of low-vicinal-angle growth at conventional temperatures of the traditional propane/silane growth.

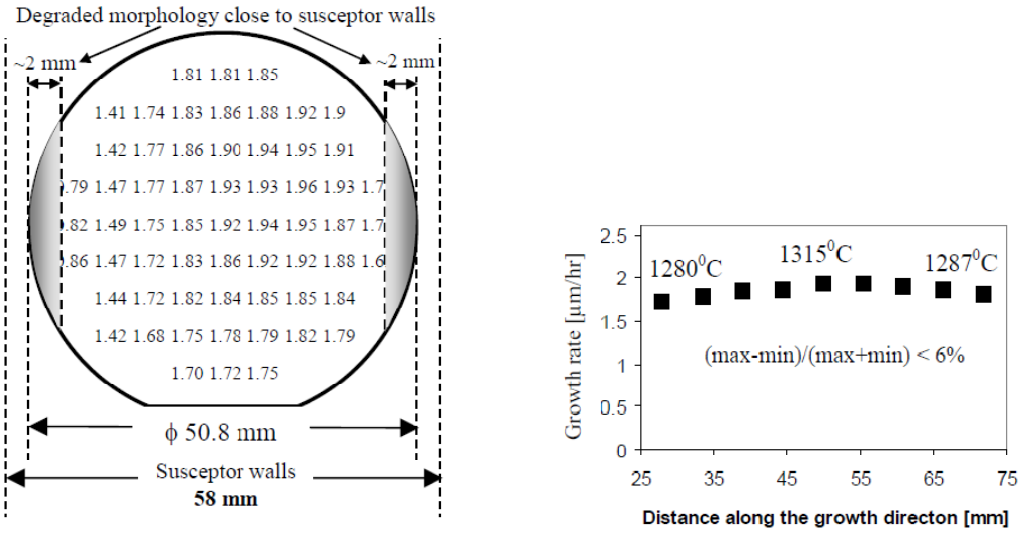


Fig.4.18: Left: thickness map of an epilayer grown at 1300°C for 1 hour on a 2" wafer (distance between the susceptor sidewalls – 58 mm; susceptor length – 100 mm). Edge exclusion – 2mm; Right: thickness line-scans at the middle of the susceptor along the gas flow direction.

### 4.3 HCl Additive for the Low-Temperature Epitaxial Growth

As was demonstrated in the previous sections, at temperatures below 1300°C, the growth rate ($R_g$) with specular epilayer surface was found to be limited by silicon cluster formation in the gas phase and did not exceed 2-2.5 μm/hr. Silicon clustering was responsible for the depletion of silicon growth species; therefore the effective Si/C ratio at the growth surface was reduced compared to the input Si/C ratio.

It was demonstrated by different groups that significant suppression of the homogeneous gas-phase nucleation (i.e., etching of Si gas-phase clusters) may take place when HCl is added during SiC homoepitaxy at regular temperatures [136-137]. While Cl

is provided by $CH_3Cl$ carbon precursor during the low-temperature halo-carbon growth, it appears that its amount may be not sufficient to fully suppress homogeneous nucleation. The objective of the experiments covered in this section was to investigate a possibility of controlling the silicon gas-phase nucleation during the low-temperature epitaxial growth by adding HCl during the growth.

As in the previous part of the work, 4H-SiC substrates used were commercial wafers vicinally cut $8^o$ towards the [11-20] direction. Epitaxial growth of 4H-SiC films was conducted in the same low-pressure hot-wall CVD reactor at 100-400 Torr with $H_2$ as the carrier gas, $SiH_4$ (3% in $H_2$) as the silicon source, and $CH_3Cl$ as the carbon source. Different flow rates of HCl were used during the growth.

### 4.3.1 The Influence of HCl on the Appearance of the Cloud of Silicon Clusters in the Gas Phase

As was described earlier in this Chapter, the $CH_3Cl$ growth at $1300^oC$ is characterized by a very high degree of Si vapor condensation. The Si gas-phase cluster cloud was routinely observed inside the susceptor during the low-temperature growth, and the cloud became increasingly denser with increasing the $SiH_4$ flow rate. Fig.4.19(a) was photographed through the rear port of the reactor during the growth at a very high $SiH_4$ flow rate of 20 sccm without HCl. It confirmed that strong silicon polymerization occurred at such low growth temperatures. Attempts of increasing the growth rate and/or Si/C ratio by adding more silane resulted in proportional densification of the cloud.

Comparison of the silicon cluster cloud inside the susceptor without and with HCl added during the growth (Fig.4.19(a) and Fig.4.19(b), respectively) offered the first

strong evidence that additional Cl-containing species (the products of the gas-phase reactions involving HCl) enhanced dissociation of the silicon gas-phase clusters during halo-carbon low-temperature epitaxial growth. The density of the silicon cluster-related cloud in the experiment with HCl (Fig.4.19(b)) was significantly reduced.

Due to the design and the geometry of the reactor, there is no practical way to know where the Si clusters start forming and where the HCl attacks those clusters the most. Therefore, relevant growth dependencies on HCl flow rate were obtained to provide some information for those questions.

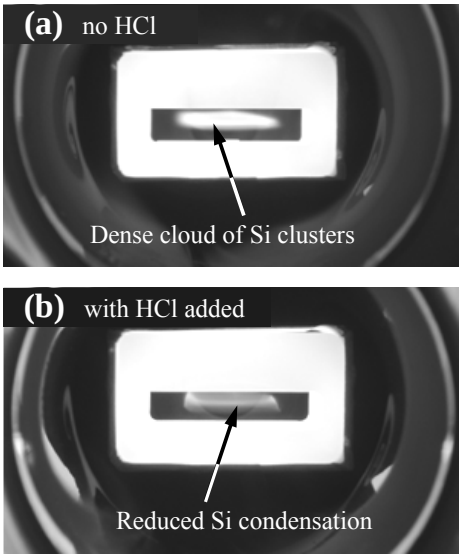


Fig.4.19: Rear view of the glowing susceptor and the cloud of Si clusters inside the susceptor during 1300$^{o}$C epitaxial growth: (a) without HCl and (b) with HCl added. Enhanced cluster etching by Cl-related species is evidenced by the drastically reduced density of the Si cluster cloud.

### 4.3.2 The Growth Rate and the Si/C Ratio versus the HCl Flow Rate

The growth conditions that produced deteriorated surface morphology during the growth without HCl were chosen for the further investigation. Fig.4.20(a)-(c) shows the micrographs of the epilayers with deteriorated surface morphology in the absence of HCl due to too high growth rate and too low Si/C ratio. The flow rates of $CH_3Cl$ and $SiH_4$ precursors were 8 sccm and 30 sccm, respectively. HCl was added to explore the possibility of etching Si clusters in the gas phase in order to enhance the supply of Si growth species to the substrate surface. The drastic improvement of the epilayer morphology by adding HCl is shown in Fig.4.20(d)-(f) compared to the growth without HCl (Fig.4.20(a)-(c)). The island nucleation in Fig.4.20(a)-(c) completely disappeared and the major part of the epilayer surface became mirror-like. Simultaneously, some triangular surface defects were formed. Other than that, the epilayer morphology improvement was obvious.

For the majority of the growth conditions attempted in this study (including the growth results shown in Fig.4.20), a significant increase of the growth rate with the morphology improvement was observed when HCl was added during the growth. Normally, it could be expected that surface processes (i.e., surface etching by HCl products) are responsible for the morphology improvement. However, the surface etching would cause reduction (or at least no increase) of $R_g$. The increase of $R_g$ accompanying the improvement of the epilayer morphology indicated that the positive influence of HCl addition primarily came from the gas-phase silicon cluster etching rather than surface etching, even though a positive role of surface processes cannot be completely excluded. In Fig.4.20, the

maximum growth rate after adding HCl increased from 5.2 to almost 7 μm/hr. Under certain growth conditions, the increase of the growth rate after adding HCl exceeded the factor of two (e.g., from 1.5 μm/hr without HCl to 3.4 μm/hr with HCl added), which confirmed the strong release of additional growth species due to Cl-assisted silicon cluster etching.

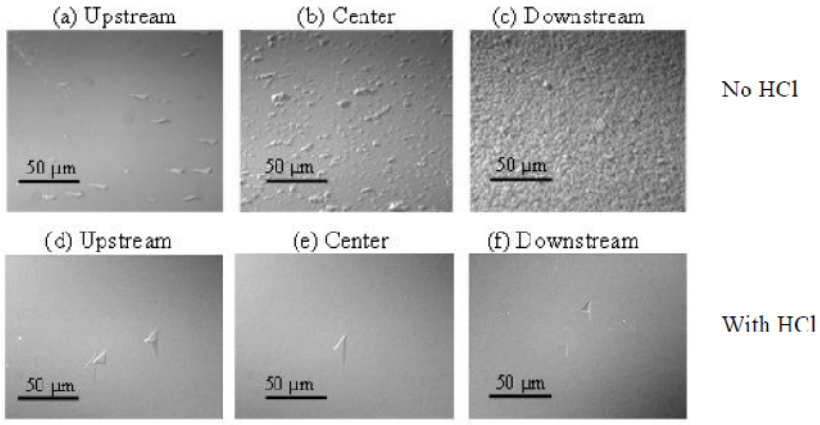


Fig.4.20: Optical micrographs of 4H-SiC epitaxial layers grown at 1300°C and high $CH_3Cl$ flow without adding HCl ((a)-(c)) and with adding HCl ((d)-(f)) during the growth.

Fig.4.21 shows the growth rate dependence on the HCl flow rate. At these growth conditions, the $R_g$ homogeneity was fairly good when the HCl addition was not used. With the addition of a small flow of HCl (2 sccm), the $R_g$ increased more than 40%, while preserving a good $R_g$ homogeneity. A further increase of the HCl flow rate to 5 sccm caused increase of the value of $R_g$ upstream of the growth zone up to 70% compared to that without using HCl, but $R_g$ at the center of the growth zone increased

much less. At the downstream portion of the growth zone, $R_g$ was actually lower than that of HCl flow rate at 2 sccm.

Even more unexpected result was observed at 8 sccm of HCl flow rate. The value of $R_g$ decreased compared to that for 5-sccm HCl flow rate while the non-homogeneity of the $R_g$ profile remained qualitatively similar. Qualitatively similar strange reduction of $R_g$ was observed at a variety of the growth conditions. The corresponding HCl flow rates at which this effect happened were different for different gas flow conditions. However, the qualitative trend was always present.

Further increase of the HCl flow rate resumed the trend of $R_g$ increase with the increasing HCl supply, but the increase of $R_g$ was much less than that at lower HCl flow rates, which showed that the trend approached saturation at higher HCl flows.

With all this complexity of $R_g$ behavior, two main results of adding HCl can be separated: (1) a non-monotonous change of $R_g$ with HCl flow rate, and (2) higher growth rate upstream in comparison to downstream when higher HCl flow rates were used. The

trend of decreasing growth rate from upstream to downstream is quite similar to the effect of a depletion mechanism (i.e., higher growth rate upstream consumes more growth-related species and leaves less available sources for the growth downstream). However, the magnitude of such depletion mechanism is not sufficient to cause the $R_g$ non-homogeneity even remotely close to the trend shown in Fig.4.21. Another precursor depletion model is needed to explain these experimental results.

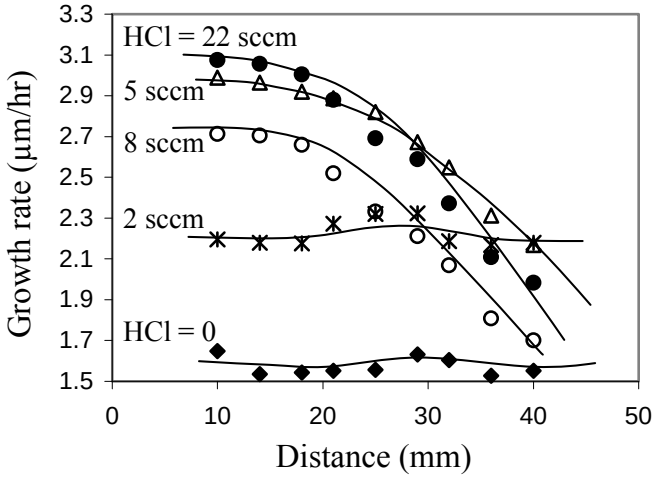


Fig.4.21: Growth rate ($R_g$) as a function of the distance from the leading edge of the susceptor for different values of HCl flow rates compared to the growth without HCl. The growth rate reduces when the HCl flow rate was increased from 5 to 8 sccm.

The $R_g$ dependence on HCl flow rate at a selected location close to the middle of the growth zone is shown in Fig.4.22. Generally, the change of the $R_g$ can be caused by the change of silicon or carbon supply or both to the growth surface. Let us consider the regular expectations that one would have when adding HCl during the epitaxial growth of SiC [122-123]. Usually anticipated effect of adding HCl during the epitaxial growth is relatively simple: (1) the increase of the $R_g$ and (2) the increase of the effective Si/C ratio caused by the enhanced supply of Si species released from the Si gas-phase clusters. In order to establish if the experimental results of adding HCl during our low-temperature epitaxial growth fit this simple picture, both the $R_g$ dependence and donor concentration dependence on the HCl flow rate are shown in Fig.4.22.

The doping dependence is used in this work as a non-direct measure of the effective Si/C ratio, which cannot be easily measured directly by any of the existing experimental techniques. Simultaneously, the qualitative relationship between the doping and the effective Si/C ratio caused by site-competition mechanism is known and can be used as a valuable source of information.

It is obvious that the changes of the effective Si/C ratio (as estimated from the changes in doping of Fig.4.22) do not follow the simple trend expected by the enhanced release of Si species from the gas-phase clusters because the donor concentration shows a complex dependence on the HCl flow rate. The origin of the complex behavior of $R_g$ and the effective Si/C ratio is discussed below.

In Fig.4.22, $R_g$ increases rapidly with increasing the HCl flow rate in the range of small HCl flow rates (below 3 sccm). This increase could be consistent with the simple expectation of an additional supply of Si growth species caused by HCl-enhanced dissociation of Si clusters.

However, the donor doping concentration reduces instead of increasing. The decrease of the donor concentration means the decrease of the effective Si/C ratio, according to the site-competition mechanism. It indicated that the HCl effect at low HCl flow rates included an additional supply of carbon (not just an increase of Si supply). This cannot be explained by the conventional model of the HCl effect. The source of this carbon is discussed below.

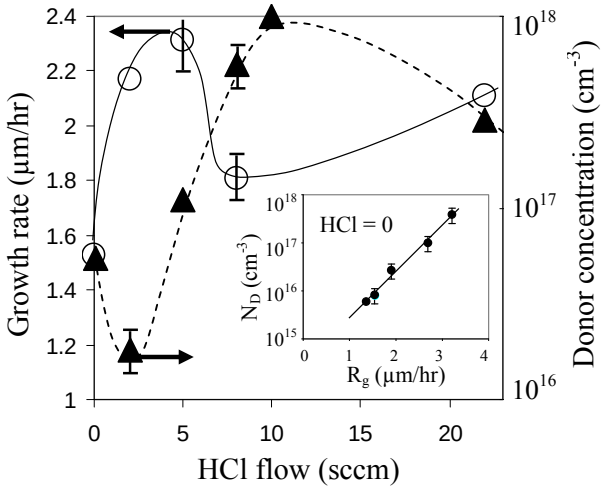


Fig.4.22: Schematics of Growth rate (empty circles) and net donor concentration (solid triangles) as a function of the HCl flow rate. Low HCl flow rates cause reduction of the Si/C ratio (the donor concentration) even though the growth rate is increasing. The inset shows the previously determined dependence of the donor concentration ($N_D$) on the growth rate without HCl when the other factors were kept the same.

In the range of 3- to 5-sccm HCl supply, both $R_g$ and donor concentration increase with HCl flow, which (by itself) would be consistent with the model of an enhanced supply of Si species due to the cluster etching by HCl.

From 5 to 8 sccm of HCl flows, the growth rate drops, but the donor concentration keeps increasing. This indicates that the effective Si/C ratio increases with the HCl flows. However, the decreasing growth rate suggested that a reduction of the carbon supply must be taking place, which outweighed the additional Si supply. The conventional model for HCl effect is also unable to explain why the carbon supply to the growth surface is reduced in this range of the HCl flow rate.

For even higher HCl flow rates, a much slower increase of $R_g$, a slow decrease of the Si/C ratio, and their gradual saturation were observed.

It follows from the above discussion that HCl addition causes complex changes in the effective Si/C ratio in the vicinity of the growth surface, which involves much more than enhanced supply of Si species released from the gas-phase clusters. Before proceeding with the discussion of the mechanisms for this behavior, one must eliminate a possibility that the changes in doping observed in Fig.4.22 could be caused by factors other than changes in the effective Si/C ratio. We consider two alternative possibilities that in general could also cause the changes in doping concentration.

1. Unintentional dopant impurities (e.g., nitrogen) are brought into the epilayer by HCl additive without any change in the value of the effective Si/C ratio.
2. The doping concentration can be a function of $R_g$ [155]; therefore the changes of the growth rate caused by HCl addition could lead to changes in doping without varying the effective Si/C ratio.

Considering the first possibility, the amount of the nitrogen should be presumably proportional to the HCl flow rate if it were delivered by adding HCl. This is inconsistent with the experimental results, especially at HCl flow rates below 3 sccm and higher than 10 sccm.

As for the second possibility, the dependence of doping concentration on $R_g$ at a constant Si/C ratio without HCl from Ref. [156] is shown in the inset of Fig.4.22. It shows that the doping increases with increasing $R_g$ at a constant Si/C ratio. Consequently, the increase of $R_g$ with increasing the HCl flow rate in the range of the HCl flow rates

below 3 sccm should cause the increase of the doping concentration (rather than decrease) if the Si/C ratio were constant.

An additional confirmation that changes in doping shown in Fig.4.22 indeed reflect changes in the effective Si/C ratio can be obtained from the surface morphology of the grown epilayers. Numerous prior experiments gave consistent evidences that the surface morphology degradation happened when the Si/C ratio was reduced. Fig.4.23(a)-(d) show the changes of the epilayer morphology for different values of the HCl flow rates and support the conclusion about the changes of the effective Si/C ratio caused by HCl addition. In Fig.4.23(b) the epilayer morphology degraded when HCl was flowing at 2 sccm. Fig.4.23(c) shows a clear improvement of the surface morphology at 5 sccm of

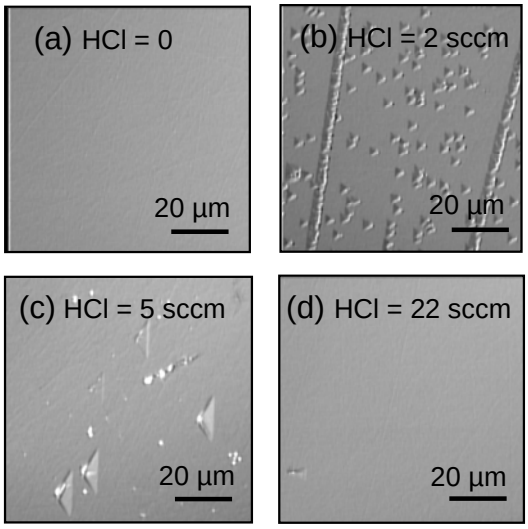


Fig.4.23: Optical micrographs of epitaxial layers grown with different HCl flow rates: (a) without HCl, (b) HCl = 2 sccm, (c) HCl = 5 sccm, (d) HCl = 22 sccm. The morphology of these epilayers corresponds to the data points in Fig.4.22.

HCl. The deterioration of the surface morphology in Fig.4.23(b) could be caused by a reduction of Si/C or an increase of the growth rate. The surface morphology improved when the HCl flow rate was increased from 2 to 5 sccm. The growth rate keeps increasing at HCl flow rate of 0 to 5 sccm in Fig.4.22. If the increase of the growth rate was the dominating factor that caused the degradation, Fig.4.23(c) should look worse than Fig.4.23(b) (instead of an improving morphology). Therefore, the change of the Si/C ratio is responsible and the dominating factor for the outcome of adding HCl. The epilayer morphology at higher HCl flows (including the flow of 22 sccm shown in Fig.4.23(d)) is nearly featureless, which is also consistent with the higher values of the effective Si/C ratio.

From the discussion above, it follows that adding HCl indeed caused changes in the effective Si/C ratio. However, the Si/C ratio did not have a straightforward relation with increasing HCl flows, judging from Fig.4.22. In some growth conditions, more HCl (which expectedly caused release of more Si species) caused lower Si/C ratios. It was speculated that the release of C species was also happening during the growth with HCl. The conventional model of adding HCl suggests that only Si species would be released from the gas-phase clusters to enhance the supply of Si source to the growth surface. The conventional model is incapable of explaining why the carbon supply is enhanced during the HCl-assisted dissociation of the Si gas-phase clusters in certain ranges of the HCl flow rates shown in Fig.4.22. Consequently, carbon involvement in the gas-phase homogeneous nucleation process should be considered. Also, reduction of $R_g$ with HCl addition for some ranges of HCl flow rates requires an additional precursor depletion

mechanism caused by HCl. A model for C involvement in the gas-phase clusters and a model for additional precursor depletion are introduced further in this work.

### 4.3.3 The Growth Rate Dependence on the Precursor Flow Rates

As was described above, in the experiments without HCl, the growth rate dependence on the silane flow rate at growth temperature of 1300$^{o}$C was complex (Fig.4.13). The dependence was influenced by the homogeneous gas-phase nucleation and the resulting saturation of Si supply to the growth surface at high $SiH_4$ flows. It was expected that this kind of saturation would be eliminated by adding HCl and lead to higher growth rates when $SiH_4$ flow is increased. The effect of adding HCl on $R_g$ was expected to be more pronounced for higher $SiH_4$ flow rate than for the lower ones.

The experimental results of the precursor flow dependencies for HCl-assisted growth showed a more complex trend than what was expected. The $R_g$ dependence on $CH_3Cl$ flow was normal when HCl was added. The $R_g$ increased with the increasing $CH_3Cl$ flow rate. However, the $R_g$ dependence on $SiH_4$ flow became more complicated when HCl was present during the growth. The $R_g$ showed a weak dependence on $SiH_4$ flow rate for a wide range of $SiH_4$ flows from below 4 to above 30 sccm. Moreover, at yet higher $SiH_4$ flow rate, $R_g$ downstream of the growth zone was decreasing.

In combination with the observation of the deteriorated $R_g$ homogeneity from upstream to downstream and $R_g$ reduction with HCl flow at certain HCl flow rates reported in section 4.3.2, the weak growth rate dependence on the $SiH_4$ flow suggested a possibility of an additional mechanism of growth rate species depletion in the presence of HCl. The rapid increase of the $R_g$ upstream and the fast drop of the $R_g$ downstream when

HCl was used suggested that the thermal decomposition of $SiH_4$ might start even before entering the growth zone of the susceptor. It may be possible to observe what was happening in the upstream portion of the hot zone (before the gas flow enters the growth zone) if the carrier gas flow is increased. By increasing the carrier gas flow, the gas-phase reactions will be delayed and shift into the growth zone. The differences will reflect on the changes happened to the substrates. Therefore, the dependences were also investigated at higher $H_2$ carrier gas flow rates to evaluate the earlier stages of the gas-phase kinetics. At $H_2$ flow of 2.5 slm, the $R_g$ dependence on the $CH_3Cl$ flow rate remained normal. The $R_g$ was increasing with increasing the $CH_3Cl$ flow (Fig.4.24 and 4.25(a)). Fig.4.24 shows the growth rate dependence of the center point on each sample,

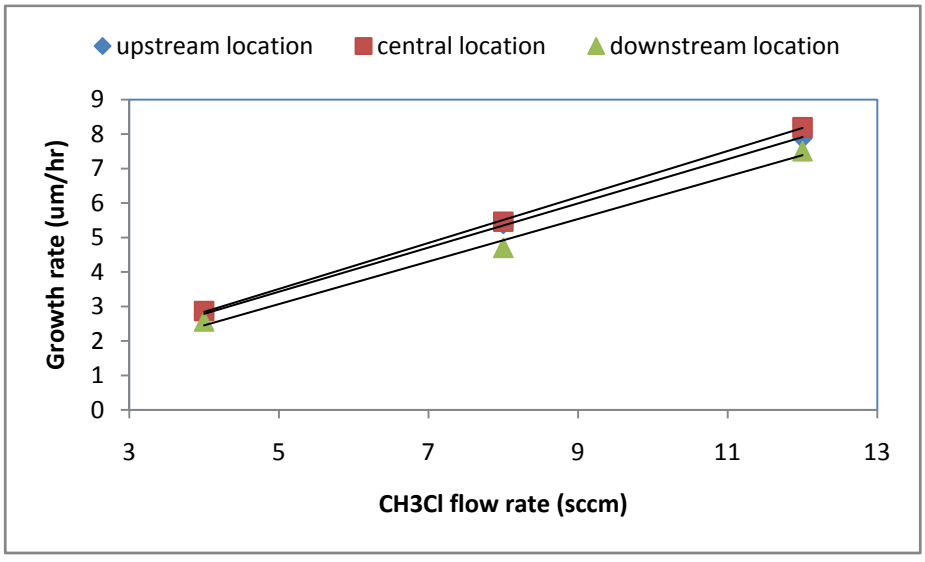


Fig.4.24: The $R_g$ dependence on the $CH_3Cl$ flow rate with HCl additive. The growth rate data were taken at the center of each sample. The samples were placed at the upstream, center, and downstream portion of the growth zone. All the other conditions were the same except the $CH_3Cl$ flow rate. The $R_g$ has a linear dependence on the $CH_3Cl$ flow.

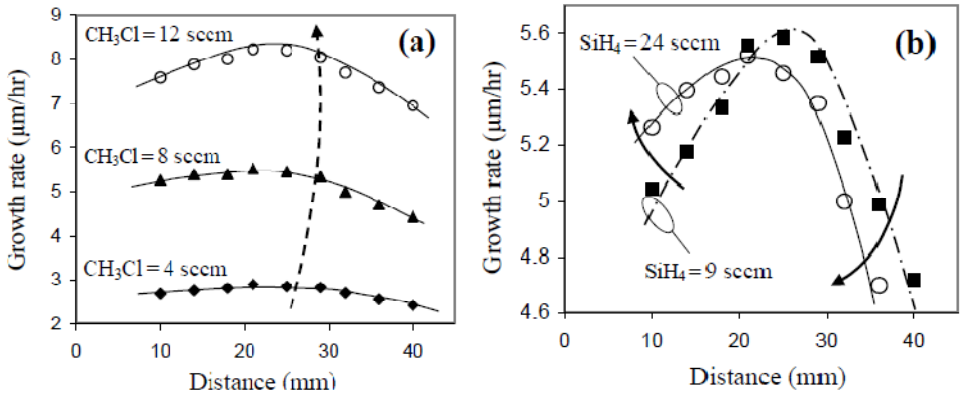


Fig.4.25: Growth rate at higher carrier gas flow velocity as a function of the distance from the leading edge of the growth zone downstream for **(a)** different values of $CH_3Cl$ flow rates, and **(b)** different values of $SiH_4$ flow rates. The HCl flow rate was 22 sccm.

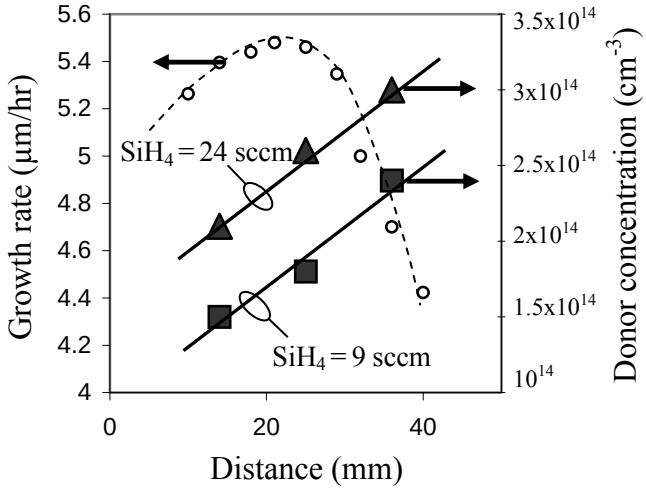


Fig.4.26: The net donor concentration at higher carrier gas flow velocity as a function of the distance from the leading edge of the growth zone for different values of $SiH_4$ flow rates. The growth rate profile for the $SiH_4$ flow of 24 sccm from Fig.4.25(b) is also shown for comparison. The HCl flow rate used was 22 sccm.

placed at upstream, center, and downstream portion of the growth zone, on the $CH_3Cl$ flow rate. A linear relationship was revealed for the $R_g$ dependence on the $CH_3Cl$ flow rate (Fig.4.24). However the $R_g$ dependence on the $SiH_4$ flow in presence of HCl remained weak (Fig.4.25(b)), similar to the HCl-assisted growth with a lower carrier gas flow rate. While $R_g$ in the upstream portion of the growth zone did show a slight increase (~5%) when the $SiH_4$ flow rate changed from 9 to 24 sccm, the downstream region showed a reverse correlation (lower $R_g$ at higher $SiH_4$ flows). In order to reveal the cause(s) of the weak dependence of $R_g$ on $SiH_4$ flow rate, the net donor concentration was examined.

Fig.4.26 shows that the net donor concentration somewhat increases from upstream to downstream, even though $R_g$ was reduced downstream. The increase of the donor concentration indicates that the Si/C ratio increases. More depletion of the Si source should cause decrease of the Si/C ratio, but in fact, the Si/C ratio increases. A plausible explanation is that the carbon source depletion overweighed the silicon source depletion under these growth conditions.

In summary, it can be concluded that a significant depletion of carbon species must be taking place in presence of HCl based on the following observations:

(1) $R_g$ decreases from upstream to downstream, when $SiH_4$ flow is increased.

(2) $R_g$ also decreases (at least in the downstream regions) with increasing the $SiH_4$ flow, and

(3) the decrease of $R_g$ from upstream to downstream is accompanied with little change or even slight increase (not decrease) of the effective Si/C (as determined from changes in doping).

### 4.3.4 HCl-enhanced Polycrystalline Deposition in the Upstream Portion of the Hot Zone

Severe morphology degradation in the form of polycrystalline islands appeared in the upstream portion of the growth zone when $H_2$ flow rate increased to 2.5 slm (Fig.4.27(a)). The $R_g$ non-homogeneity caused by HCl from upstream to downstream did not improved, either. The size of the polycrystalline islands and the island concentration reduced from upstream to downstream. The average size of the islands observed on the substrate was proportional to the HCl flow rate (Fig.4.27(b)). In contrast, the polycrystalline deposition in the growth zone was insignificant in the growth experiments at the same flow conditions but without HCl.

To investigate the formation of the polycrystalline islands in the more upstream portions of the hot zone, a few small pieces of SiC substrates were placed in the upstream region of the susceptor at different distances from the leading edge of the susceptor, as well as on the protruding portion of the thermal insulation foam upstream from the susceptor. Observation of the pattern of the island formation on those pieces provided some information about the gas-phase and surface reactions at the corresponding location of the upstream portion of the hot zone.

The surface morphology for a no-HCl growth experiment and for a growth experiment with the HCl flow rate at 22 sccm is shown in Fig.4.28(a-e) and Fig.4.28(f-j),

respectively. Micrographs (a) and (f) correspond to the most upstream samples. The numbers in units of mm at the bottom of Fig.4.28 correspond to the distance of each substrate from the leading edge of the susceptor. A positive number means that the sample was positioned on the susceptor, and a negative number means that the sample was position on the insulation foam (upstream from the susceptor). The upstream edge of the susceptor is the reference zero.

No epitaxial growth and no polycrystalline deposition were observed till the position that is 20 mm from the leading edge of the susceptor (Fig.4.28(a) and (f)). Obviously, there is no precursor decomposition at this distance from the susceptor.

At the location closer to the hot region of the susceptor (-10 mm upstream from the leading edge of the susceptor), quick decomposition of $SiH_4$ takes place. As a result of the availability of high concentration of silicon growth species, polycrystalline deposit formed in Fig.4.28(b) and (g). Powder XRD spectra shown in Fig.4-29(a) indicated that the polycrystalline deposits at this position contained only Si. XRD also indicated that somewhat higher concentration of the polycrystalline deposits in the sample without HCl compared to the experiments with HCl addition was found at these locations.

More pronounced differences between the polycrystalline deposits for the growth processes with and without HCl took place in the regions closer to the growth zone. For the sample placed inside the susceptor at 10 mm downstream from its leading edge, the growth without HCl showed drastic reduction of the polycrystalline deposits (Fig.4.28(c)). Separated polycrystalline islands observed are surrounded by areas with the normal epitaxial growth. XRD revealed that carbon is also present in those deposits at this

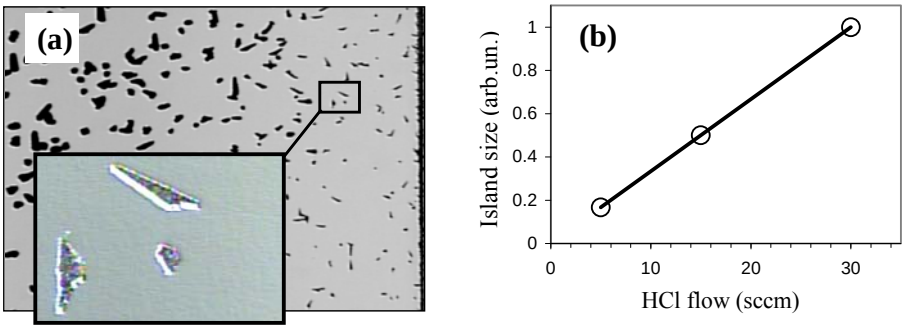


Fig.4.27: (a) Polycrystalline islands formed at the upstream portion of the SiC substrate when the gas flow velocity was increased in an attempt to improve $R_g$ homogeneity. (b) The average normalized size of the islands as a function of the HCl flow rate.

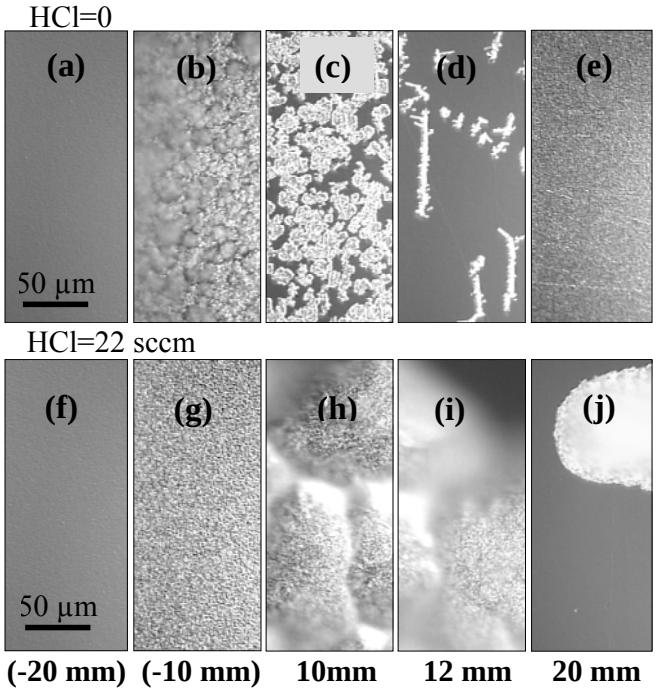


Fig.4-28: Optical micrographs of the polycrystalline deposits on pieces of SiC wafers placed in the upstream regions of the hot zone: the top - no HCl, and the bottom - with HCl=22 sccm. Location of (a), (f) was 20 mm upstream from the susceptor, (b), (g) 10 mm upstream from the susceptor, (c), (h) inside the susceptor 10 mm from its upstream edge, (d), (i) inside the susceptor 12 mm from its upstream edge, and (e), (j) inside the susceptor 20 mm from its upstream edge (which is 5 mm from the substrate).

location in the form of polycrystalline SiC (Fig.4.29(b)) while polycrystalline Si is still dominating. The presence of carbon in the polycrystalline deposits at this location and its absence at more upstream locations can be explained by the fact that $CH_3Cl$ decomposes slower than $SiH_4$, so carbon becomes available for incorporating in the polycrystalline deposits only closer to the susceptor. As discussed in more details below, the reduction in the concentration of the polycrystalline islands at the locations of Figs. 4.28(c)(d) compared to the more upstream location of Fig. 4.28(b) can be explained by consumption of Si species in the gas-phase homogeneous-nucleation process thus making less silicon species available to participate in the polycrystalline deposition.

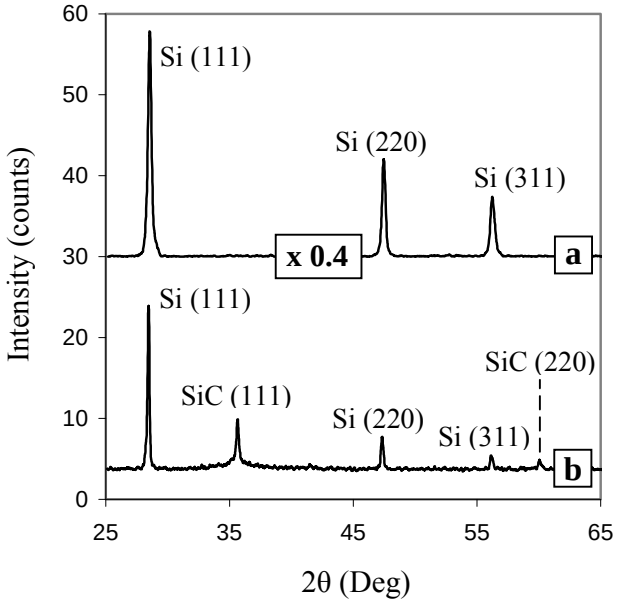


Fig.4.29: XRD spectra of the polycrystalline deposits after epitaxial growth without HCl at different locations of the hot zone along the gas flow direction: (a) more upstream location corresponding to Fig.4-28(b), and (b) more downstream location corresponding to Fig.4-28(c). The spectra are shifted in the vertical direction for clarity. The spectrum (a) is scaled down 0.4 times.

At the location of 12mm downstream from the leading edge of the susceptor, the islands become even rarer (Fig.4.28(d)). At the distance of 20 mm from the leading edge of the susceptor (Fig.4.28(e)), no polycrystalline deposits were observed in the experiments without HCl, but the epilayer morphology deteriorated (very rough), which could suggest low value of the effective Si/C ratio at these locations.

For the growth with high HCl flows, the most pronounced differences from the no-HCl case started with the sample placed inside the susceptor 10mm downstream from its leading edge (Fig.4.28(h)). There is no reduction of the polycrystalline deposits in this region compared to the more upstream locations in contrast to the no-HCl growth (Fig.4.28(c)). Actually, the polycrystalline deposition appears to be more significant according to XRD results.

The polycrystalline deposition rate in the experiment with HCl starts gradually decreasing from upstream to downstream when approaching the growth zone, but the transition is much slower than that in the experiments without HCl. The sample placed 12 mm downstream from the susceptor leading edge (Fig.4.28(i)) shows almost as strong deposits as the more upstream sample (Fig.4.28(h)), with only rare space between the polycrystalline islands.

Fig.4.28(j) shows the relatively large islands of polycrystalline deposits even at the location of 20 mm downstream from the leading edge of the susceptor (only 5mm from the growth zone). This is in contrast to the growth without HCl (Fig.4.28(e)), in which polycrystalline deposits are absent at the same location. In addition, the surface morphology of the epilayer in this region, in the locations free from polycrystalline

deposits, is much better in the growth with HCl than that in the growth without HCl. A better morphology allows one to suggest that the effective Si/C ratio in this region is higher when HCl is used.

Fig.4.30 shows the relative intensity of the XRD lines as a function of the distance along the gas flow direction, which was used as a more quantitative measure of the density of the polycrystalline deposits. The distance of 45 mm in Fig.4.30 corresponds to the leading edge of the susceptor. Therefore, the polycrystalline deposition started at approximately the same distance from the susceptor for any HCl flow, which happens before the gas mixtures entered the susceptor or the growth zone. The end of the polycrystalline zone clearly depends on the HCl flow rate. The end-zone extended farther into the growth zone when higher HCl flow rates were used.

It is important to understand at what position along the gas-flow direction the transition from the upstream formation of polycrystalline deposits (or a coexistence of polycrystalline deposition and epitaxial growth) to the desirable epitaxial growth without polycrystalline phases more downstream takes place, and what factors are responsible for this transition. It can be speculated that this transition happens due to the temperature increase when approaching the hot susceptor and then moving deeper inside the susceptor.

It is suggested in this work that the influence of the temperature increase inside the susceptor can be excluded as the main factor responsible for this transition. From Fig.4.27, the experiments with higher $H_2$ flow rates indicated that polycrystalline deposits may form even inside the susceptor where the temperature is at its maximum value. According to the computational fluid dynamics simulations (conducted in our group),

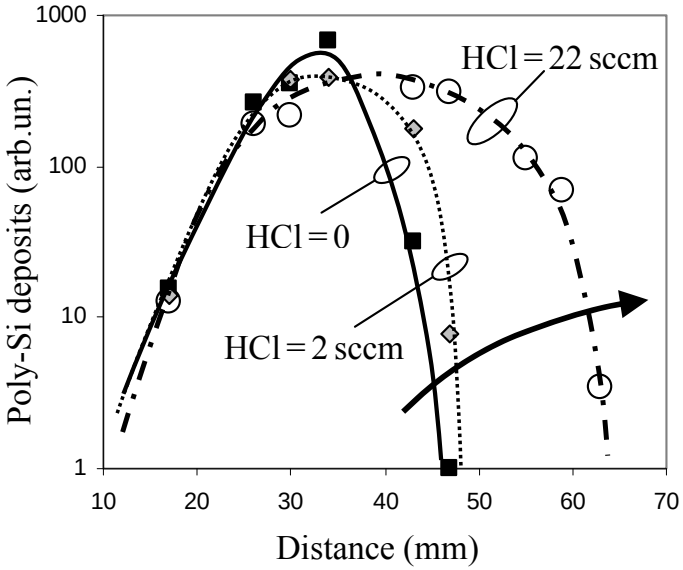


Fig.4.30: Relative amount of the polycrystalline Si deposition in the upstream portion of the hot zone as a function of the distance along the gas flow direction for two different values of HCl flow rates compared to growth without HCl. The amount of deposition was determined from XRD spectra.

higher $H_2$ flow rates do not influence the temperature profile in the growth zone significantly enough to be responsible for the polycrystalline deposition in the growth zone shown in Fig.4.27.

It is more logical to consider the gas-phase reaction kinetics to be responsible for the boundaries of the polycrystalline deposits. The early decomposition products of $SiH_4$ and/or very high concentrations of species delivered to the wall surfaces are responsible for the polycrystalline deposition when the supply of $SiH_4$ is sufficiently high (e.g., Fig.4.28(b) and (g)).

The quick reduction of the polycrystalline deposition in the regions of the hot zone closer to the growth zone (i.e., regions shown in Fig.4.28(c)-(d)) in the growth without HCl can be explained by the Si gas-phase homogeneous nucleation discussed above. Consumption of Si-containing products of $SiH_4$ decomposition by the Si clusters in the gas phase makes less Si available for the polycrystalline deposition. Consequently, there is less Si further downstream and consequently less polycrystalline deposits (Fig.4.28(c)). Meanwhile, the temperature at these locations is high enough to cause significant decomposition of the carbon precursor $CH_3Cl$. The depletion of Si by the gas-phase clustering and the significant supply of carbon results in a low value of Si/C ratio and the deterioration of the surface morphology of the epitaxial growth (Fig.4.28(e)).

Deeper inside the susceptor, the higher temperatures in the growth zone cause the reverse process - dissociation of the Si gas-phase clusters. As a result, the effective Si/C ratio increases, which results in the good epilayer quality. However, significant amount of clusters remains intact and limits the Si-species supply to the growth surface and consequently the growth rate [124].

The kinetics is different when HCl is added. Formation of intermediate $Si_xCl_y$ products in the gas phase or the etching/dissociation of newly formed Si clusters by Cl-containing reaction products in the upstream portion of the hot zone significantly reduces the Si consumption by the clustering mechanism. However, this surplus supply of Si species causes a higher polycrystalline deposition in the upstream portion of the hot zone than that without HCl (Fig.4.28(h)-(j) versus Fig.4.28(c)-(e)).

At the location that is closer to the growth zone, HCl reduces the depletion of Si species by the homogeneous nucleation mechanism, which ensures higher values of the effective Si/C ratio and improve the epilayer morphology in Fig.4-28(j) compared to that in Fig.4.28(e).

The broader zone of polycrystalline deposition when HCl is present serves as an additional mechanism for depletion of silicon and carbon precursors. The release of Si species from gas-phase clusters causes the formation of polycrystalline Si islands. Formation of those islands intensifies consumption of carbon species that also get incorporated in those islands. Consequently, the islands consume (i.e., deplete) both Si and C precursors, which may cause the reduction of $R_g$ in the growth zone.

It follows from the above discussion that dissociation of the gas-phase clusters may serve as a source of additional supply of the growth species, but it may also intensify their depletion by the polycrystalline deposition upstream of the growth zone. Consequently, the effect on the growth rate may be complicated, which is what was observed in section 4.3.2 (Fig. 4.21 and 4.22). In the light of the new evidences, the growth rate increase upstream in Fig.4-21 (with HCl addition) can still be explained by the dissociation of the gas-phase clusters. Compared to the growth without HCl, these gas-phase clusters get etched or dissociated by HCl, and the released species can reach the growth zone of the reactor to increase the $R_g$. When higher HCl flow rates were delivered, the overwhelming release of the Si species caused the polycrystalline deposition; therefore $R_g$ increased less than expected, and it also reduced from upstream to downstream inside the growth zone.

This new mechanism of depletion is also likely to be responsible for the complex dependence of $R_g$ on the HCl flow rate (Fig.4.22). At some HCl flow rates, the depletion of the growth species caused by the polycrystalline deposition outweighed the enhancement of the Si supply to the growth zone caused by HCl-induced dissociation of the gas-phase clusters. This additional depletion mechanism results in insufficient increase of the $R_g$ or even its reduction (e.g., downstream of the growth zone).

As mentioned previously, the precursor depletion by the polycrystalline deposition involves not only silicon but also carbon species. The results of XRD revealed the presence of carbon in the polycrystalline deposits (Fig.4.29(b)). However, apparently, the depletion of silicon and carbon gas-phase species is not equal and depends on the HCl flow rate. This could at least partially explain the complex dependence of the effective Si/C ratio on the HCl flow rate (Fig.4.22). To explain the entire dependence of the effective Si/C ratio on the HCl flow rate, the involvement of carbon in the gas-phase clusters should be considered.

### 4.3.5 The Involvement of Carbon in Gas-Phase Clusters

Most of the investigations of the homogeneous gas-phase nucleation for SiC epitaxial growths suggest that the clusters in the gas phase contain only Si when the concentration of Si vapor reaches a supersaturation value. Only a few references proposed the involvement of carbon in the Si gas-phase clusters (i.e., the formation of Si-$Si_xC_{1-x}$ clusters) in the high-temperature CVD experiments [122-123]. In those papers, the growth temperature was at the range of 1620~1900$^oC$. It has been reported that 3C-SiC microcrystals existed in the gas-phase clusters in the case of atmospheric CVD using a

$SiH_4$-$CH_4$-$H_2$ system at 1400°C [157]. For amorphous $Si_xC_{1-x}$ particles, severe $H_2$ etching occurs at temperature over 1400°C [158]. In the case of our low-temperature epitaxial growth, the $Si_xC_{1-x}$ particles might be formed in the gas-phase clusters and etched by HCl additive, and this results in complex change of the effective Si/C ratio at the surface of the growing epilayer when HCl is added. This will be discussed in the following paragraphs.

It is difficult to explain the reduction of the effective Si/C ratio accompanied by the increase of $R_g$ at low HCl flow rates up to 3 sccm in Fig.4.22 without suggesting that gas-phase clusters involves a significant amount of carbon in addition to silicon. A possible release of carbon, which outweighed that of Si, from the gas-phase clusters, would explain the increase of $R_g$ and the reduction of Si/C ratio at low HCl flows. Since the carbon precursor $CH_3Cl$ dissociates later (i.e., farther downstream) than $SiH_4$, the carbon probably gets incorporated in the gas-phase clusters after the silicon core of the clusters

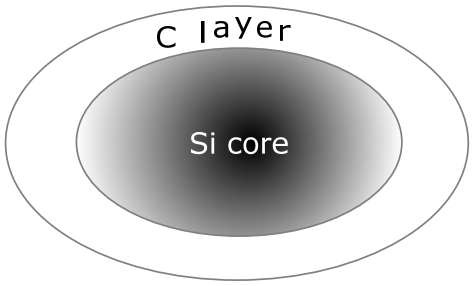


Fig.4.31: A schematic representation of the structure of a Si-C-cluster formed by the gas-phase homogeneous nucleation. The predominantly Si core of the cluster forms upstream of the hot zone. The carbon layer encloses the Si-cluster core because the $CH_3Cl$ precursor dissociates later in the hot zone.

had been formed (Fig.4.31). This would explain why the release of carbon is outpacing the release of Si at low HCl flows. The small HCl flow is only sufficient to etch the carbon-rich top layers of the clusters. It should be noted, that this work suggested for the first time that not only silicon but also carbon is captured in the gas-phase clusters during the low-temperature epitaxial growth.

The complex influence of adding HCl during the low-temperature epitaxial growth can be discussed as the following:

(1) At the HCl flow rate below 2 sccm shown in Fig.4.22, the predominant supply of carbon species over the silicon supply is caused by the fact that the amount of HCl is only sufficient to etch the outer layer of the gas-phase clusters containing carbon (Fig.4.31). This causes the increase of $R_g$ and the reduction of the effective Si/C ratio.

(2) The low-to-intermediate HCl supply below 5 sccm in Fig.4.22 is sufficient to etch clusters further. Once the outer carbon-rich layer is removed, the release of silicon dominates, which causes the increase of $R_g$ and the effective Si/C ratio with HCl flow. The intensive release of Si from the gas-phase clusters also causes the formation of polycrystalline deposits upstream of the hot zone. Being too much upstream, those deposits do not involve carbon species since the carbon precursor is not yet dissociated at this location.

(3) Intermediate HCl flows from 5 to approximately 8 sccm in Fig.4.22 form the polycrystalline deposits closer to the susceptor by enhanced etching of the gas-phase clusters. In this region, a significant fraction of $CH_3Cl$ is already dissociated, and this provides carbon incorporated in the polycrystalline deposits. Therefore, the carbon

gets depleted by the formation of the polycrystalline islands. Meanwhile, the enhanced etching of the clusters provides more Si species from the Si core of the clusters for both polycrystalline deposition upstream and epitaxial growth in the growth zone. The depletion of carbon with still significant silicon supply causes the sharp reduction of $R_g$ and increase of the Si/C ratio with HCl flow in this range.

When higher HCl flow rates above 10 sccm are provided (Fig.4.22), essentially all the gas-phase clusters are dissociated. No significant effect is observed for still higher HCl flows. The moderate increase of the $R_g$ and decrease of the Si/C ratio could be the results of other factors such as the influence of HCl on the surface kinetics of the epitaxial growth or/and a moderate etching of the graphite insulation foam, etc.

The effect of HCl on the pattern of the polycrystalline deposits does not affect the growth rate dependence on $CH_3Cl$ flow rates (Fig.4.25(a)). The consumption of carbon by the polycrystalline deposition is proportional to the Si-source supply by the release either from the gas-phase clusters or directly from the Si-related products of $SiH_4$ thermal decomposition; therefore the increase of the $CH_3Cl$ flow rates does not affect the efficiency of the deposits' formation. Consequently, the growth rate dependence on the $CH_3Cl$ flow rate showed a linear relationship with HCl (Fig.4.25(a)).

If the $SiH_4$ flow is increased in the presence of HCl, the efficiency of the polycrystalline deposition is enhanced upstream. This enhances the polycrystalline deposition-related depletion mechanism, which results in much less significant increase or even decrease of $R_g$ with increasing the $SiH_4$ flow rate.

### 4.3.6 Possible Influence of HCl addition on gas-phase reactions other than homogeneous gas-phase nucleation

The conventional consideration of the chemistry of the HCl effect on gas-phase reactions predominantly focuses on formation of Si-Cl bonds, which effectively results in suppressed formation of the homogeneous nucleation or dissociation/etching of the already formed gas-phase clusters.

In this work, the enhanced carbon supply (i.e., increased effective C/Si ratio) apparently observed at small HCl flow rates is explained by involvement of carbon in the gas clusters and its enhanced release caused by HCl. All the other possible causes for increasing C/Si ratio would provide monotonous increase of this ratio for yet higher HCl flow rates, which is not what was observed experimentally.

However, one more possible source of the enhancement of the carbon supply should be considered. It could be speculated that more carbon is coming from the HCl-enhanced gas-phase reactions leading to dissociation of $CH_3Cl$ (i.e., reactions not involving gas-phase cluster nucleation). To consider this possibility, we have to start by assuming that the reactions of $CH_3Cl$ decomposition proceed far from equilibrium, and significant portion of $CH_3Cl$ remains not dissociated when passing the growth zone of the reactor.

The kinetics of chlorocarbon precursor's ($CH_3Cl$) decomposition was investigated by Yo-Ping Wu et al. [159]. The major products of the pyrolysis of $CH_3Cl$ in the $H_2$ environment are $CH_3$, HCl, $CH_4$, $C_2H_4$, and $C_2H_6$.

The main reaction pathways for $CH_3Cl$ decomposition in $H_2$-reach ambient are:

$$CH_3Cl = CH_3 + Cl \quad (4\text{-}1)$$

$$CH_3Cl + H = CH_3 + HCl \quad (4\text{-}2)$$

Some of the minor pathways are:

$$CH_3Cl = CH_2(S) + HCl \quad (4\text{-}3)$$

$$CH_3Cl + Cl = CH_2Cl + HCl \quad (4\text{-}4)$$

Presence of extra chlorine (as coming from HCl addition) favors the reverse reaction according to the equations (4-1)-(4-3), thus effectively reducing (not enhancing) the efficiency of the carbon source dissociation and supply of adatoms to the growth surface.

Only in the minor pathway according to the reaction (4-4), addition of Cl (as a product of HCl decomposition) appears to favors the forward reaction of the carbon precursor decomposition. However, this is a very minor pathway; also presence of HCl simultaneously favors the reverse reaction. The presence of both Cl and HCl are expected at our growth temperatures. Therefore, dissociation of the carbon precursor providing C species for the epitaxial growth will be suppressed rather than enhanced when HCl is added according to all possible reaction pathways (not involving homogeneous nucleation of the gas-phase clusters). This eliminates also this mechanism for explaining the increase of the effective C/Si ratio at certain HCl flow rates, which leaves us with the explanation that the extra carbon supply is coming from the dissociated $Si_xC_{1-x}$ layers.

### 4.3.7 Summary

The experimental results showed that the effect of adding HCl introduced more complex gas-phase reactions than just etching the silicon clusters in the gas phase. The enhanced dissociation of the silicon clusters in the gas phase indeed took place. It led to an additional supply of silicon species for the epitaxial growth, but the apparent value of the effective Si/C ratio on the growing surface exhibited a very complex dependence on the HCl flow rate. The results suggested that significant amount of carbon species (in addition to silicon) was incorporated in the gas-phase clusters and was released from the gas-phase clusters along with the silicon cluster etching by HCl. In addition, polycrystalline island formation at the upstream portion of the hot zone was revealed as a new mechanism for precursors' depletion.

HCl was found efficient in dissociating clusters in the gas phase not only at the traditionally high epitaxial growth temperatures [136-137], but also at temperatures as low as 1300$^{o}$C and below investigated in this work. However, new properties of the gas-phase clusters have been identified. Dissociation of the gas-phase clusters results in the increase of not only silicon supply but also carbon supply during the epitaxial growth. The experimental results are consistent with a hypothesis that the gas-phase clusters are not just clusters of silicon but Si-$Si_xC_{1-x}$ complexes.

The behavior of the polycrystalline deposition in the upstream portion of the hot zone revealed how exactly the gas-phase cluster etching by HCl progressed along the gas flow direction from the upstream portion of the hot zone (upstream the susceptor) and closer towards the growth zone inside the susceptor. The enhanced supply of $SiH_4$ does

not contribute to any significant increase of the polycrystalline deposition in the growth experiments without HCl because of the quick capture of Si by the homogeneous gas-phase nucleation. Consequently, in the absence of HCl, the gas-phase clustering effect prevents the polycrystalline deposition from extending further into the growth zone. When HCl is added, significant release of silicon and carbon causes the development of the polycrystalline deposition farther downstream inside the hot zone closer to the growth zone. This additional deposition depletes significant amount of silicon and carbon, which may cause much less significant increase or even decrease of the $R_g$ in the growth zone when HCl is added. It also causes changes of the Si/C ratio depending on the HCl flow rate. The additional polycrystalline deposition-related precursors' depletion mechanism qualitatively explained all major experimental results of our halo-carbon low-temperature epitaxial growth. A quantitative model for the HCl-assisted growth is under development for a more comprehensive understanding of the kinetics of the gas-phase reactions.

# CHAPTER 5

# CONCLUSIONS AND FUTURE WORK

The experimental results reported in this work demonstrated a possibility of conducting homoepitaxial growth of 4H-SiC at temperatures significantly lower than what was previously believed possible. High-quality 4H-SiC epitaxial films with specular surfaces at growth temperatures of 1300$^{o}$C (or lower) were achieved by using halo-carbon precursor chloromethane. Differences in gas-phase kinetics and surface reactions allow one to achieve the desirable step-flow growth at such low temperatures, which is not possible or difficult to achieve when using the conventional $SiH_4$-$C_3H_8$-$H_2$ systems.

The growth-rate-limiting mechanisms during the low-temperature halo-carbon epitaxial growth were investigated. The main process dependencies and activation energies were established. The homogeneous nucleation leading to formation of silicon clusters in the gas phase was found to be the major limiting factor for increasing the growth rate without morphology degradation.

A capability of HCl to suppress homogeneous nucleation was investigated. By adding HCl during the low-temperature epitaxial growths, a significant reduction of the Si condensation was achived, which increased supply of Si-related species for the epitaxial growth and resulted in drastic increase of the growth rate and improved surface morphology.

However, it was established that complex trends of low-temperature growth in presence of HCl can not be explained by the commonly accepted mechanisms of HCl influence. The investigation of the polycrystalline deposition at the upstream section of the hot zone of the reactor provided justification for a new precursors' depletion hypothesis. Also, the common assumption that only silicon species are involved in the gas-phase clusters failed to explain the complex behaviors of the dependences of the $R_g$ and the doping concentration on the HCl flow rate. The complex non-monotonous dependences indicated that HCl-assisted dissociation of the gas-phase clusters leads to release of not only silicon but also carbon. Only a few groups in the world speculated about involvment of carbon in the gas-phase clusters during the epitaxial growth. This work indicated that carbon consumption by homogeneous nucleation (gas-phase cluster formation) as well as its release during cluster dissociation (thermally induced or HCl-enhanced) plays an important role during the low-temperature epitaxial growth.

The newly established precursor depletion mechanism (HCl-enhanced polycrystalline deposition) and the mechanism of additional supply of carbon caused by gas-phase cluster dissociation qualitatively explained the experimental results reported in this work. However, a quantitative model will be needed for better understanding of the epitaxial growth mechanism when HCl is present in the $SiH_4$-$CH_3Cl$-$H_2$ growth system.

In summary, the sole use of $CH_3Cl$ was found not sufficient for eliminating the Si cluster formation in the gas phase. Although adding HCl improves the growth rate and surface morphology, the growth rate homogeneity along the gas-flow direction was compromised due to the additional precursor depletion mechanisms summarized above.

Replacing silane with chlorinated Si-precursor (for example: $SiCl_4$) may provide additional chlorine-containing intermediate species and further increase the growth rate without morphology degradation and improve the growth rate homogeneity. A further investigation of using halo-precursors should benefit the 4H-SiC epitaxial growths for the industrial applications.

# BIBLIOGRAPHY


[1] Adrian R. Powell and Larry B. Rowland, member, IEEE, "*SiC materials-progress, status, and potential roadblocks*", *PROCEEDINGS OF THE IEEE, VOL. 90, NO. 6, JUNE 2002.*

[2] F. Bechstedt, P. Käckell, A. Zywietz, K. Karch, B. Adolph, K. Tenelsen, and J. Furthmüller, *"Polytypism and Properties of Silicon Carbide", phys. Stat. sol. (b) 202, 35 (1997).*

[3] N. W. Jepps and T. F. Page, *"Polytypic transformations in silicon carbide"*, *Progr. Cryst. Growth Charact. 7, 259 (1983).*

[4] M. G. Spencer, John Palmour, and Calvin Carter, *"Substrate and Epitaxial Issues for SiC Power Devices", IEEE TRANSACTIONS ON ELECTRON DEVICES, VOL. 49, NO. 5, MAY 2002, pp.940-945.*

[5] Neudeck, P. G., Huang, W. & Dudley, M. *"Breakdown degradation associated with elementary screw dislocations in 4H-SiC p + n junction rectifiers", Solid-State Electron.* ***42****, 2157−2164 (1998).*

[6] Lendenmann, H. *et al. "Long term operation of 4.5 kV PiN and 2.5 kV JBS diodes", Materials Science Forum Vols. 353−356(2001) pp.727−730.*

[7] Robert T. Bondokov, Tsanko Lashkov and Tangali S. Sudarshan, *"Influence of Structural Defects on the Polishing of Silicon Carbide Single Crystal Wafers", J. J. Appl. Phys. Vol. 43, No. 1 (2004), pp. 43-49.*

[8] Malhan, R. K., Nakamura, H., Onda, S., Nakamura, D. & Hara, K. *"Impact of SiC structural defects on the degradation phenomenon of bipolar SiC devices", Material Science Forum Vols. 433−436(2003) pp. 917−920.*

[9] Philip G. Neudeck, *"Electrical Impact of SiC Structural Crystal defects on High Electric Field Devices", Materials Science Forum Vols. 338-342 (2000) pp. 1161-1166.*

[10] M. R. Goulding, *"The selective epitaxial growth of silicon", Mater. Sci. Eng. B17, 47 (1993).*

[11] K. Kojima, H. Okumura, S. Kuroda, K. Arai, *"Homoepitaxial growth of 4H-SiC on on-axis (000-1) C-face substrates by chemical vapor depositon", Journal of Crystal Growth 269 (2004) pp.367-376.*

[12] Tsunenobu Kimoto and Hiroyuki Matsunami, *"Nucleation and step motion in chemical vapor deposition of SiC on 6H-SiC{0001} faces", J. Appl. Phys. 76 (1994), pp.7322-7327.*

[13] Y. Chen, T. Kimoto, Y. Takeuchi, H. Matsunami, *"Selective homoepitaxy of 4H-SiC on (0 0 0 1) and (11-20) masked substrates", Journal of Crystal Growth 237-239 (2002) pp.1224-1229.*

[14] A. S. Grove, *"Mass Transfer in Semiconductor Technology", Ind. & Eng. Chem., **58**, 48 (1996).*

[15] S. Wolf and R.N. Tauber, *"Silicon Processing for the VLSI Era, Volume 1-Process Technology", Chapter 6, second edition, LATTICE PRESS.*

[16] P. Singer, *"Techniques of Low Pressure CVD", Semiconductor International, pp. 72, May 1984.*

[17] R. S. Rosler, *"Low Pressure CVD Production Processes for Poly, Nitride, and Oxide", Solid State Technology **20**(4), 63 (April 1977).*

[18] S. Wolf and R. N. Tauber, *"Silicon Processing for the VLSI Era", Volume 1, Process Technology, LATTICE PRESS, ISBN: 0-9616721-6-1, chapter 6.*

[19] Masato Hiramatsu, Yoshinobu Kimura, Masayuki Jyumonji, Mikihiko Nishitaniy and Masakiyo Matsumura*,"Deposition of Pure Hydrogenated Amorphous Silicon by Plasma-Enhanced Chemical Vapor Deposition for Polycrystalline Silicon Thin Film Transistors", J. J. Appl. Phys**.** Vol. 44, No. 6A (2005), pp.3813-3816.*

[20] Shinya Tsuda, et. al., *"Preparation and Properties of High-Quality a-Si films with a Super Chamber (Separated Ultra-High Vacuum Reaction Chamber)", J. J. Appl. Phys**.** Vol. 26, No.1 January 1987, pp.33-38.*

[21] Lely J. A. 1955 *Silicium, Schwefel, Phosphate, Colloq. Sek. Anorg. Chem. Intern. Union Reine u. Angew. Chem. (Munster) pp.20–24.*

[22] Yu. M. Tairov and V. F. Tsvetkov, *"Investigation of growth processes of ingots of silicon carbide single crystals", Journal of Crystal Growth 43 (1978) pp.209-212.*

[23] Nishizawa S I, Kato T, Kitou Y, Oyanagi N, Hirose F, Yamaguchi H, BahngWand Arai K, *"High-Quality SiC Bulk Single Crystal Growth Based on Simulation and Experiment", Materials Science Forum Vols. 457-460 (2004) pp.29-34.*

[24] Nakamura D, Gunjishima I, Yamaguchi S, Ito T, Okamoto A, Kondo H, Onda S and Takatori K, *"Ultrahigh-quality silicon carbide single crystals", Nature (London) 430, pp.1009-1012(26 August 2004).*

[25] C. Basceri, I. Khlebnikov, Y. Khlebnikov, P. Muzykov, M. Sharma, G. Stratiy, M. Silan, and C. Balkas, *"Growth of Micropipe-Free Single Crystal Silicon Carbide (SiC) Ingots Via Physical Vapor Transport (PVT)", Materials Science Forum Vols. 527-529 (2006) pp.39-42.*

[26] O. Kordina, C. Hallin, A. Ellison, A. S. Bakin, and I. G. Ivanov, *"High temperature chemical vapor deposition of SiC", Appl. Phys. Lett. 69 pp.1456-1458 (1996).*

[27] Alexsandre Ellison, B. Magnusson, Björn Sundqvist, G.R. Pozina, J.P. Bergman, Erik Janzén, A. Vehanen, *"SiC Crystal Growth by HTCVD", Materials Science Forum Vols. 457-460 (2004) pp.9-14.*

[28] Peter Wellmann, Ziad Herro, Albrecht Winnacker, Roland Püsche, Martin Hundhausen, Pierre Masri, Alexey Kulik, Maxim Bogdanov, Sergey Karpov, Mark Ramm and Yuri Makarov, *"In situ visualization of SiC physical vapor transport crystal growth", Journal of Crystal Growth 275 (2005) pp.e1807-e1812.*

[29] Peter Wellmann, Patrick Desperrier, Ralf Müller, Thomas Straubinger, Albrecht Winnacker, Francis Baillet, Elisabeth Blanquet, Jean Marc Dedulle and Michel Pons, *"SiC single crystal growth by a modified physical vapor transport technique", Journal of Crystal Growth 275 (2005) pp.e555-e560.*

[30] Didier Chaussende, Magali Ucar, Laurent Auvray, Francis Baillet, Michel Pons,§ and Roland Madar, *"Control of the Supersaturation in the CF-PVT Process for the Growth of Silicon Carbide Crystals Research and Applications", Crystal Growth & Design, **5** (4), pp.1539 -1544, 2005.*

[31] D.Chaussende, C.Balloud, L.Auvray, F.Baillet, M.Zielinski, S.Juillaguet, M.Mermoux, E.Pernot, J.Camassel, M.Pons4 and R.Madar, *"Characterization of thick 2-inch 4H-SiC layers grown by the Continuous Feed - Physical Vapor Transport method",Materials Science Forum Vols. 457-460 (2004) pp.91-94.*

[32] D. Chaussende, L. Latu-Romain, L.Auvray, M.Ucar, M. Pons and R. Madar, *"Large Area DPB Free (111) b-SiC Thick Layer Grown on (0001) a-SiC Nominal Surfaces by the CF-PVT Method", Mater. Science Forum Vols. 483–485(2005) pp.225–228.*

[33] Daisuke Nakamura, Itaru Gunjishima, Satoshi Yamaguchi, Tadashi Ito, Atsuto Okamoto, Hiroyuki Kondo, Shoichi Onda, and Kazumasa Takatori, *"Ultra-high quality silicon carbide single crystals", Nature 430, 1009-1012 (26 August 2004).*

[34] Waage, P.; Guldberg, C. M. *"Studies Concerning Affinity" Forhandlinger: Videnskabs-Selskabet i Christiana* **1864,** 35.

[35] Jérôme Meziere e.t. al., *"Contribution of numerical simulation to silicon carbide bulk growth and epitaxy", J. Phys.: Condens. Matter **16** (2004) S1579–S1595.*

[36] Alessandro Veneroni, e.t. al., *"Modeling of epitaxial silicon carbide deposition", Journal of Crystal Growth 275 (2005) pp.e295–e300.*

[37] Ö. Danielsson, A. Henry, E. Janzén, *"Growth rate predictions of chemical vapor deposited silicon carbide epitaxial layers", Journal of Crystal Growth 243 (2002) pp.170–184.*

[38] C. D. Stinespring, J. C. Wormhoudt, *"Gas phase kinetics analysis and implications for silicon carbide chemical vapor deposition", Journal of Crystal Growth 87(1988) pp.481-493.*

[39] Mark D. Allendorf, and Robert J. Kee, *"A Model of Silicon Carbide Chemical Vapor Deposition", J Electrochem. Soc.* ***138****, pp.841-852 (1991).*

[40] P. M. Lofgren, W. Ji, C. Hallin, and C.-Y. Gu, *"Modeling of Silicon Carbide Epitaxial Growth in Hot-Wall Chemical Vapor Deposition Processes", J. Electrochem. Soc.* ***147****(1), pp.164-175 (2000).*

[41] Keiji Wadaa, Tsunenobu Kimotoa, Kimito Nishikawab, Hiroyuki Matsunami, *"Epitaxial growth of 4H–SiC on 4$^o$ off-axis (0 0 0 1) and (0 0 0-1 ) substrates by hot-wall chemical vapor deposition", Journal of Crystal Growth 291 (2006), pp.370–374.*

[42] Kazutoshi Kojima, Takaya Suzuki, Satoshi Kuroda, Johji Nishio and Kazuo Arai, *"Epitaxial Growth of High-Quality 4H-SiC Carbon-Face by Low-Pressure Hot-Wall Chemical Vapor Deposition", J. J. Appl. Phys. Vol. 42 (2003) pp. L 637–L 639.*

[43] Keiji Wada, Tsunenobu Kimoto, Kimoto Nishikawa, Hiroyuki Matsunami, *"Epitaxial growth of 4H-SiC on 4$^o$ off-axis (0001) and (000-1) substrates by hot-wall chemical vapor deposition", Journal of Crystal Growth 291 (2006) pp. 370-374.*

[44] Kodigala Subba Ramaiah, I. Bhat, T. P. Chow, J. K. Kim, E. F. Schubert, D. Johnstone, and S. Akarca-Biyikli, *"Growth and characterization of SiC epitaxial layers on Si- and C-face 4H-SiC substrates by chemical vapor deposition", J. Appl. Phys.* ***98.*** *106108 (2005).*

[45] Katsunori Danno, Koichi Hashimoto, Hiroaki Saitoh, Tsunenobu Kimoto, and Hiroyuki Matsunami, *"Low-Concentration Deep Traps in 4H-SiC Growth with High Growth Rate by Chemical Vapor Deposition", J. J. Appl. Phys. Vol. 43, No. 7B, 2004, pp. L 969-L 971.*

[46] Hiroyuki Matsunami, Tsunenobu Kimoto, *"Step-controlled epitaxial growth of SiC: high quality homoepitaxy", Materials Science and Engineering, R20 (1997) pp. 125-166.*

[47] Eric Pearson, Tadayoshi Takai, Timur Halicioglu and William A. Tiller, *"Computer modeling of Si and SiC surfaces and surface processes relevant to crystal growth from the vapor", Journal of Crystal Growth 70 (1984) pp. 33-40.*

[48] Tsunenobu Kimoto and Hiroyuki Matsunami, *"Surface diffusion lengths of adatoms on 6H-SiC{0001} faces in chemical vapor deposition of SiC", J. Appl. Phys.* ***78****(5), 1 September 1995.*

[49] Hiroyuki Matsunami, *"Technological Breakthroughs in Growth Control of Silicon Carbide for High Power Electronic Devices", J. J. Appl. Phys. Vol. 43, No. 10, 2004, pp. 6835-6847.*

[50] C. Hallin, A. O. Konstantinov, O. Kordina and E. Janzen: *Silicon Carbide and Related Materials 1995, eds.* S. Nakashima, H. Matsunami, S. Yoshida and H. Harima (Inst. of Phys., Bristol, 1996) pp. 85.

[51] A. A. Burk, Jr. and L. B. Rowland, *"The role of excess silicon and in situ etching on 4H-SiC and 6H-SiC epitaxial layer morphology", Journal of Crystal Growth* ***167*** *(1996) 586.*

[52] Akira Itoh, Hironobu Akita, Tsunenobu Kimoto, and Hiroyuki Matsunami, *"High-quality 4H-SiC homoepitaxial layers grown by step-controlled epitaxy", Appl. Phys. Lett. 65 (1994) 1400.*

[53] Kentaro Shibahara, Naotaka Kuroda, Shigehiro Nishino, and Hiroyuki Matsunami, *"Fabrication of P-N Junction Diodes Using Homoepitaxially Grown 6H-SiC at Low Temperature by Chemical Vapor Deposition***",** *J. J. Appl. Phys***.** *Vol. 26(1987) L1815-L1817.*

[54] J. A. Powell, D. J. Larkin, L. G. Matus, W. J. Choyke, J. L. Bradshaw, L. Henderson, M. Yoganathan, J. Yang, and P. Pirouz, *"Growth of high quality 6H-SiC epitaxial films on vicinal (0001) 6H-SiC wafers", Appl. Phys. Lett., vol. 56, no. 15, pp. 1442-1444, Apr. 1990.*

[55] Tsunenobu Kimoto, Hironori Nishino, Woo Sik Yoo, and Hiroyuki Matsunami, *"Growth mechanism of 6H-SiC in step-controlled epitaxy", J. Appl. Phys.* ***73*** *(2), 15 January 1993.*

[56] T. Kimoto, A. Itoh, and H. Matsunami, *"Step-Controlled Epitaxial Growth of High-Quality SiC Layers", phys. stat. sol. (b) 202, 247 (1997).*

[57] D. J. Larkin, *"SiC Dopant Incorporation Control Using Site-Competition CVD", phys. stat. sol. (b) 202, 305 (1997).*

[58] HS. KarmannH, HW. SuttropH, HA. SchönerH, HM. SchadtH, HC. HaberstrohH, HF. EngelbrechtH, HR. HelbigH, HG. PenslH, HR. A. SteinH, and HS. LeibenzederH, *"Chemical vapor deposition and characterization of undoped and nitrogen-doped single crystalline 6H-SiC", J. Appl. Phys. 72, 5437 (1992).*

[59] David J. Larkin, Philip G. Neudeck, J. Anthony Powell, and Lawrence G. Matus, *"Site-competition epitaxy for superior silicon carbide electronics", Appl. Phys. Lett. 65 (13), 26 September 1994.*

[60] Tsunenobu Kimoto, Akira Itoh, and Hiroyuki Matsunami, *"Incorporation mechanism of N, Al, and B impurities in chemical vapor deposition in SiC ", Appl. Phys. Lett. 67 (16), 16 October 1995.*

[61] Ö. Danielsson, U. Forsberg, and E. Janzeźn, *"Predicted nitrogen doping concentrations in silicon carbide epitaxial layers grown by hot-wall chemical vapor deposition", Journal of Crystal Growth 250 (2003) pp. 471-478.*

[62] Wenzhou Chena, Kung-yen Lee, and Michael A. Capano, *"Growth and characterization of nitrogen-doped C-face 4H-SiC epilayers", Journal of Crystal Growth 297 (2006) pp. 265-271.*

[63] Philip G. Neudeck, David J. Larkin, J. Anthony Powell, Lawrence G. Matus, and Carl S. Salupo, *"2000 V 6H-SiC p-n junction diodes grown by chemical vapor deposition", Appl. Phys. Lett.* ***64****(11), 14 March 1994 pp. 1386-1388.*

[64] J.B. Petit, P.G. Neudeck, C.S. Salupo, D.J. Larkin and J.A. Powell. In: (2nd Edn ed.), *Inst. Phys. Conf. Ser.* ***137*** *(1994), p. 679.*

[65] P. G. Neudeck, J. B. Petit, and C. S. Salupo, *2nd Internat. High Temperature Electronic Conference, Vol. 1, Eds. D. B. King and F. V. Thomes, Sandia National Laboratories, Charlotte (NC), 1994 (p. X).*

[66] Tsunenobu Kimoto, Akira Itoh, and Hiroyuki Matsunami, *"Step bunching in chemical vapor deposition of 6H– and 4H–SiC on vicinal SiC(0001) faces", Appl. Phys. Lett.* ***66*** *(26), 26 June 1995.*

[67] Hiroyuki Matsunami, Tsunenobu Kimoto, *"Step-controlled epitaxial growth of SiC: high quality homoepitaxy", Materials Science and Engineering, R20(1997) 125-166.*

[68] Conyers Herring, *"Some Theorems on the Free Energies of Crystal Surfaces", Phys. Rev. 82(1951) 87.*

[69] W.A. Tiller, *"The Science of Crystallization: Microscopic Interfacial Phenomena", Cambridge University Press, Cambridge, 1991, Chapter 2.*

[70] Tsunenobu Kimoto, Akira Itoh, Hiroyuki Matsunami, and Tetsuyuki Okano, *"Step bunching mechanism in chemical vapor deposition of 6H- and 4H-SiC {0001}", J. Appl. Phys.* ***81*** *(8), 15 April 1997.*

[71] F. C. Frank, *"Growth and Perfection of Crystals", edited by R. H. Doremus, B. W. Roberts, and D. Turnbull (Wiley, New York, 1958), p. 411.*

[72] R. L. Schwoebel and E. J. Shipsey, *"Step Motion on Crystal Surfaces", J. Appl. Phys.* ***37****, 3682 (1966).*

[73] M. Kasu and N. Kobayashi, *"Equilibrium multiatomic step structure of GaAs(001) vicinal surfaces grown by metalorganic chemical vapor deposition"Appl. Phys. Lett.* ***62****, 1262 (1993).*

[74] Ellen D. Williams, R. J. Phaneuf, Jian Wei, N. C. Bartelt and T. L. Einstein, *"Thermodynamics and statistical mechanics of the faceting of stepped Si(111)", Surf. Sci.* ***294****, 219 (1993).*

[75] V. Heine, C. Cheng, and R. J. Needs, *"The Preference of Silicon Carbide for Growth in the Metastable Cubic Form", J. Am. Ceram. Soc. 74, 2630 (1991).*

[76] F. R. Chien, S. R. Nutt, W. S. Yoo, T. Kimoto, and H. Matsunami, *"Terrace growth and polytype development in epitaxial β-SiC films on α-SiC (6H and 15R) substrates", J. Mater. Res.* ***9****, 940 (1994).*

[77] Philip G. *Neudeck, Member, IEEE and J . Anthony Powell, Member, IEEE, "Performance Limiting Micropipe Defects in Silicon Carbide Wafers", IEEE ELECTRON DEVICE LETTERS, VOL. 15, NO. 2, pp. 63-65, FEBRUARY 1994.*

[78] S. E. Saddow, T. E. Schattner, J. Brown, L. Grazulis, K. Mahalingam, G. Landis, R. Bertke, and W. C. Mitchel. *"Effects of Substrate Surface Preparation on Chemical Vapor Deposition Growth of 4H-SiC Epitaxial Layers", Journal of ELECTRONIC MATERIALS, Vol. 30, No. 3, 2001.*

[79] J. A. Powell and D. J. Larkin, *"Process-Induced Morphological Defects in Epitaxial CVD Silicon Carbide", phys. stat. sol. (b) 202, 529 (1997).*

[80] Jianwei Wan, Seung-Ho Park, Gilyong Chung, and Mark loboda, *"A Comparative Study of Micropipe Decoration and Counting in Conductive and Semi-Insulating Silicon Carbide Wafers", Journal of Electronic Materials, Vol. 34, No. 10, 2005, pp.1342-1348.*

[81] Philip G. Neudeck, *Senior Member, IEEE*, Wei Huang, and Michael Dudley, *"Study of Bulk and Elementary Screw Dislocation Assisted Reverse Breakdown In Low-Voltage (<250V) 4H-SiC $p^+n$ Junction Diodes – Part I: DC Properties", IEEE TRANSACTIONS ON ELECTRON DEVICES, VOL. 46, NO. 3, MARCH 1999, pp. 478-484.*

[82] Tsunenobu Kimoto, Nao Miyamoto, and Hiroyuki Matsunami, *Member, IEEE, "Performance Limiting Surface Defects in SiC Epitaxial p-n Junction Diodes", IEEE TRANSACTIONS ON ELECTRON DEVICES, VOL. 46, NO. 3, MARCH 1999, pp.471-477.*

[83] Philip G. *Neudeck, Member, IEEE and J . Anthony Powell, Member, IEEE, "Performance Limiting Micropipe Defects in Silicon Carbide Wafers", IEEE ELECTRON DEVICE LETTERS, VOL. 15, NO.* ***2,*** *FEBRUARY 1994, pp.63-65.*

[84] Uwe Zimmermann, John Österman, Dan Kuylenstierna, and Anders Hallén, Andrey O. Konstantinov, William M. Vetter and Michael Dudley, *"Material defects in 4H-silicon carbide diodes", J. Appl. Phys.* ***93*** *(1), pp.611 -618, January 2003.*

[85] Philip G. Neudeck, and J . Anthony Powell,*"Performance Limiting Micropipe Defects in Silicon Carbide Wafers", IEEE ELECTRON DEVICE LETTERS, VOL. 15, NO.* ***2,*** *FEBRUARY 1994, pp.63-65.*

[86] H. Fujiwara, T. Kimoto, T. Tojo, and H. Matsunami, *"Characterization of in-grown stacking faults in 4H–SiC (0001) epitaxial layers and its impacts on high-*

*voltage Schottky barrier diodes", Appl. Phys. Lett.* ***87****, 051912 (2005), pp.051912-1 – 051912-3.*

[87] Frank Slootman, Jean-Claude Parent, "*Homogeneous gas-phase nucleation in silane pyrolysis", J. Aerosol Sci.* ***25*** *pp.15-21 (1994).*

[88] R. Robertson, D. Hils, A. Gallagher, *"Silane pyrolysis", Chem. Phys. Lett.* ***103*** *pp.397-404 (1994).*

[89] R. T. White, R. L. Espino-Rios, D. S. Rogers, M. A. Ring, H. E. O'Neal, *"Mechanism of the silane decomposition. I. Silane loss kinetics and rate inhibition by hydrogen. II. Modeling of the silane decomposition (all stages of reaction)", Int. J. Chem. Kinet.* ***17*** *pp.1029-1065 (1985).*

[90] J. W. Erwin, M. A. Ring, H. E. O'Neal, *"Mechanism and kinetics of the silane decomposition in the presence of acetylene and in the presence of olefins", Int. J. Chem. Kinet.* ***17*** *pp.1067-1083 (1985).*

[91] Morey A. Ring, M. J. Puentes, and H. Edward O'Neal, *"Pyrolysis of monosilane", J. Am. Chem. Soc. 92 pp.4845-4848 (1970).*

[92] P. Neudorfl, A. Jodhan, O. P. Strausz, *"Mechanism of the thermal decomposition of monosilane", J. Phys. Chem.* ***84****, pp.338-339 (1980).*

[93] W. G. Breilan, M. E. Coltrin, P Ho, *"Comparisons between a gas-phase model of silane chemical vapor deposition and laser-diagnostic measurements", J. Appl. Phys.* ***59****, pp.3267-3273 (1986).*

[94] W. G. Breiland, P. Ho, M. E. Coltrin, *"Gas-phase silicon atoms in silane chemical vapor deposition: Laser-excited fluorescence measurements and comparisons with model predictions", J. Appl. Phys.* ***60****, pp.1505-1513 (1986).*

[95] S. K. Iya, R. N. Flagella, F. S. DiPaolo, *"Heterogeneous decomposition of silane in a fixed bed reactor", J Electrochem. Soc.* ***129****, pp.1531-1535 (1982).*

[96] B. A. Scott, R. D. Estes, *"Role of gas phase reactions in silicon chemical vapor deposition from monosilane", Appl. Phys. Lett.* ***55****, pp.1005 (1989).*

[97] G. Hsu, R. Hogle, N. Rohatgi, A. Morrison, *"Fines in Fluidized Bed Silane Pyrolysis", J. Electrochem. Soc.* ***131****, pp.660-663 (1984).*

[98] A. A. Onischuk, V. P. Strunin, M. A. Ushakova, V. N. Panfilov, *"Studying of silane thermal decomposition mechanism", Int. J. Chem. Kinet.* ***30****, pp.99-110 (1998).*

[99] A. A. Onischuk, A. I. Levykin, V. P. Strunin, K. K. Sabelfeld, V. N. Panfilov, *"Aggregate Formation Under Homogeneous Silane Thermal Decomposition", J. Aerosol Sci. 31, pp.1263-1281 (2000).*

[100] C. G. Newman, H. E. O'Neal, M. A. Ring, F. Leska, N. Shipley, *"Kinetics and mechanism of the silane decomposition", Int. J. Chem. Kinet. 11, pp.1167-1182 (1979).*

[101] Charles G. Newman, Morey A. Ring, and H. Edward O'Neal, *"Kinetics of the silane and silylene decompositions under shock tube conditions", J. Am. Chem. Soc.* ***100****, pp.5945-5946 (1978).*

[102] Mitsuo Koshi, Shin Kato, and Hiroyuki Matsui, *"Unimolecular decomposition of silane, fluorosilane, and difluorosilane at high temperatures", J. Phys. Chem.* ***95****, pp.1223-1227 (1991).*

[103] A. A. Onischuk, V. P. Strunin, R. I. Samoilova, A. V. Nosov, M. A. Ushakova and V. N. Panfilov, *"Chemical composition and bond structure of aerosol particles of amorphous hydrogenated silicon forming from thermal decomposition of silane", J. Aerosol Sci. 28, pp.1425-1441 (1997).*

[104] R. G. Aivazyan, V. V. Azatyan, L. F. Satunkina, *"Kinetic Regularities of Monosilane Pyrolysis and the Role of Reaction Chains", Kinet. Katal.* ***37****, pp.461-468 (1996).*

[105] B. A. Scott, R. D. Estes, J. M. Jasinski, *"The role of surface reactions in monosilane pyrolysis", J. Chem. Phys. 89, pp.2544-2549 (1988).*

[106] M. Frenklach, L. Ting, H. Wang and M.J. Rabinowitz , *"Silicon particle formation in pyrolysis of silane and disilane", Isr J Chem 36 (1996), pp.293–303.*

[107] R. Robertson, A Gallagher, *"Reaction mechanism and kinetics of silane pyrolysis on a hydrogenated amorphous silicon surface", J. Chem. Phys. 85, pp.3623-3630 (1986).*

[108] Rosa Becerra and Robin Walsh, *"Some mechanistic problems in the kinetic modeling of monosilane pyrolysis", J. Phys. Chem. 96, pp.10856-10862 (1992).*

[109] A. A. Onischuk, V. N. Panfilov, *"Mechanism of thermal decomposition of silanes", Russian Chemical Reviews 70 (4) pp.321-332 (2001).*

[110] A.N. Vorob'ev, S.Yu. Karpov, A.I. Zhmakin, A.A. Lovtsus,Yu.N. Makarov, A. Krishnan, *"Effect of gas-phase nucleation on chemical vapor deposition of silicon carbide", Journal of Crystal Growth 211 (2000) pp.343-346.*

[111] R. Rupp (a), Yu. N. Makarov (c), H. Behner (b), and A. Wiedenhofer, *"Silicon Carbide Epitaxy in a Vertical CVD Reactor: Experimental Results and Numerical Process Simulation", phys. stat. sol. (b) 202, 281 (1997).*

[112] Shin-ichi Nishizawa, Kazutoshi Kojima, Satoshi Kuroda, Kazuo Arai, Michel Pons, *"Modeling of SiC-CVD on Si-face/C-face in a horizontal hot-wall reactor", Journal of Crystal Growth 275 (2005) pp. e515–e520.*

[113] H. Pedersen, S. Leone, A. Henry, F.C. Beyer, V. Darakchieva, E. Janzén, *"Very high growth rate of 4H-SiC epilayers using the chlorinated precursor methyltrichlorosilane (MTS)", Journal of Crystal Growth 307 (2007) pp.334-340.*

[114] Z. M. Qian, H. Michiel, A. Van Ammel, J. Nijs, and R. Mertens, *"Homogeneous Gas Phase Nucleation of Silane in Low Pressure Chemical Vapor Deposition (LPCVD)", J. Electrochem. Soc. 135, pp.2378-2379 (1988).*

[115] C. H. J. Van Den Brekel, L. J. M. Bollen, *"Low pressure deposition of polycrystalline silicon from silane", Journal of Crystal Growth 54 (1981) pp.310-324.*

[116] Jin Jwang Wu and Richard C. Flagan, *"Onset of runaway nucleation in aerosol reactors", J. Appl. Phys.* ***61*** *, pp.1365-1371 (1987).*

[117] M. K. Alam; R. C. Flagan, *"Controlled Nucleation Aerosol Reactors: Production of Bulk Silicon", Aerosol Sci. Technol.* ***5****, pp.237-248 (1986).*

[118] Toshinori Kojima, Kimitoshi Usui and the late Takehiko Furusawa, *"Properties of Silicon Produced by Monosilane Pyrolysis", J. Chem. Eng. Jpn. 22, pp.683-686 (1989).*

[119] Carlyle S. Herrick and David W. Woodruff, *"The Homogeneous Nucleation of Condensed Silicon in the Gaseous Si-H-Cl System", J. Electrochem. Soc.* ***131****, pp.2417-2422 (1984).*

[120] V. P. Pimenov, V. I. Chernyak, A. I. Gorbunov, *Khim. Fiz. 7 1520 (1988)*[a].

[121] Mark T. Swihart and Steven L. Girshick, *"Thermochemistry and Kinetics of Silicon Hydride Cluster Formation during Thermal Decomposition of Silane", J. Phys. Chem., B* ***103****, pp.64-76 (1999).*

[122] A. Ellison, J. Zhang, J. Peterson, A. Henry, Q. Wahab, J. P. Bergman, Y. N. Makarov, A. Vorob'ev, A. Vehanen, E. Janzén, *"High temperature CVD growth of SiC", Mater. Sci. Eng. B 61-61(1999), pp. 113-120.*

[123] Yuuki Ishida, Tetsuo Takahashi, Hajime Okumura, Kazuo Arai, and Sadafumi Yoshida, *"In situ Observation of Clusters in Gas Phase during 4H-SiC Epitaxial Growth by Chemical Vapor Deposition Method", J. J. Appl. Phys. Vol. 43, No.8A, (2004), pp.5140-5144.*

[124] Yaroslav Koshka, Huang-De Lin, Galyna Melnychuk, Colin Wood, *"Epitaxial growth of 4H–SiC at low temperatures using $CH_3Cl$ carbon gas precursor: Growth rate, surface morphology, and influence of gas phase nucleation", Journal of Crystal Growth 294 (2006) pp.260-267.*

[125] Yaroslav Koshka, Huang-De Lin, Galyna Melnychuk, Colin Wood, *"Lower-temperature epitaxial growth of 4H-SiC using carbon gas precursor", Materials Science Forum Vols. 527-529 (2006) pp.167-170.*

[126] A. Veneroni, F. Omarini, and M. Masi, *"Silicon carbide growth mechanisms from $SiH_4$, $SiHCl_3$ and $nC_3H_8$", Cryst. Res. Technol.* ***40****, No. 10-11, pp.967-971 (2005).*

[127] Mark T. Swihart and Robert W. Carr, *"On the Mechanism of Homogeneous Decomposition of the Chlorinated Silanes, Chain Reactions Propagated by Divalent Silicon Species", J. Phys. Chem. A* ***1998****, 102, pp.1542-1549.*

[128] Vladimir S. Ban and Stephen L. Gilbert, *"Chemical Processes in Vapor Deposition of Silicon, I. Deposition from $SiCl_2H_3$ and Etching by HCl", J. Electrochem. Soc.* ***122****, pp. 1382-1388 (1975).*

[129] Vladimir S. Ban, *"Chemical Processes in Vapor Deposition of Silicon, II. Deposition from $SiCl_3H$ and $SiCl_4$", J. Electrochem. Soc. 122, pp. 1389-1391 (1975).*

[130] K. Ikoma, M. Yamanaka, H. Yamaguchi, and Y. Shichi, *"Heteroepitaxial Growth of β-SiC on Si(111) by CVD Using a CH3Cl-SiH4-H2 Gas System", J. Electrochem. Soc.* ***138****, pp. 3028-3031 (1991).*

[131] Z. Y. Xie, S. F. Chen, J. H. Edgar, K. Barghout, and J. Chaudhuri, *"Polytype Controlled SiC Epitaxy on On-axis 6H-SiC(0001) by Adding HCl during Growth", Electrochemical and Solid-State Letters,* ***3****(8) pp.381-384 (2000).*

[132] H. J. Chung, A. Y. Polyakov, S. W. Hub, S. Nigam, M. Skowronski, M. A. Fanton, B. E. Weiland, and D. W. Snyder, *"Bulk growth of high-purity 6H-SiC single crystals by halide chemical-vapor deposition", J. Appl. Phys.* ***97,*** *084913 (2005).*

[133] L. Calcagno, G. Izzo, G. Litrico, G. Foti, F. La Via, G. Galvagno, M. Mauceri, and S. Leone, *"Optical and electrical properties of 4H-SiC epitaxial layer grown with HCl addition", J. Appl. Phys.* ***102****, 043523 (2007).*

[134**]** S. Nigam, H.J. Chung, A.Y. Polyakov, M.A. Fanton, B.E. Weiland, D.W. Snyder, M. Skowronski, *"Growth kinetics study in halide chemical vapor deposition of SiC", Journal of Crystal Growth 284 (2005) pp.112-122.*

[135] Rong Wang, Ronghui Ma, *"Kinetics of halide chemical vapor deposition of silicon carbide film", Journal of Crystal Growth 308 (2007) pp.189-197.*

[136] D. Crippa et al., *"New Achievements on CVD Based Methods for SiC Epitaxial Growth", Materials Science Forum Vols. 483-485 (2005) pp67-72.*

[137] Rachael L. Myers-Ward, Olle Kordina, Z. Shishkin, Shailaja P. Rao, R. Everly, S.E. Saddow, *"Increased Growth Rate in a SiC CVD Reactor Using HCl as a Growth Additive", Materials Science Forum Vols. 483-485 (2005) pp.73-76.*

[138] Shigehiro Nishino, Toshiyuki Miyanagi, Y. Nishio, *"Epitaxial Growth of SiC on α-SiC Using $Si_2Cl_6 + C_3H_8 + H_2$ System", Materials Science Forum Vols. 264-268 (1998) pp.139-142.*

[139] Jie Zhang, Janice Mazzola, Carl Hoff, Yaroslav Koshka, Jeff B. Casady, *"High Growth Rate (up to 20 μm/h) SiC Epitaxy in a Horizontal Hot-Wall Reactor", Materials Science Forum Vols. 483-485 (2005) pp.77-80.*

[140] Katsunori Danno, Tsutomu Hori, and Tsunenobu Kimoto, *"Impacts of growth parameters on deep levels in n-type 4H-SiC", J. Appl. Phys. 101, 053709 (2007).*

[141] G. Aylward, T. Findlay, SI Chemical Data, fourth ed., Wiley, Milton, Australia, 1998, pp.115.

[142] F. La Via, G. Galvagno, G. Foti, M. Mauceri, S. Leone, G. Pistone, G. Abbondanza, A. Veneroni, M. Masi, G. L. Valente, D. Crippa, *"4H-SiC Epitaxial Growth with Chlorine Addition", Chem. Vap. Deposition 12 (2006), pp.509-515.*

[143] H.D. Lin, G. Melnychuk, J.L. Wyatt, and Y. Koshka, *"Low-Temperature Halo-Carbon Homoepitaxial Growth of 4H-SiC:Morphology, Doping, and Role of HCl Additive", Materials Science Forum Vols. 556-557 (2007) pp.133-136.*

[144] Stefano Leone, Marco Mauceri, Giuseppe Pistone, Giuseppe Abbondanza, F. Portuese, Giovanni Abagnale, Gian Luca Valente, Danilo Crippa, Milo Barbera, Ricardo Reitano, Gaetano Foti, Francesco La Via, *"SiC-4H Epitaxial Layer Growth Using Trichlorosilane (TCS) as Silicon Precursor", Materials Science Forum Vols. 527-529 (2006) pp.179-182.*

[145] Mike F. MacMillan, Mark J. Loboda, Gil Yong Chung, E.P. Carlson, Jian Wei Wan, *"Homoepitaxial Growth of 4H-SiC Using a Chlorosilane Silicon Precursor", Materials Science Forum Vols. 527-529 (2006) pp.175-178.*

[146] Govindhan Dhanaraj, Michael Dudley, Yi Chen, Balaji Ragothamachar, Bei Wu, Hui Zhang, *"Epitaxial growth and characterization of silicon carbide films", Journal of Crystal Growth 287 (2006) pp.344-348.*

[147] Dieter K. Schroder, *"Semiconductor Material and Device Characterization", 3rd Edition, John Wiley & Sons, Inc., ISBN-13: 978-0-471-73906-7, pp. 61-63.*

[148] Kentaro Shibahara, Naotaka Kuroda, Shigehiro Nishino and Hiroyuki Matsunami, *"Fabrication of P-N Junction Diodes Using Homoepitaxially Grown 6H-SiC at Low Temperature by Chemical Vapor Deposition", J. J. Appl. Phys. Vol. 26, No.11, 1987, pp. L1815-L1817.*

[149] A. Ellison, J. Zhang, A. Henry, E. Janzén, *"Epitaxial growth of SiC in a chimney CVD reactor", Journal of Crystal Growth 236 (2002) pp.225-238.*

[150] Jih-Jen Wu, Shih-Hsien Yeh, Chin-Ta Su, and Franklin Chau-Nan Hong, *"Characterization of diamond deposition from chloromethane reactants by laser reflective interferometry", Appl. Phys. Lett. 68 pp.3254-3256 (1996).*

[151] D. J. Larkin, S. G. Sridhara, R. P. Devaty and W. J. Choyke, *"Hydrogen incorporation in boron-doped 6H-SiC CVD epilayers produced using site-competition epitaxy", J. Electron. Mater. Vol.24, No.4 (1995), pp.289-294.*

[152] J. Anthony Powell and Herbert A. Will, *"Epitaxial growth of 6H SiC in the temperature range 1320–1390°C", J. Appl. Phys. 44 (11) (1973), pp.5177-5178.*

[153] Atsushi Yamashita, Woo Sik Yoo, Tsunenobu Kimoto and Hiroyuki Matsunami, *"Homoepitaxial Chemical Vapor Deposition of 6H-SiC at Low Temperatures on {01-14} Substrates", J. J. Appl. Phys. Vol. 31, No.11, (1992), pp.3655-3661.*

[154] Shunichi Nakamura, Tsunenobu Kimoto, Hiroyuki Matsunami, *"Homoepitaxy of 6H–SiC on nearly on-axis (0 0 0 1) faces by chemical vapor deposition Part I: Effect of C/Si ratio on wide-area homoepitaxy without 3C–SiC inclusions", Journal of Crystal Growth 256 (2003) pp.341-346.*

[155] F.F. Abraham, *"Homogeneous Nucleation Theory", Academic Press, New York, 1974.*

[156] K. Chindanon, H. Lin, G. Melnychuk, and Y. Koshka, *"Nitrogen and Aluminum Doping in Low-temperature Halo-Carbon Homoepitaxial Growth of SiC", International Conference on Silicon Carbide and Related Materials 2007, Oct. 14-19, 2007, Otsu, Japan, paper Th-P-39.*

[157] M. Sadakata: *"CVD Handbook, ed. The Society of Chemical Engineers, Japan" (Asakura-Shoten, Tokyo, 1991) Chap. 3, p. 519 [in Japanese]*.

[158] K. Masahara, Y. Ishida, H. Okumura, T. Takahashi, M. Kushibe, T. Ohno, T. Suzuki, T. Tanaka, S. Yoshida and K. Arai, *"Pre-Growth Treatment of 4H-SiC Substrates by Hydrogen Etching at Low Pressure", Materials Science Forum Vols. 338-342 (2000) pp.1037-1040.*

[159] Yo-Ping Wu, Yang-Soo Won, *"Pyrolysis of Chloromethanes", Combustion and Flame 122:312-326(2000).*